Project 2549

S/C Project 2406

S/C Project 2570

C

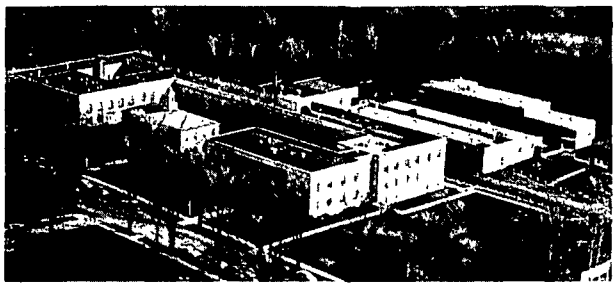

THE INSTITUTE OF PAPER CHEMISTRY, APPLETON, WISCONSIN

THE INSTITUTE OF PAPER CHEMISTRY
Appleton, Wisconsin

HYDRODYNAMIC EVALUATION OF FIBER SURFACE AREA AND SWOLLEN VOLUME

A CRITICAL REVIEW

March 31, 1967

THE INSTITUTE OF PAPER CHEMISTRY
Appleton, Wisconsin

HYDRODYNAMIC EVALUATION OF FIBER SURFACE AREA AND SWOLLEN VOLUME

A CRITICAL REVIEW

March 31, 1967

To the memory of Dr. William L. Ingmanson

TABLE OF CONTENTS

THE INSTITUTE OF PAPER CHEMISTRY
Appleton, Wisconsin

HYDRODYNAMIC EVALUATION OF FIBER SURFACE AREA AND SWOLLEN VOLUME

SUMMARY

The method of fluid permeation has been successfully used for measuring the surface area of nearly spherical solid particles in loose aggregations. Its application to fibers, however, involves certain difficulties. Because of their elongated shape the fibers in the medium can have preferred orientations leading to high porosities. Most natural fibers are of irregular cross sections and may possess internal porous structures which are subject to swelling by permeating fluids. They are more or less flexible and sometimes deformable, constituting a compressible medium. Cellulosic fibers also have complicated surfaces which are readily changeable by mechanical or chemical means. For these and other reasons precise determinations of surface area and swollen volume by the hydrodynamic or other means have not yet been fully achieved.

At the present time the hydrodynamic evaluation of the two important fiber properties of surface area and swollen volume appears to be more reliable in common papermaking practices than other techniques and more amenable to further refinements for future utilizations. This review will therefore be restricted to a discussion of the status and prospects of the hydrodynamic method.

This review begins with the underlying principle of permeability and the experimental verification of the phenomenon. It proceeds to the static compressibility which is not only required in the analysis of filtration but

is also by itself a tool for pulp evaluation. Utilizing the knowledge of compressibility, the filtration data obtained under controlled conditions are analyzed in detail with the aid of the theories recently developed at the Institute. The results of analysis are compared with the ubiquitous "freeness" to indicate the latter's usefulness as well as its limitations. Finally, a number of actual applications of the hydrodynamic pulp evaluation are cited as illustrations with the hope that its intelligent use may be expanded when a somewhat simplified and relatively inexpensive instrument becomes available.

Some interpretations of the findings presented here are more or less controversial; their validity needs confirmation or refutation. Other evidence, which is dubious or inconsistent, suggests further experimental investigations for clarification and utilization. Continuing development of rigorous theories is the crying need in this research area. Without appropriate mathematical models capable of predictions, the mere accumulation of data will be neither adequate nor effective in advancing the technology of pulp evaluation.

INTRODUCTION

HISTORICAL DEVELOPMENT

Cellulosic fibers have a wide distribution of length, width, and thickness. Their cross sections vary somewhat along the length and their surfaces are more or less fibrillated. In a wet state they are considerably swollen and tend to deswell under moderate pressures. They are not only flexible in bending but also conformable on contact. Because of their irregular geometry, the surface area and swollen volume of cellulosic fibers are difficult to measure in a simple, direct, and positive way. Yet by experience and logic the papermaker has long realized the importance of these two fiber properties in pulp processing and sheet forming.

In the olden days the beaterman used to test a pulp by squeezing a sample in his hand. He tried to judge how easily the water drained, how slippery the fibers felt, and how clear the drainage appeared. Essentially, he sensed the "freeness," "wetness," or fineness" of the pulp. As the art advanced, the squeezing test was replaced by a freeness test, purported to measure the same thing in terms of a quantity rather than a feeling. The measurement was supposed to indicate the drainage of a pulp in a definable way. However, in the transition from a qualitative to quantitative mensuration, some of the complications and implications of the test were often ignored. As an unfortunate consequence, the freeness test in its various modifications has sometimes been misused or misinterpreted, possibly with overconfidence or merely by oversimplification.

Some twenty years ago extensive investigations of the hydrodynamics of fiber suspensions were undertaken with particular regard to pulp drainage

characteristics. By controlled experiments of permeation, filtration, and compression, the factors governing flow of water through fiber mats have since been clarified to a considerable extent. In this review it is intended to summarize the major findings of the past work and to indicate the unresolved problems for future research.

PRESENT STATUS

The phenomenological description of flow through a porous medium begins with the Darcy law, which relates the velocity of flow to the gradient of pressure by a proportionality factor. If the fluid properties are separated from this factor, the remainder represents Darcy's permeability, which is characteristic of the porous medium in the dynamic sense. The Kozeny-Carman equation is a refinement of Darcy's law, which resolves permeability in terms of pore volume and surface area. This relationship, within its limitations, is often used to determine the specific surface and volume of irregularly shaped particles from permeability data.

Permeability measurements are made under the steady condition of slow flow through a uniform medium at constant pressure and temperature. When the method of permeation was first applied to cellulosic fibers, certain experimental difficulties were encountered at once. The fibrous medium, being easily compressible, results in decreasing porosity under increasing fluid stresses in the direction of flow. To maintain a nearly uniform structure, the medium was subjected to high mechanical compaction and permeated at low pressure drops. These conditions restricted the range and precision of usable data. More serious was the problem of permeability decay, which has not yet been completely solved.

To overcome the shortcomings of permeation the method of filtration was adopted. In a controlled filtration experiment a very dilute suspension of fibers is caused to flow at either constant pressure or constant rate through a septum on which the fibers are formed into a relatively thick mat with complete retention. The constant-pressure technique necessitates a series of runs in order to cover a sufficient range of pressure drops. For this and other reasons the constant-rate technique has come into favor.

The analysis of filtration, however, is more involved than that of permeation. Firstly, because of the variation of porosity with pressure drop, the mat compressibility must be known. Secondly, a fiber mat being highly porous, does not strictly follow the Kozeny-Carman relationship, which holds only for the moderate porosity range. Thirdly, the deswelling tendency as well as the conformability of swollen fibers needs to be taken into account. These complications have been largely resolved through systematic investigations which will be critically reviewed in the following sections.

The freeness test inherits the same complications as filtration. In addition, because it is carried out under falling head and with fines loss, the drainage results so obtained are not readily amenable to analysis for fiber surface area and swollen volume. Without knowledge of these fiber properties the hydrodynamic behavior of pulps cannot be easily comprehended.

PERMEABILITY

PERMEABILITY CONCEPT

Steady, isothermal, slow flow of an incompressible Newtonian fluid in the downward direction through a homogeneous, undeformable, macroporous medium bounded by horizontal plane areas of equal size A and with thickness L obeys Darcy's law (1):

$$U = K_0 \frac{\Delta p + \rho g L}{L} \qquad (1) .$$

The superficial velocity U is defined as the volumetric flow rate per unit area. The pressure drop Δp is the difference between the static pressures at the upper and lower boundaries of the medium. The term $\rho g L$ accounts for the gravitational pressure, ρ being the fluid density and g the gravitational constant. The proportionality factor K_0 is considered to be the permeability of the medium to a particular fluid.

It has been well established that K_0 is independent of the fluid density and inversely proportional to the fluid viscosity μ, so that

$$K_0 = \frac{K}{\mu} \qquad (2) ,$$

where the new factor K is generally referred to as the Darcy permeability or is sometimes called the specific permeability. It serves as a dynamic characterization of the porous structure and has the dimension of a length squared. As a numerical example, suppose that water flows downward through a medium, 10 sq. cm. in cross-sectional area and 1 cm. thick, at a rate of 10 cu. cm./sec. Then the superficial velocity is 1 cm./sec. If the total head Δh (the sum of the static and gravitational heads), as measured by two

open water manometers located across the medium, is 10 cm., the dynamic pressure drop ($\Delta \underline{P} \approx \rho \underline{g} \Delta \underline{h}$) is 9800 dynes/sq. cm., taking ρ to be 1 g./cu. cm. and $\underline{g}$ 980 cm./sq. sec. The static pressure drop $\Delta \underline{p}$ is 8820 dynes/sq. cm. or 9 g./sq. cm., which would be the difference indicated by two pressure gages instead of manometers. Taking μ to be 1 cp. or 10^{-2} g./cm. sec., the specific permeability, $\underline{K}$, of the medium is 1.02×10^{-6} sq. cm.

Permeation is an irreversible process, the pressure and potential energy being dissipated as heat due to the friction of flow by viscous action. The permeability of a medium is, therefore, a statistical average quantity characterizing the complex pore geometry.

PORE GEOMETRY

For a random medium, a statistical description of the pore structure is possible, as discussed by Pragar (2). A function $f(\vec{\underline{r}})$ of a position vector $\vec{\underline{r}}$ within the porous medium is introduced such that the function has the value of unity if $\vec{\underline{r}}$ is in the void region and zero if $\vec{\underline{r}}$ is in the solid region. A complete knowledge of $f(\vec{\underline{r}})$ will amount to a detailed specification of the pore geometry.

The volume average of the function itself is the porosity or void fraction:

$$\epsilon = \langle f(\vec{r}) \rangle = \frac{1}{V} \int_V f(\vec{r}) d\vec{r} \qquad (3),$$

where $\langle f(\vec{\underline{r}}) \rangle$ is called the one-point average. It represents the probability that if a pin is thrown at random on a much enlarged cross section of an isotropic medium, the pinhead will land in the void region.

The surface of the void region may be ascertained by adding a length vector $\vec{\delta}$ to the position vector $\vec{r}$ and carrying out the averaging process over all possible orientations of $\vec{r}$. The resulting two-point average,

$$S(\vec{\delta}) = \langle f(\vec{r}) f(\vec{r} + \vec{\delta}) \rangle \qquad (4),$$

indicates the probability that a pin having the length and direction of the vector $\vec{\delta}$ will land with both its ends in voids. For an isotropic medium, $S(\vec{\delta})$ will depend on the magnitude of $\vec{\delta}$ only. When $\delta = 0$, the product of $f(\vec{r})$ by itself is unity and its volume average is ϵ. When $\delta = \infty$, the probabilities of two events in two voids wide apart are independent of each other. The volume average of each being ϵ, the product is therefore ϵ^2. Thus, the correlation function $S(\delta)$ decays continuously from ϵ to ϵ^2 as δ varies from 0 to ∞. The theoretical function derived by Debye, Anderson, and Brumberger (3) is

$$\frac{S(\delta) - \epsilon^2}{\epsilon(1 - \epsilon)} = \exp\left[- \frac{S_v \delta}{4\epsilon(1 - \epsilon)} \right] \qquad (5),$$

where S_v is the surface area per unit volume of the medium.

To define the shapes of the void region, at least the three-point average is required:

$$G(\vec{\delta}, \vec{\delta}') = \langle f(\vec{r}) f(\vec{r} + \vec{\delta}) f(\vec{r} + \vec{\delta}') \rangle \qquad (6).$$

For an isotropic medium, G will be a symmetrical function of the three distances δ, δ', and δ'', the last quantity being $|\vec{\delta}' - \vec{\delta}|$. If a triangle with these three lengths is thrown at random on a cross section of the medium, then G is the probability that all three vertices will land in void regions. G varies from the maximum value of ϵ when the three lengths

are all equal to zero to ϵ^3 when they are infinite. If δ'' vanishes while δ and δ' remain finite, $\underline{G}$ reduces to $\underline{S}(\delta)$, and if δ' becomes infinite while δ remains finite, $\underline{G}$ goes to $\epsilon\underline{S}(\delta)$. The correlation function $\underline{G}$ serves to describe some minor departure from a spherical surface. Its functional form has not been established. For a more detailed description of irregular void regions, the use of four- or five-point average becomes desirable, but hardly practicable.

GEOMETRIC MODELS

To resolve Darcy's permeability in terms of of pore geometry, model simulation of porous media has been employed as a useful tool of analysis. The Kozeny-Carman model (4) consists of a system of parallel channels, the size of which is represented by the hydraulic radius $\underline{m}$. The hydraulic radius of a dynamically simulated channel is defined by the ratio of cross-sectional area to wetted perimeter. Extending the definition to a porous medium, $\underline{m}$ assumes the ratio of porosity ϵ to specific surface $\underline{S_0}$. By dimensional considerations, the permeability of the model is taken to be proportional to the hydraulic radius squared. Since the average velocity in the channels or pores is equal to $\underline{U}/\epsilon$, the ratio of $\underline{K}$ for the porous medium to $\underline{m}^2$ of the model is proportional to ϵ. The resulting Kozeny-Carman expression of Darcy's permeability is simply

$$K = \frac{\epsilon^3}{kS_0^2} \qquad (7),$$

where $\underline{k}$ is known as the Kozeny constant.

According to Carman's interpretation, the Kozeny constant is the product of a pore shape factor and a tortuosity factor squared. The value of

the former lies in the range 2-3 for simple geometrical shapes, and that of the latter is estimated to be $\sqrt{2}$ for beds of spheres. Thus, $\underline{k}$ has a value between 4 and 6. Its average value is generally accepted to be 5 for roughly spherical particles in the range of porosity from 0.3 to 0.5.

The Kozeny-Carman equation has received some severe criticisms as well as partial justifications. Only recently, Snyder and Stewart (5) solved by Galerkin's method the basic hydrodynamic equations of continuity and motion for creeping flow of a Newtonian fluid through a dense cubic packing arrangement of uniform spheres under the exact boundary conditions. Their solution is in almost complete agreement with the Kozeny-Carman equation, the value of the Kozeny constant being 4.76.

By virtue of their elongated shape, fibers can be formed into mats of high porosities. In early work it was soon found that at high porosities the Kozeny "constant" itself is porosity dependent.

In the high porosity range, Happel's free-surface model (6) appears to be the most successful. In his model each cylinder in a regular assemblage is considered to be surrounded by a concentric envelope of fluid with a free surface, the combination constituting a unit cell. While the real boundary condition of zero velocity at the cylinder surface is maintained as in any rigorous treatment, the other boundary condition of zero shear or velocity gradient at the free surface is at best an approximation. Happel's solution for creeping flow perpendicular to an array of cylinders yields the following permeability expression for the Kozeny factor:

$$k = \frac{2\epsilon^3}{(1-\epsilon)\left[\ln \frac{1}{1-\epsilon} - \frac{1-(1-\epsilon)^2}{1+(1-\epsilon)^2}\right]} \qquad (8) .$$

By the free-surface model, Happel also obtained permeability expressions for flow parallel to cylinders as well as flow around spheres. The variations of the Kozeny factor with porosity for all the three cases are shown in Table I. As pointed out by Happel, the free-surface model is not suitable for porosities below about 0.5.

TABLE I

VALUES OF THE KOZENY FACTOR
ACCORDING TO THE FREE-SURFACE MODEL

Porosity	Flow Perpendicular to Cylinders	Flow Around Spheres	Flow Parallel to Cylinders
0.5	5.38	4.74	3.67
0.6	5.62	5.11	3.96
0.7	6.19	5.79	4.42
0.8	7.46	7.22	5.23
0.9	11.03	11.34	7.31

EXPERIMENTAL PROCEDURE

A general procedure for permeation experiments is outlined as follows: Dry and clean fibers are introduced into hot water in a suction flask which is then gradually evacuated to a gently boiling condition for the purpose of deaeration. The deaerated fiber slurry is siphoned into the dilution water in a feed tank, care being taken to prevent the free surface from disturbances which might cause entrainment of air bubbles on the fiber surfaces. The dilute fiber suspension in the tank is mildly agitated to break up any fiber bundles and to maintain a state of uniform dispersion, the consistency of the suspension being about 0.01%.

The septum which is a perforated plate covered with a coarse backing wire (35 mesh) and a fine face wire (100 mesh) is thoroughly cleaned and dried. After it is assembled with the permeation tube, flushing water flows upward through the tube to wet the septum and to remove air bubbles. The tube is then completely filled with water and the fiber suspension is admitted to the tube beneath the free surface. A mat is formed at a constant flow rate, sufficiently high to maintain turbulent dispersion in the tube but low enough to avoid irregular eddies.

A permeable piston is gently lowered and compresses the mat to the desired porosity. The water recirculating line is connected to the tube, and any air entrapped in the flow system is removed by bleeding through a vent. Flow through the mat is then initiated and slowly increased to the desired rate. At a steady state the corresponding pressure drop is noted and if necessary, corrected for that of the septum, which has been separately determined. A series of successive points at increasing flow rates is obtained in a single run. The last point is limited to a pressure drop not exceeding 1% of the load of the piston in order to maintain a uniform mat. The water used in permeation is deionized and distilled. The recirculating water is thoroughly filtered in each cycle to prevent the mat from contaminations.

Glass fibers, being relatively rigid, can be formed into mats of very high porosities, but they are not particularly satisfactory for porosities lower than 0.8 because of their fragile nature under mechanical compacting pressure during permeation. Nylon fibers are suitable for the intermediate porosities by virtue of their flexibility, but not practicable for porosities larger than 0.9 on account of the long durations required for forming thick mats from dilute suspensions at very low pressure drops.

The dimensions of these fibers can be precisely determined microscopically and the densities pycnometrically. The nylon fibers are known to be slightly swollen in water (about 3%). The compressibility constants, M and N, of the simple power function (to be discussed in the next section) are used to establish the mat porosities. The characterization of these fibers is summarized in Table II.

TABLE II

CHARACTERIZATION OF CYLINDRICAL FIBERS

Fiber	L_f, mm.	d_f, microns	ρ_f, g./cm.^{3}	S_v, cm.^{2}/cm.^{3}	v, cm.^{3}/g.	N	M, (g./cm.^{3})/(dynes/cm.^{2})^N
Glass	0.94	16.5	2.60	2420	0.384	(0.22)	(0.009)
Nylon	6.47	19.5	1.14	2050	0.904	0.225	0.0066

An example of permeation data for glass fibers is given in Fig. 1, in which the flow rate per unit mat area is plotted vs. the pressure drop across the mat with porosity as the parameter. Within the experimental range the data indicate direct proportionality in agreement with Darcy's law. From the slopes of these lines the permeability coefficients are calculated with the known viscosities.

EMPIRICAL CORRELATIONS

For fiber structures Davis (7) correlated the variation of the Kozeny factor with porosity in the following form:

$$k = k_1 \frac{\epsilon^3}{(1 - \epsilon)^{1/2}} [1 + k_2 (1 - \epsilon)^3] \qquad (9) ,$$

where k_1 and k_2 are two constants and have the values 4.0 and 56, respectively, based on air permeability data for loose fiber filters. Ingmanson

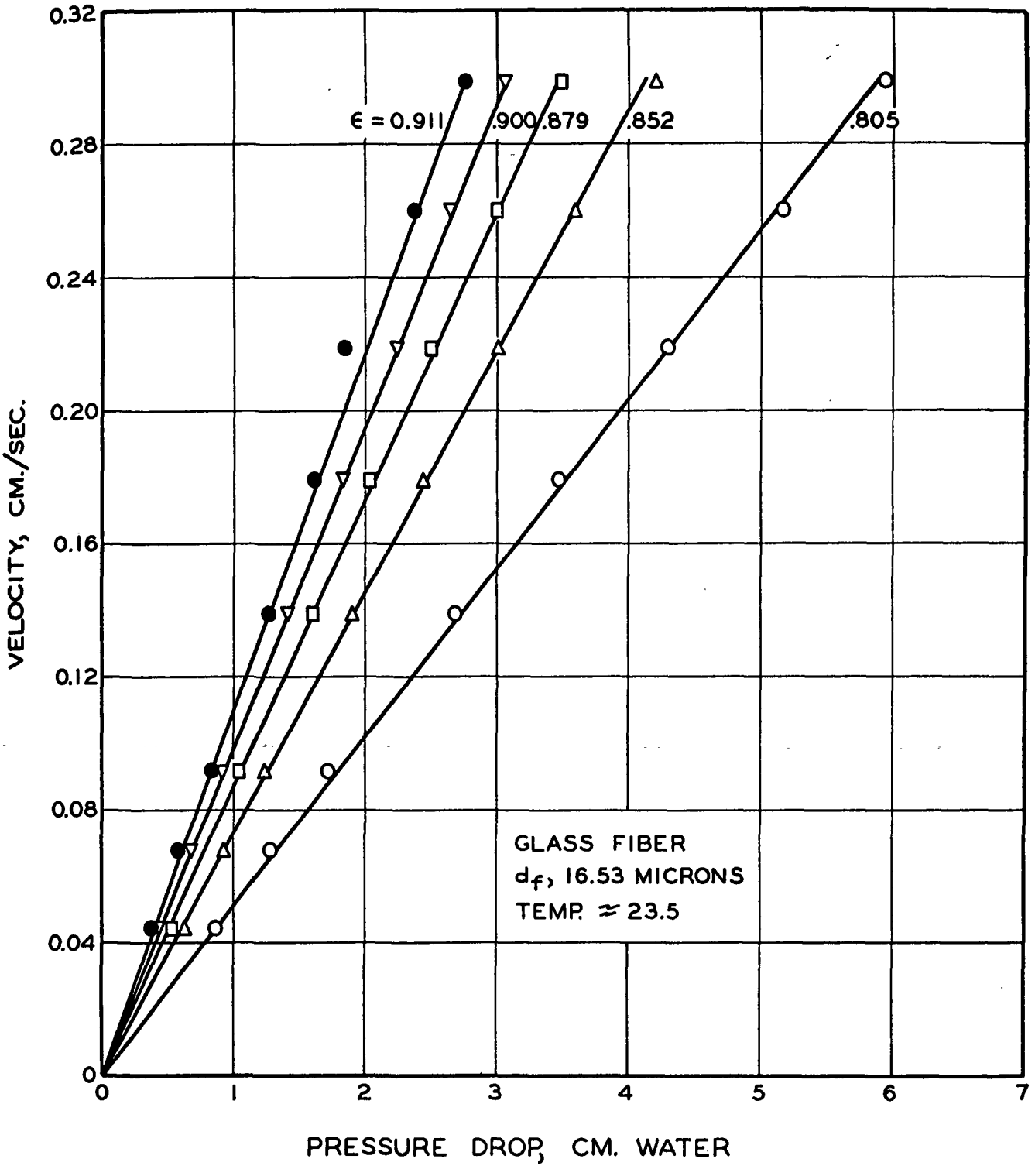

Figure 1. Permeation Data of Uniform Fiber Mats

and coworkers (8, 9) made very careful water permeability experiments with uniform mats of glass and nylon fibers oriented randomly in a plane with their axes perpendicular to flow, and arrived at the values 3.5 and 57 for k_1 and k_2, respectively. Their data are shown in Fig. 2. It is seen that the Davis-Ingmanson equation correlates the data quite satisfactorily. Their expression, however, should not be used for porosities lower than about 0.6 as it will yield rapidly decreasing values of k, while it has been amply demonstrated that the Kozeny factor remains practically constant at medium porosities.

Recently, Carroll (10) proposed the following correlation:

$$k = 5.0 + \exp[14(\epsilon - 0.80)] \qquad (10),$$

which is also shown in the same figure. Carroll's curve seems to fit the whole experimental range somewhat better than that of Davis-Ingmanson. However, his equation is not as adaptable as Davis-Ingmanson's to subsequent mathematical manipulations. For this reason and by inertia as well, we continue to use the latter's correlation, with which Darcy's permeability for cylindrical fibers becomes

$$\frac{1}{K} = k_1 S_v^2 (1 - \epsilon)^{3/2} [1 + k_2 (1 - \epsilon)^3] \qquad (11).$$

COMPLICATING EFFECTS

The permeability of fibers is affected by their cross-sectional shape. Bliesner (11) found an increase of flow resistance in mats of flattened fibers from his air permeability data. Labrecque (12) confirmed Bliesner's findings with nylon fibers of quasi-elliptical shape at different aspect (width-thickness) ratios. Their studies, however, were complicated by the change of the wetted surface area with porosity.

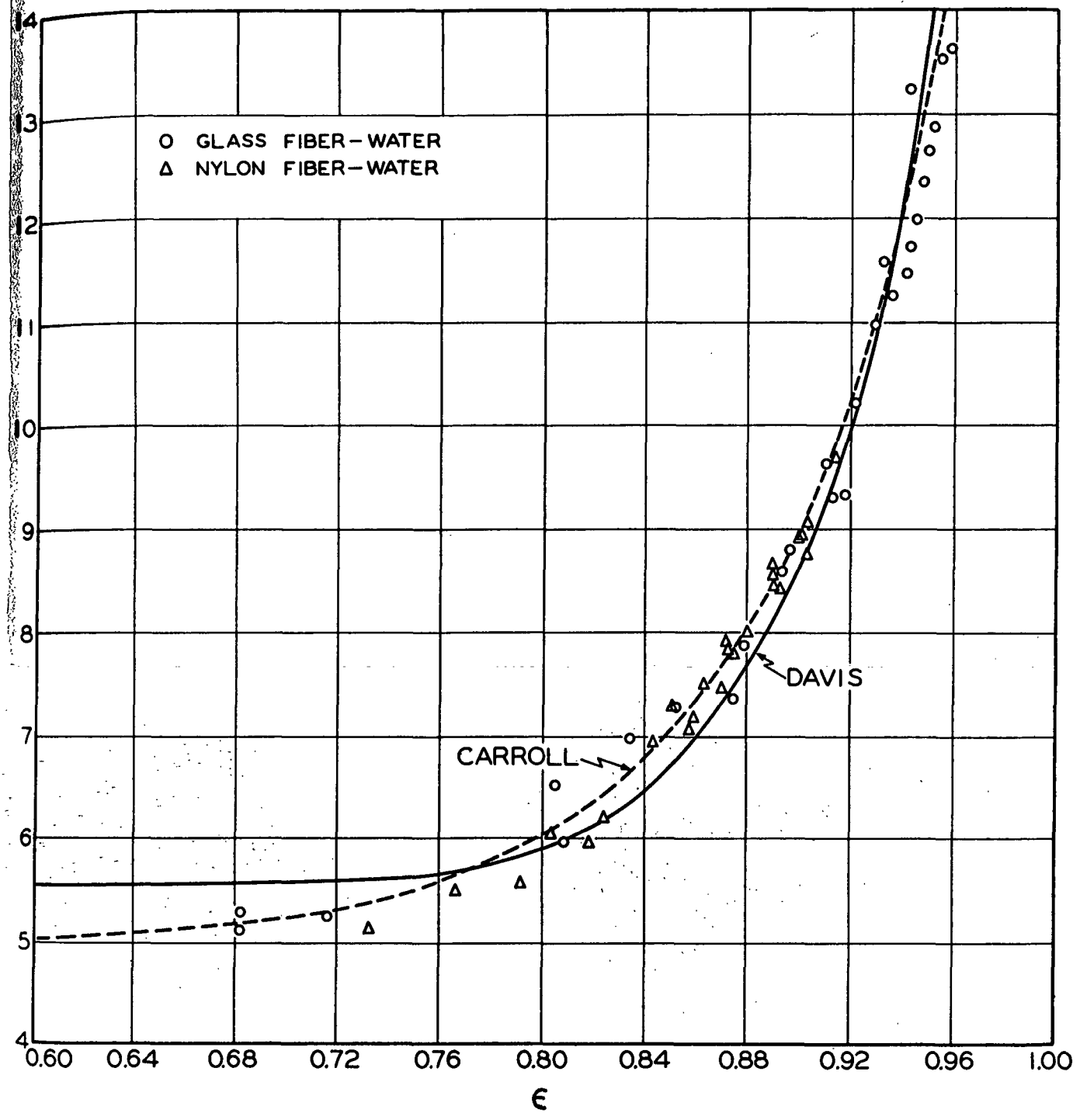

Figure 2. Correlation of Kozeny Factor with Porosity

For relatively rigid cylindrical fibers it is reasonable to expect a constant surface area exposed to flow in the high-porosity range under the assumption of point contact at the fiber intersections. In such a case, the specific surface $\underline{S_v}$ based on a unit volume of the fibers may be calculated directly from the fiber diameter, $\underline{d_f}$:

$$S_0 = S_v(1 - \epsilon) = \frac{4}{d_f}(1 - \epsilon) \qquad (12),$$

in which the cross-sectional area of the fiber ends is neglected.

For deformable fibers, the contact area formed at the fiber intersections does not contribute to the resistance to flow, and should be deducted from the total fiber surface area in permeability considerations. In estimating the contact area it is necessary first to know the number of intersections in the fiber mat at a given porosity. Labrecque used the Onogi-Sasaguri theory (13) for this purpose, taking the effect of fiber shape into account. Next, he calculated the average contact area per fiber intersection according to the equation of Van den Akker (14) for projected contact area, which is further corrected for incomplete contact, based on photomicrographical measurements of the fiber cross sections in a random array. Finally, with the known wetted surface area he analyzed the permeability data for the Kozeny factor. His results for high porosities are summarized in Table III.

TABLE III

EFFECT OF FIBER SHAPE ON PERMEABILITY

Aspect Ratio	Porosity	Specific Contact Area, $cm.^3/cm.^3$	Specific Wetted Area, $cm.^3/cm.^2$	Kozeny Factor
1.0	0.80	0	1535	6.18
2.64	0.80	50	1670	6.24
4.12	0.80	106	1754	6.97
4.69	0.78	138	1852	7.92

There appears a definite trend of a very mild increase in the Kozeny factor up to an aspect ratio of about 3, beyond which the value of $\underline{k}$ increases rather rapidly. Labrecque's data for lower porosities indicate the same trend. However, his correlation of the Kozeny factor with porosity for cylindrical fibers tends to be nearly linear, rather than exponential as correlated in Fig. 2. The discrepancy is probably attributable to a consistent error in the estimate of contact area with the variation of porosity.

By the same treatment Labrecque recalculated Bliesner's data. The results as shown in Fig. 3 serve to indicate the general trend of the effect of fiber shape on the Kozeny factor in the useful porosity range.

CELLULOSIC FIBERS

Wet wood fibers generally have aspect ratios less than 3.5, as revealed by photomicrographs of their cross sections made in the frozen state. Therefore, the extension of either Davis-Ingmanson's or Carroll's correlation to permeability of wood fibers is justifiable. However, the permeability method for determination of specific surface and volume of wood fibers involves an additional problem of decay.

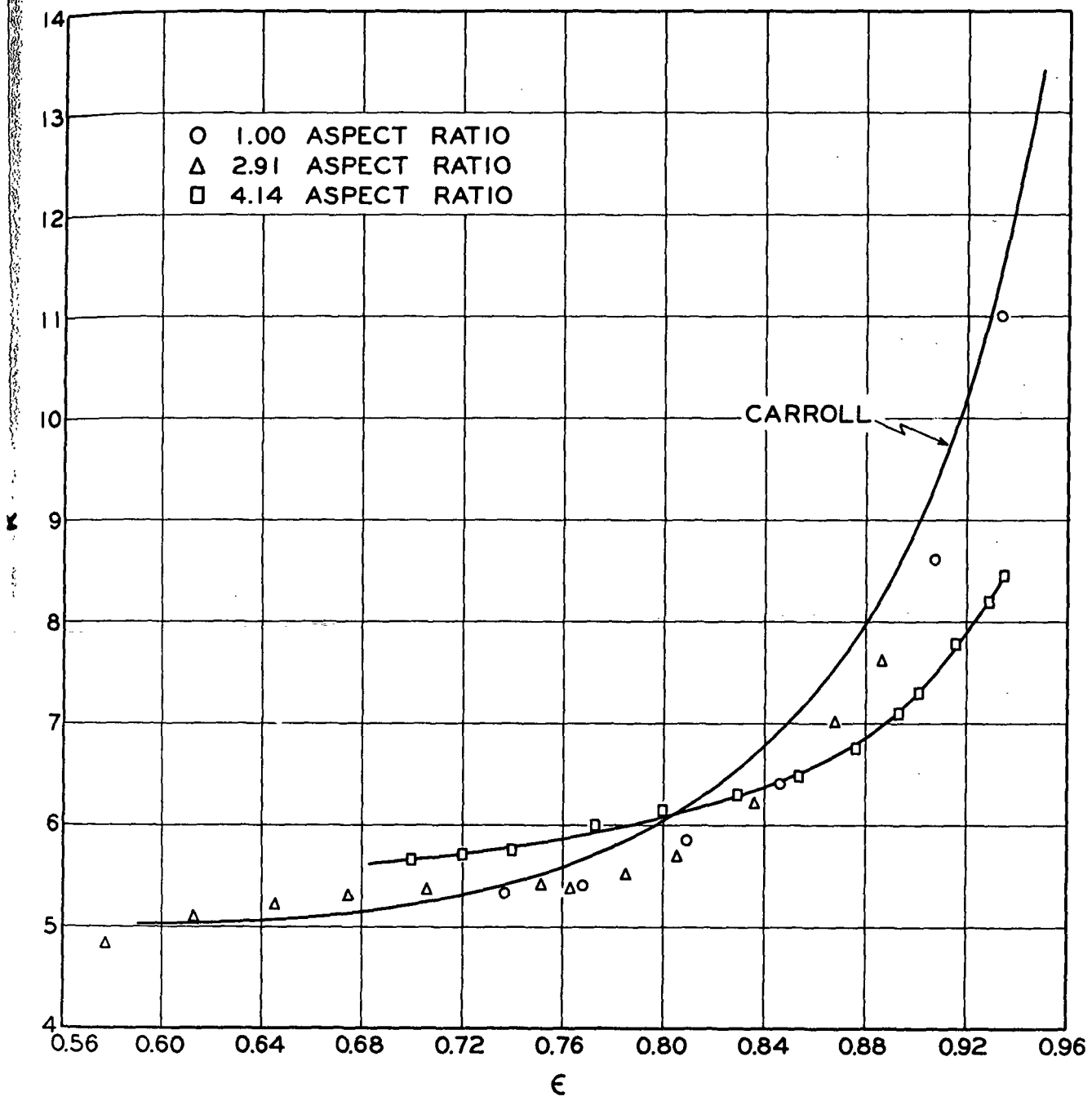

Figure 3. Effect of Fiber Shape on the Kozeny Factor

The decay of permeability of wood pulp mats is a familiar phenomenon which exhibits slow decrease of flow at constant pressure drop or creeping rise of pressure drop at the same flow (Fig. 4). A common experimental condition causing decay is the gradual retention of impurities in a mat from the permeating water. By thoroughly cleaning the entire experimental system and using highly purified water, this source of trouble may be eliminated with extreme care. Another factor is the fines in wood pulp, which may be removed by means of extra fiber classification.

With these precautions, a permeation experiment was carried out to ascertain other possible causes of decay. A freshly formed mat was permeated at increasing flow rates over a range of 10-160 cm./sec. When the highest flow was attained, the velocity was successively decreased, allowing the mat to expand at each interval until the lowest point was reached again. After repeating the procedure for six cycles, it was found that the same pressure drop-velocity curve could be duplicated. The whole conditioning process took eight hours, after which permeation was maintained at the highest flow for one hour. During this period no decay was observed. The result of this experiment appears to be in general agreement with the stabilizing effect of mechanical conditioning on the compressibility behavior of wood fiber mats, which will be reviewed in the next section.

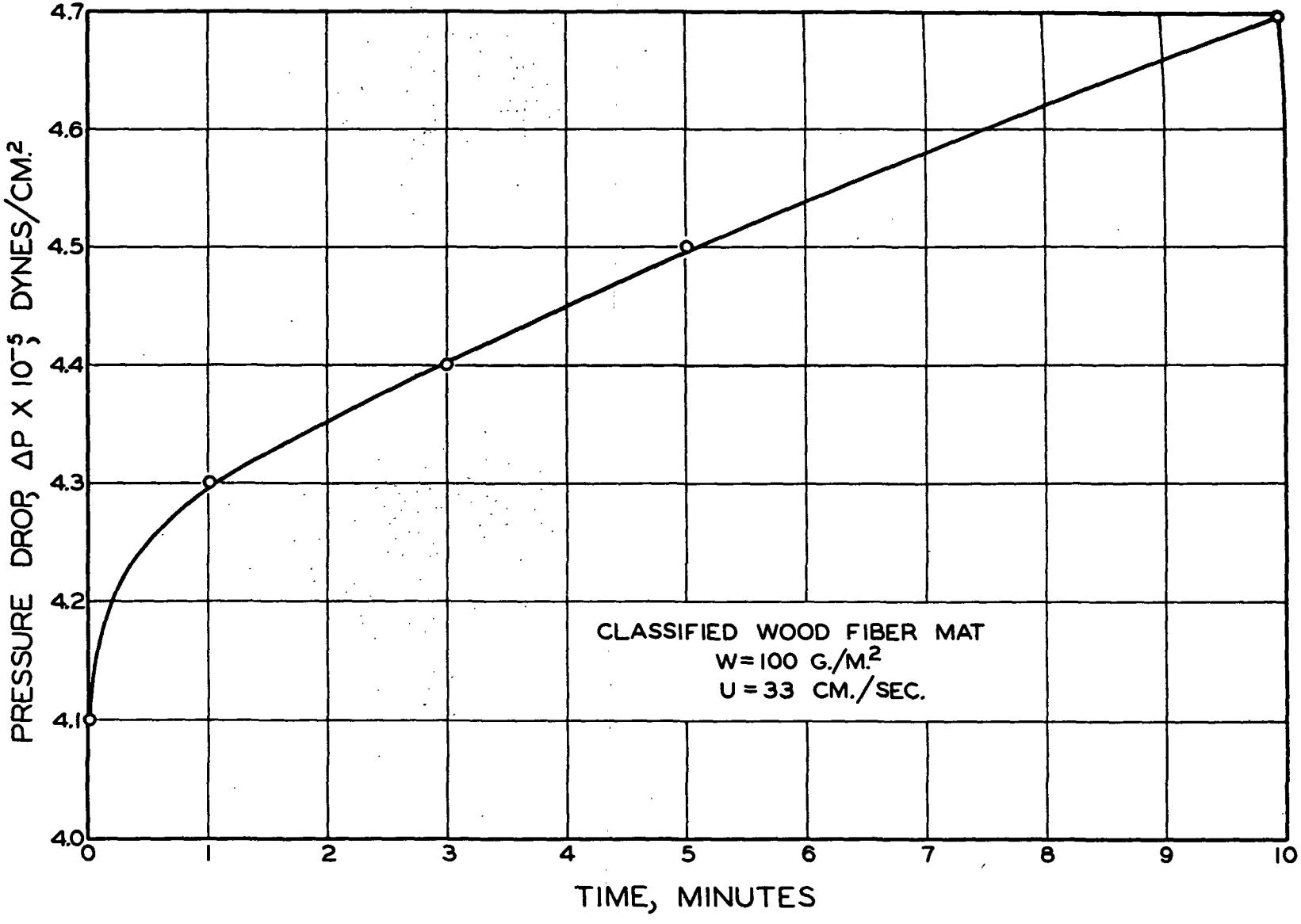

Figure 4. Permeability Decay

COMPRESSIBILITY

GENERAL BEHAVIOR

In a static compressibility test a thick mat is formed on a rigid septum from a very dilute and well-dispersed fiber suspension at a slow, constant rate. Steady application of a compacting load is achieved by means of a movable piston guided in its downward travel and counterbalanced by a weight; additional weights are then gently placed on the piston. The mat thickness may be measured either with a cathetometer or a dial micrometer. The test results are usually reported as mat density vs. applied pressure. The mat density is expressed as the mass of dry fibers per unit mat volume and the applied pressure as the load per unit mat area.

The complex response of a fiber mat to compression and recovery is illustrated in Fig. 5, taken from Jones' study (15). These data are for loblolly pine summerwood pulp prepared by the kraft process, bleached to 0.3% Klason lignin and classified for the removal of fines. In the log-log plot of mat density vs. applied pressure, the first-compression data for freshly formed mats under successively increasing loads may be divided into the linear and curved regions. The linear region extends upward from approximately 10 g./sq. cm. Toward lower pressures the data tend to curve with diminishing slopes. It is to be noted that the two sets of the first-compression data taken at two different loading intervals, using identical loads, have closely the same slopes with a slight displacement in position. The gradual increase of deformation with time in response to constant applied stress is called "creep."

At any time during the first compression, if the load is decreased, the mat recovers, but never quite reaches the extent corresponding to the original

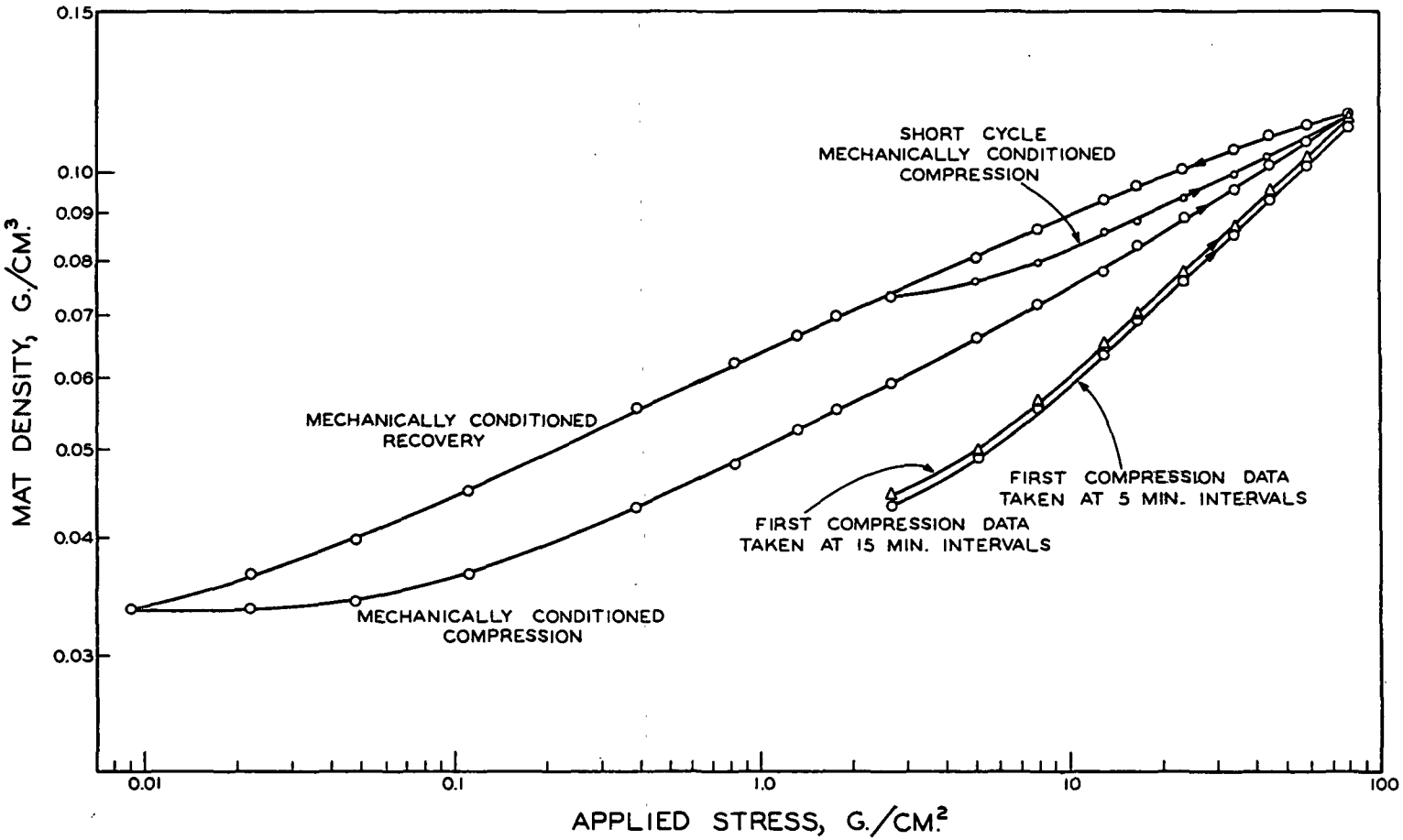

Figure 5. Compressibility of a Wood Fiber Mat

compression. The recovery which is also time dependent proceeds with further decrease of load. At a certain point of recovery, if the mat is subjected to compression again, the deformation in the second compression will be less than that of the first. Thus, a compression-recovery cycle exhibits hysteresis. The portion of the data indicated in Fig. 5 represents the sixth cycle. After several cycles the mat is said to be mechanically conditioned when the response to further compression becomes stabilized although there remains partial recovery or minor hysteresis. Rapid compression-recovery cycles such as vibrations produce higher compressibility than slow cycles, as shown in Fig. 6.

POSSIBLE MECHANISMS

A fiber mat formed by filtration of a dilute suspension possesses a highly anisotropic and porous structure. The fibers are randomly oriented in the horizontal plane with their axes generally perpendicular to the vertical direction. The essential feature of the fibrous structure is its large number of fiber-fiber contacts. When the mat is subject to compaction, it is quite conceivable that the number of contacts, real or apparent, will increase by virtue of fiber bending. Furthermore, one fiber may reposition itself with respect to another as a result of relative movement. Finally, the contact surfaces may conform to each other under compression. These possible mechanisms of compressibility will be elaborated in light of available experimental evidence.

Fiber Bending

As a fiber mat is compressed with a mechanical load, the compressive stresses are transmitted through the virtual contacts and distributed throughout the fibers. The free spans supported between two points from below or above are subject to bending which causes further contacts with neighboring fibers until a stable state of a denser structure is reached.

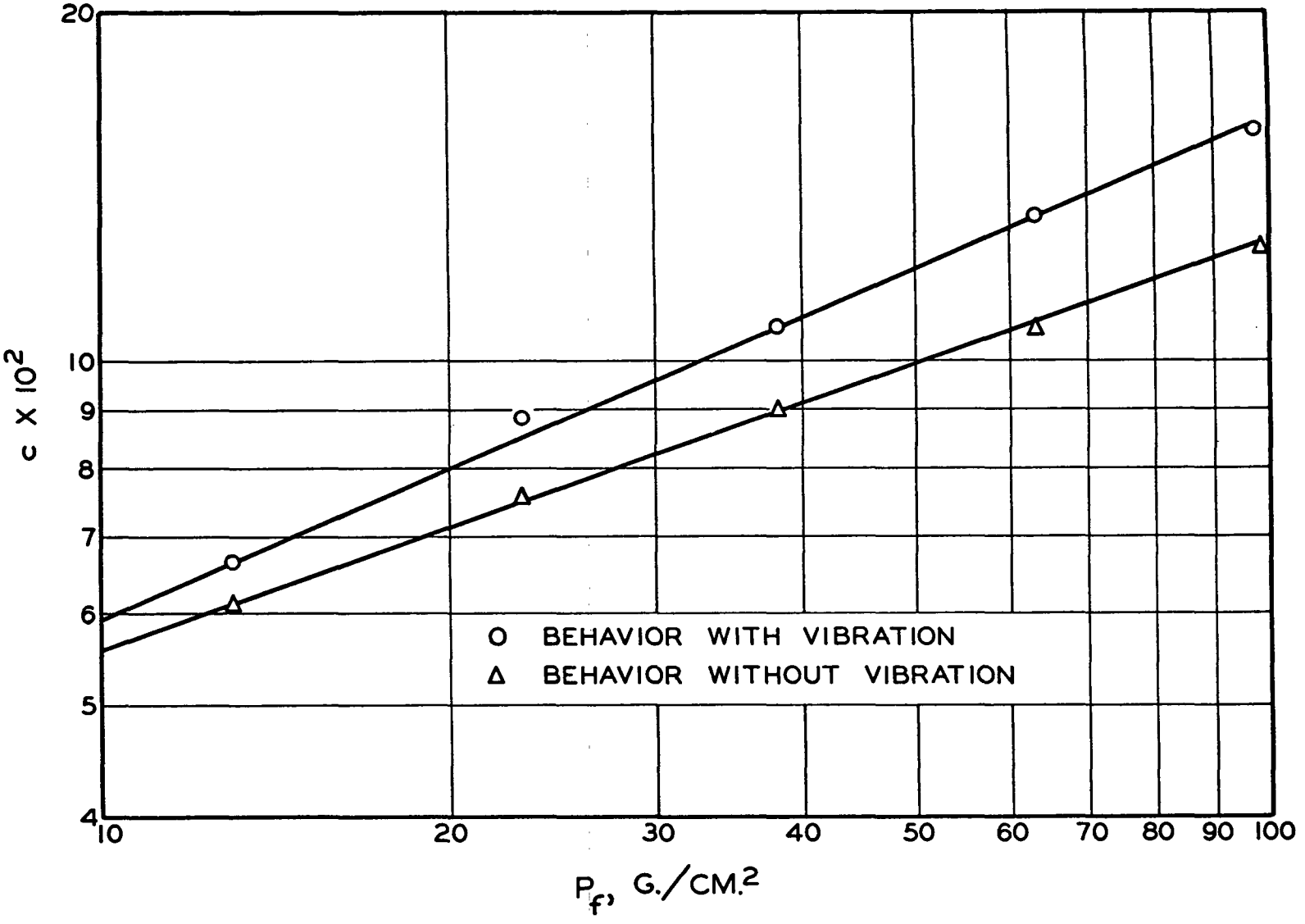

Figure 6. Effect of Vibration on Compressibility

The bending of glass fibers under compression has been demonstrated by Elias (16), who was able to observe microscopically the configuration of a silvered fiber in a mat of untreated fibers saturated with a special oil of the same refractive index as that of the glass fibers. Figure 7 shows the configurations of a silvered fiber at four values of solid fraction. The increase of inflection points along this fiber with increasing loading is vividly recorded in these photomicrographs. Elias further estimated the number of contact points from the configuration of the fibers under observation. His results are cited in Table IV.

TABLE IV

FIBER CONTACTS UNDER COMPRESSION

Glass fibers: $d_f = 7.22$ microns

$\rho_f = 2.54$ g./cm.^{3}

L_f, mm.	N_c/N_f	$N_c/N_f L_f$	c/ρ_f	P_f, g./cm.^{2}
2.26	7.3	3.2	0.0310	8.5
2.26	11.4	5.0	0.0488	65
2.26	12.6	5.6	0.0545	107
4.55	21.6	4.7	0.0575	107
1.09	6.5	6.0	0.0601	107

From the limited data for 2.26-mm. fibers the number of contacts per unit fiber length appears to be directly proportional to the solid fraction, as shown in Fig. 8, by the apparent alignment of the three circles. The last three sets of data indicate that the number of contacts per unit length decreases from 6.0 to 4.7 with fiber length increasing from 1.09 to 4.55 mm. at the same loading. If the contact numbers for the other two fiber lengths

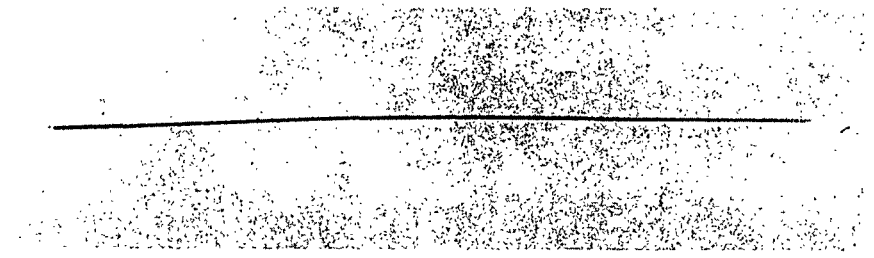

$c/\rho_f = 0.012$

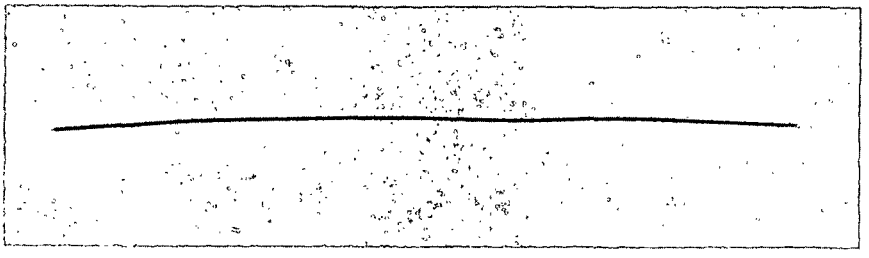

$c/\rho_f = 0.0310$

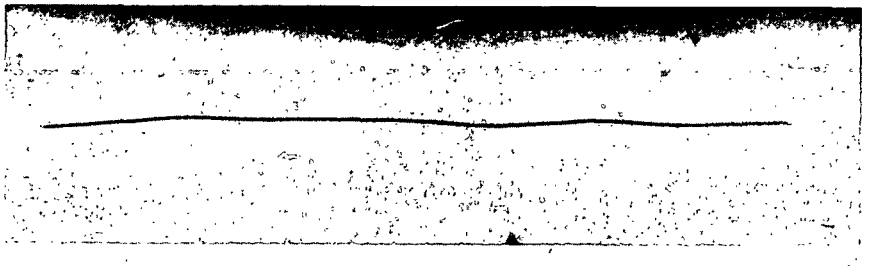

$c/\rho_f = 0.0488$

$c/\rho_f = 0.0545$

Figure 7. Bending Configurations of a Glass Fiber

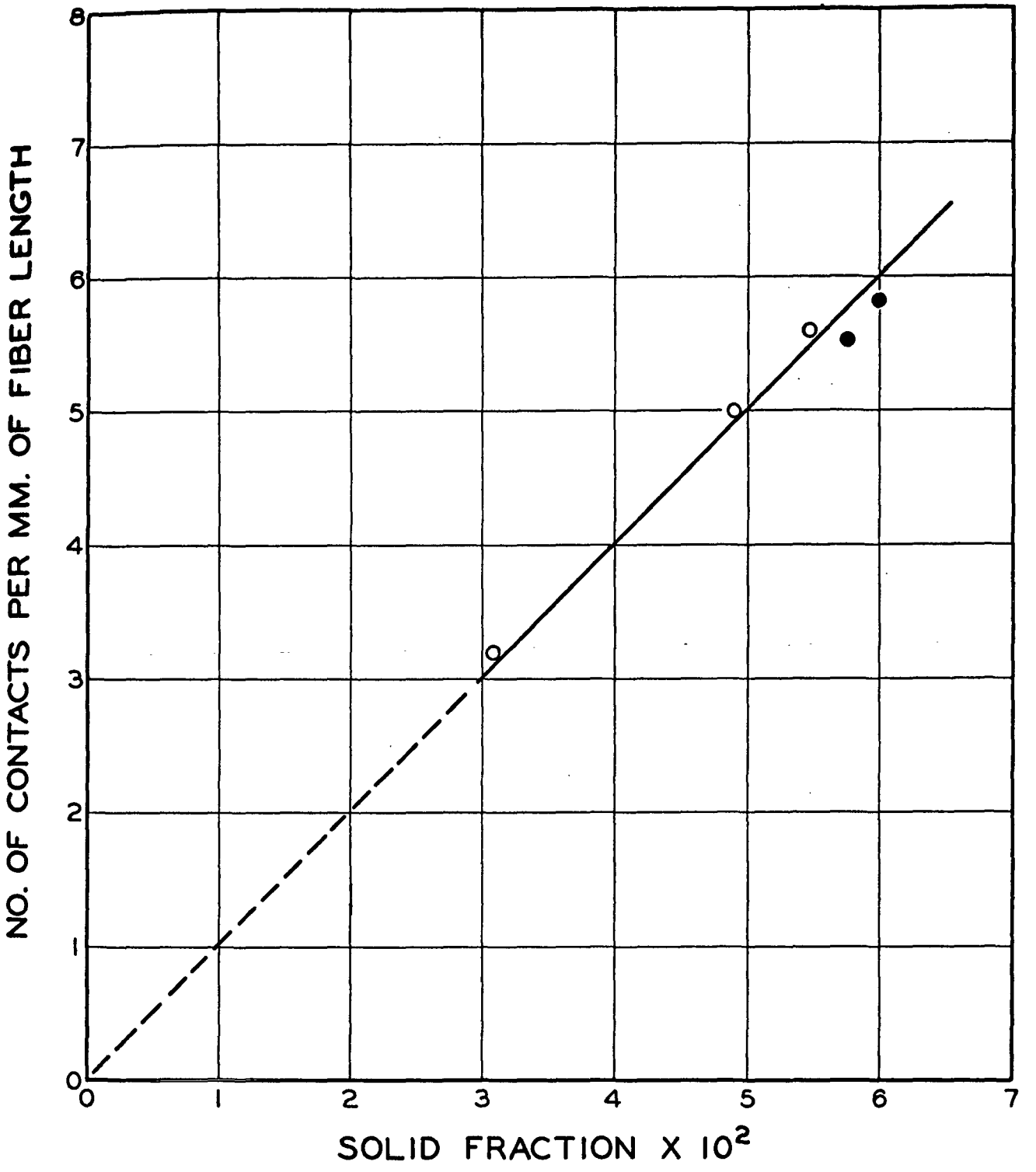

Figure 8. Change of Fiber Contacts with Solid Fractions

in Table IV are adjusted by proportion to the same 2.26 mm. length, the adjusted data points would fall slightly under the line, as indicated by the two dots. Elias further reported that at the same loading the number of contacts for 2.3 mm. by 12.9-mm. fibers was 7.2, compared with 12.6 for 2.26 mm. by 7.22-micron fibers.

Since the deflection of an elastic beam is inversely proportional to its stiffness or flexural rigidity, more contacts per unit length would be expected for more flexible fibers. This was demonstrated by Elias with the imbedding of a dacron fiber in the glass fiber mat. The stiffness of the dacron fiber was about 1/100th of that of the glass fiber. The number of contacts per mm. of the dacron fiber was observed to increase by 2-4 over the glass fiber at a solid fraction of about 0.05.

Fiber Repositioning

As a mat is being compressed, the fibers are uniformly displaced in the direction of the motion of the piston. The question arises as to whether the fibers in the plane of the mat might move in the directions perpendicular to the motion of the piston. The answer was sought by Elias through the superimposition of the photographic images of a planar area in the mat at different compactions. Figure 9 shows a set of three photographs for the first, second compression and the superimposition of these two pictures. There appears almost perfect matching of those fibers in focus. The conclusion is therefore that little reorientation of the fibers in the plane of the mat has occurred during compression and recovery.

By means of his optical technique, Elias also observed that most fibers of a freshly formed mat lay flat in the plane of the mat as expected.

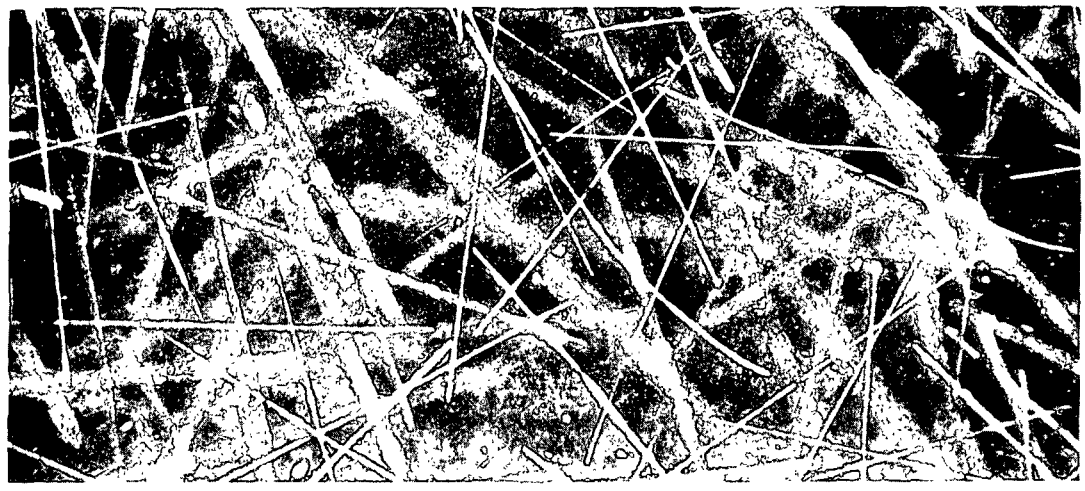

FIRST COMPRESSION $c/\rho_f = 0.0559$

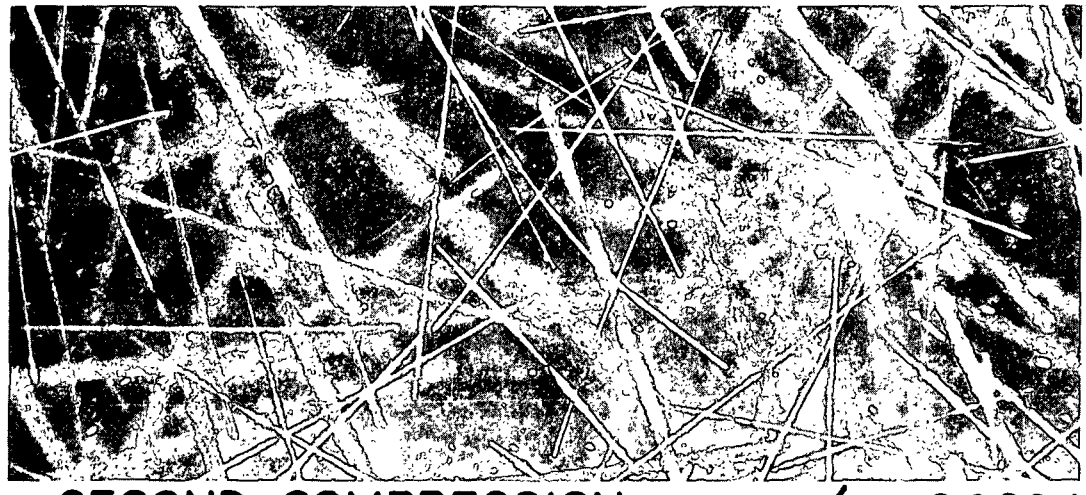

SECOND COMPRESSION $c/\rho_f = 0.0604$

SUPERIMPOSED FIRST AND SECOND COMPRESSION

Figure 9. Absence of Fiber Reorientation in a Mat Plane

However, a fraction of the fibers were oriented at appreciable angles with the vertical or z axis. The number average of such angles increased rapidly from about 78° for 1.09-mm. fibers to 85° for 2.26-mm. fibers, beyond which length it became stabilized at about 86° (4° from the horizontal plane) for 4.55-mm. fibers.

The fibers at high z-orientations (large angles with the x-y plane) would become nearly horizontal during compression. The ratio of the cosine of the angle with the z axis from an uncompressed to a compressed state would be approximately inversely proportional to the ratio of the corresponding solid fractions. This supposition was found to be essentially correct in Elias' compressibility experiments with glass fibers.

For a fiber to change its z-orientation, it would have to undergo some movement relative to other fibers which are in contact with it. Such movement would entail slippage at the contact, which introduces a second mechanism of compressibility.

As a fiber bends, either its ends must move toward each other or its spans between the points of support must stretch. For the glass fibers used by Elias, the axial tension required for stretching was estimated to be an order of magnitude greater than the frictional force preventing the fiber ends from moving closer. Elias' photographs taken through the side of a mat showed that the projected length of a visible fiber on the x-y plane was measurably greater in an uncompressed than in a compressed state. The straight distance between the two ends of several fibers 2.26 mm. long at a solid fraction of about 0.05 measured less than the distance along the fibers by an average of 4.5 microns, the shortening being about 0.2%. Thus in Elias' glass fiber mats some axial slippage of the fibers must have occurred.

Axial slippage necessitates axial tension or compression, which arises from the loading of the mat. While the maximum deflection of a beam subject to negligible axial forces is directly proportional to the load, axial tension will reduce the deflection and, conversely, axial compression will increase the deflection at the same load. By the same reasoning, the mat will assume different degrees of compaction, depending on the distribution of the axial tension and compression in the fibers.

Fiber Conformation

As a result of compression, the fibers must undergo deformation. In addition to bending due to flexibility of the fibers, there is more or less change in cross-sectional shape because of the conformability of the fibers under the pressure of contact. The contact areas will enlarge as the fibers become more flattened upon increased loading. Fiber conformation at the contact surfaces will reduce the thickness of a fiber "layer," resulting in a more compacted fibrous structure and constituting a third mechanism of compressibility. Furthermore, it is likely to alter the distribution of the stresses in the fibers and indirectly affects bending.

In the case of relatively rigid fibers, the contact area is small under moderate pressures, and the reduction in fiber thickness at contact is negligible compared to the effect of fiber bending on compressibility. However, for fibers with low modulus of elasticity, especially those with noncircular cross sections, the contact area in an unbonded structure may be appreciable. Labrecque (12) has estimated, by means of the light-scattering technique, the contact area in mats of quasi-elliptical nylon fibers with aspect ratio (width/thickness) of about 4 to 1 to be from 9 to 21% of the specific surface of these fibers in the range of solid fraction from 0.2 to

0.5. These results are in approximate agreement with those calculated from the Onogi-Sasaguri theory cited in the previous section on Permeability.

APPARENT FACTORS

The apparent factors involved in compressibility of a fiber mat should include fiber dimensions, fiber properties, and initial structure. For cylindrical fibers the principal dimensions are length L_f and diameter d_f. In the case of solid elastic fibers, the density ρ_f and the modulus of elasticity E need to be taken into account. Characterization of the initial structure presents difficulties. It is dependent on the mode of packing, which in turn is influenced by the fiber dimensions and properties. For the time being, the unstressed mat density c_o serves to represent the gross structure in the absence of an applied load. From dimensional considerations a compressibility function for such simplified fiber systems based on fiber bending alone would involve the following dimensionless variables and parameters:

$$\frac{c}{\rho_f} = f\left(\frac{c_o}{\rho_f}, \frac{L_f}{d_f}, \frac{P_f}{E}\right) \qquad (13).$$

Jones (15) provided a comprehensive set of compressibility data for water-saturated mats of synthetic fibers. The range of his experiments is cited in Table V. The interpretations of the data to follow, however, are not necessarily in conformance with his original version.

TABLE V

Jones' Compressibility Experiments

Fiber	L_f, mm.	d_f, microns	ρ_f, g./cm.^{3}	$E \times 10^{-7}$, g./cm.^{2}
Glass	0.96-6.3	5.1-12.9	2.56	71.2-103
Dacron	4.6	22.7	1.39	14.7
Nylon	0.96-6.3	16.8-46.2	1.14	0.31-1.33

P_f, g./cm.^{2} 10^{-1} - 10^2

Fiber Dimensions

For mechanically conditioned mats it is reasonable to assume that the initial structures are sufficiently stabilized so that their compressibility behavior is dependent on fiber dimensions alone at constant fiber properties. The previous dimensional consideration has indicated a possible correlation of mat density with axis (length-diameter) ratio at a given loading in such cases. Jones' compression data for glass fiber mats are so plotted in Fig. 10. The family of curves reveals a consistent trend of the mat density approaching from a high value to a possible limit with increasing axis ratio. Within the precision of the data, the mat density or solid fraction remains nearly constant above the axis ratio of about 500 for glass fibers.

According to the Onogi-Sasaguri theory for a mat of fibers randomly oriented in the x-y plane with little z orientations,

$$\frac{c}{\rho_f} = \frac{\pi^3}{16} \frac{d_f}{L_s} \qquad (14) ,$$

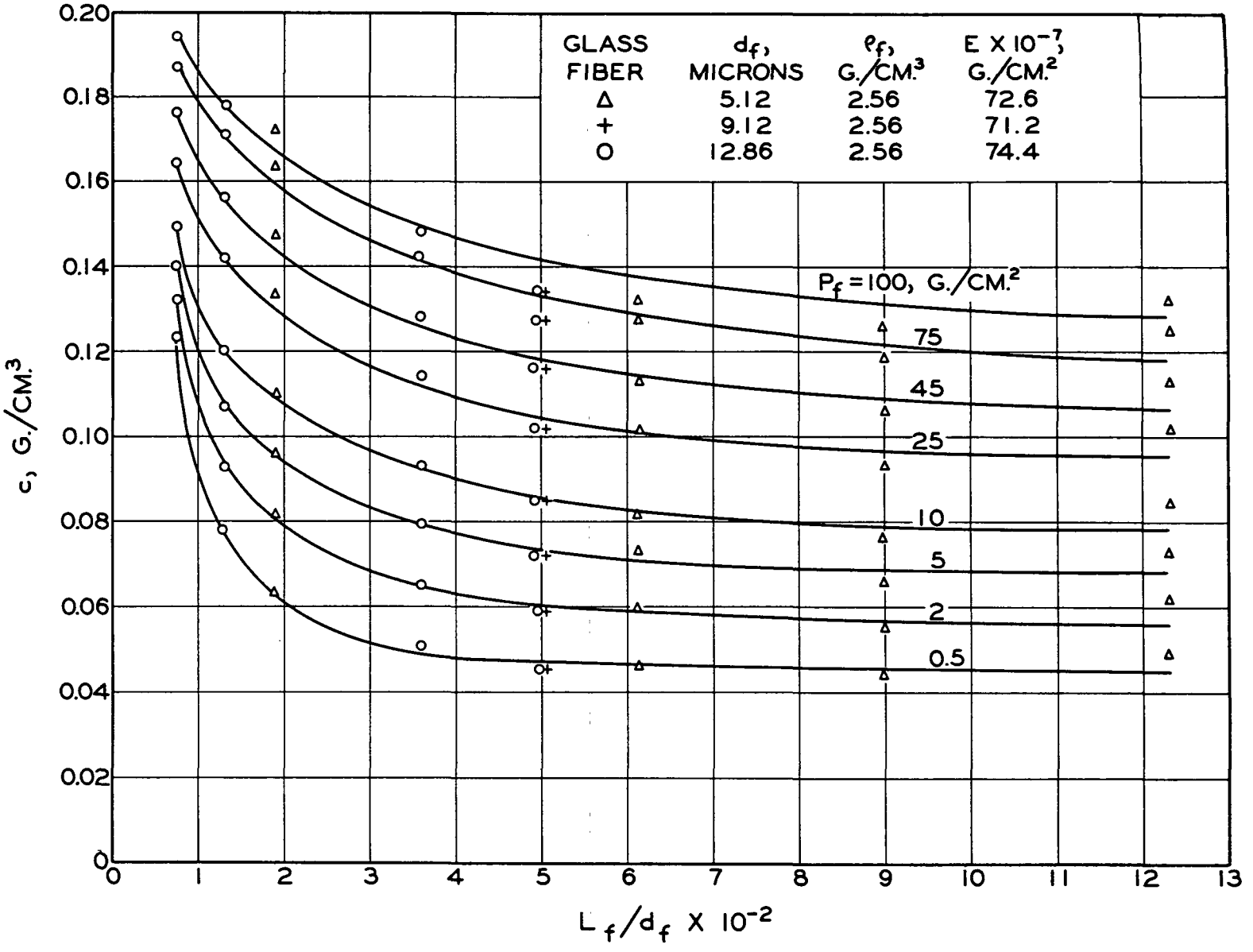

Figure 10. Compression Data for Mechanically Conditioned Glass Fiber Mats

where $\underline{L}_s$ is the average segment length or the reciprocal of twice the number of contacts per unit fiber length. As pointed out before, Elias'[7] limited data seem to support the concept of direct proportionality, as shown in Fig. 8. The experimental proportionality factor, however, is lower than the theoretical one by 28%. From Elias' observation that segment length increases slightly with increasing fiber length at the same loading, it may be inferred that solid fractions would be somewhat lower with longer fibers. Further, accepting Elias' additional observation that segment length is nearly proportional to fiber diameter at the same loading, then the net influence of fiber diameter on mat density would be a minor one. These inferences appear to be in qualitative agreement with the mildly curved part of Jones' data.

Toward very low axis ratios the curves rise rapidly with a possible tendency of convergence. This trend could be interpreted as the approach of mat structures to an incompressible bed of spherelike particles in a random isotropic packing. In the opposite direction the tendency to a limiting mat density would satisfy the intuitive expectation of constant segment length with very long fibers.

Jones' data for nylon fibers in Fig. 11 show similar trends. The flat region, however, is not as well defined. The mat densities appear to decrease much more slowly, yet significantly, in the axis ratio range of 100-136. Furthermore, there is the disturbing single evidence of substantially higher densities at the corresponding loadings for the axis ratio of 274 than for 136. If such evidence were real, the foregoing conjecture of limiting densities would be quite untenable, but the existence of a relatively flat region would still be possible.

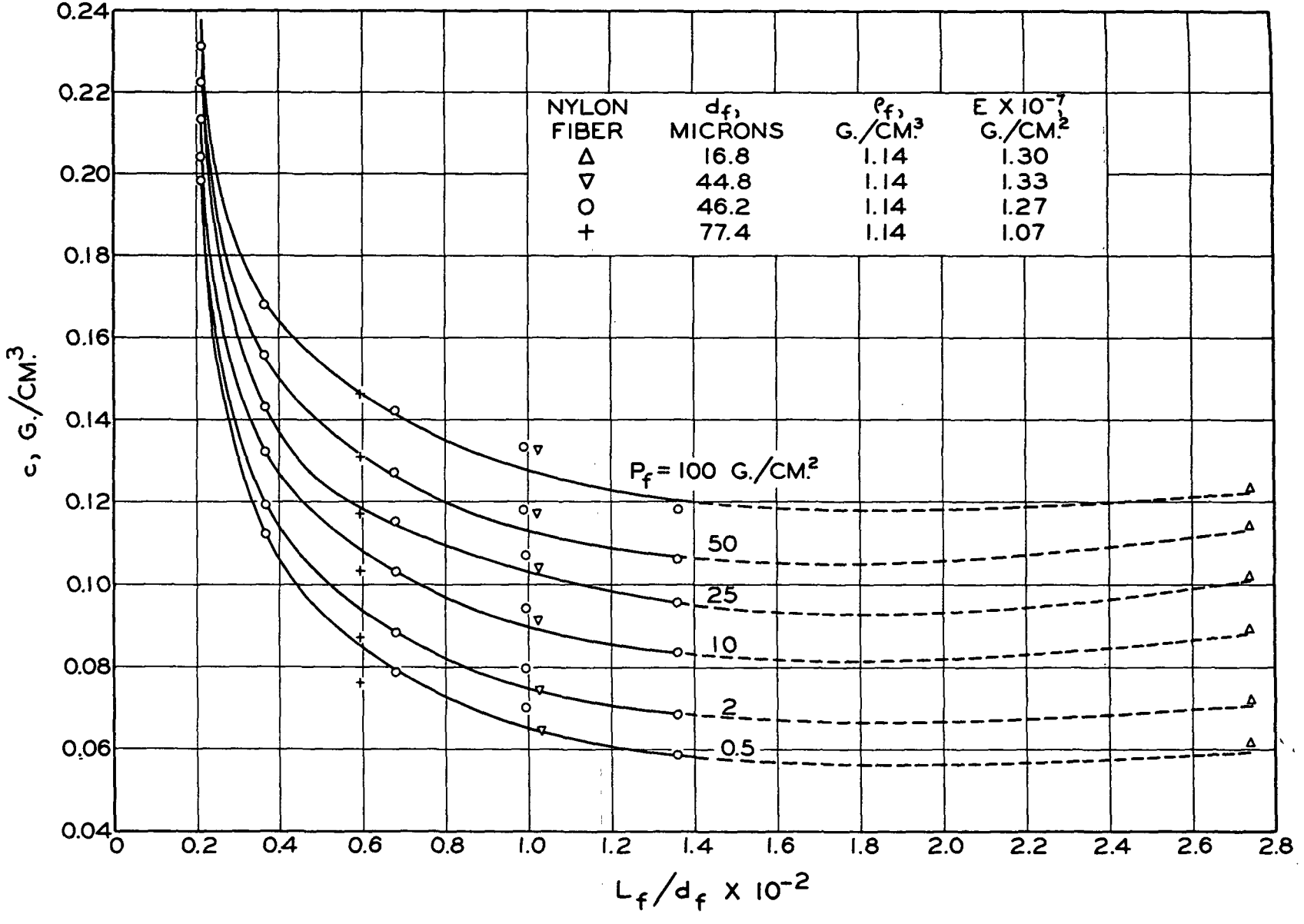

Figure 11. Compression Data for Mechanically Conditioned Nylon Fiber Mats

Fiber Properties

Compressibility represents the volume change of a system under compressive stresses. If the mat structure may be described adequately by its solid fraction, the density of fibers has been taken into account. For elastic fibers when modulus of elasticity is the sole property governing bending, then the solid fraction would be a unique function of the pressure-modulus ratio. Jones' data for mechanically conditioned mats of nylon, dacron, and glass fibers in the linear region are so compared in Fig. 12. To minimize the effects of fiber dimensions, only those fibers with sufficiently high axis ratios are included in this plot, from which the results of evaluation are summarized in Table VI.

As a general trend the data do indicate decreasing solid fraction with increasing pressure-modulus ratio as expected. However, there are significant deviations from the assumed correlation.

As first suggested by Qviller (17) and later employed by Campbell (18) and Ingmanson (19), the linear region of compressibility data can be represented by the simple power function:

$$c = MP_f^N \qquad (15),$$

in which M and N are the compressibility constants for a given fiber system, N being a pure number and M having the awkward dimensions of (mass/length^3)/(force/length^2)^N. Comparing with the simplified dimensional function, Equation (13), for mechanically conditioned mats of elastic fibers,

$$M = f(c_o/\rho_f,\ L_f/d_f)(\rho_f/E^N) \rightarrow M_b \rho_f/E^N \qquad (16).$$

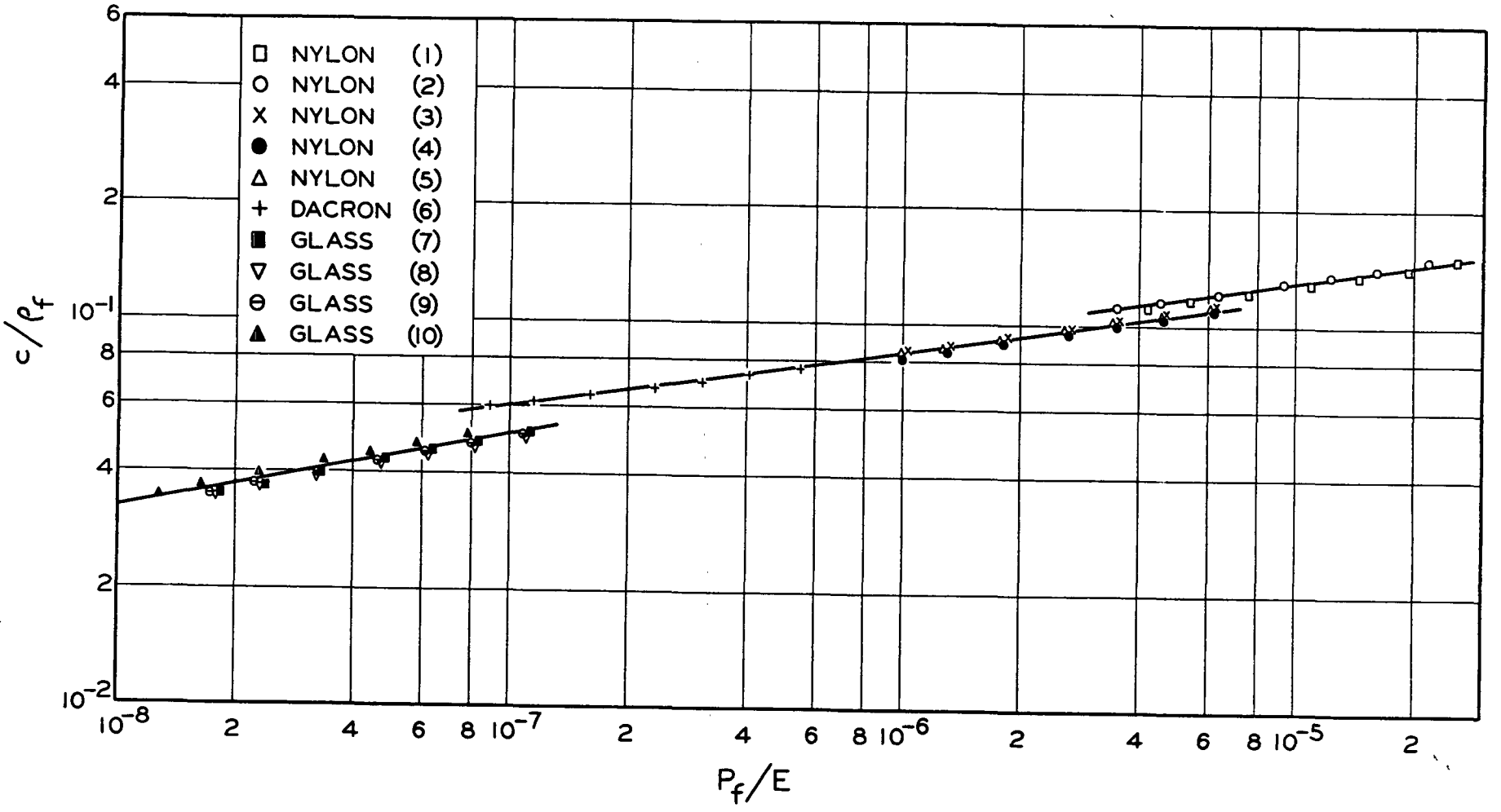

Figure 12. Effects of Fiber Bending and Slipping on Compressibility

If the previous assumptions were correct, M_b would be a dimensionless constant. In actuality the values of N, M_b, and M shown in Table VI deviate appreciably from the simple concept of beam bending.

In the beam theory, the maximum elastic deflection of a beam under distributed loads and frictionless supports is

$$\delta = \frac{L_n^3 P_n}{K_n EI} \qquad (17),$$

where L_n is the free span between two supports, I the moment of inertia, P_n the magnitude of the total load, and K_n a constant depending on load distributions. The subscript n refers to the number of spans. The value of constant K_n generally increases with increasing complexity of loading for similar beam geometry. With a single concentrated load located at the mid-point of a span supported at its two ends, K_n has a value of 48. For a continuous beam in three equal spans alternately supported and centrally loaded, K_n increases to 295.

Extending the beam theory to a mat, the span length which is twice the segment length would decrease more rapidly, as loading increases, than the possible rise of the beam constant. Thus, the increase of the solid fraction, which reflects the deflection of fiber bending, increases with the compacting pressure at a rate less than the direct proportionality in the beam equation, indicating the power N to be less than unity.

It may be demonstrated that for pure bending the value of N is 1/3. The N values for synthetic fibers in Table VI are, however, much lower--0.15 for nylon and dacron and 0.20 for glass. The lower values of N for these fibers may be attributable to fiber-fiber slippage which causes smaller

EFFECT OF FIBER PROPERTIES ON MECHANICALLY CONDITIONED COMPRESSIBILITY

Fiber	Nylon (1)	(2)	(3)	Nylon (4)	(5)	Dacron (6)	(7)	Glass (8)	(9)	(10)
L_f, mm.	4.6	4.6	4.6	4.6	4.6	4.6	4.6	6.3	4.6	6.3
d_f, microns	44.5	43.8	46.2	16.8	44.8	22.7	9.12	5.12	12.9	9.14
L_f/d_f	103	105	100	274	102	203	505	1230	490	504
ρ_f, g./cm.^{3}	1.14	1.14	1.14	1.14	1.14	1.39	2.56	2.56	2.85	2.56
$E \times 10^{-7}$, g./cm.^{2}	0.31	0.37	1.27	1.30	1.33	14.7	71.2	72.6	74.4	103
N	0.147	0.147	0.147	0.147	0.147	0.147	0.196	0.196	0.196	0.196
M_b	0.707	0.707	0.635	0.635	0.635	0.635	0.0423	0.0423	0.0423	0.0423
$M = M_b \rho_f / E^N \times 10^2$	8.95	8.75	6.56	6.50	6.47	4.54	5.61	5.60	5.55	5.85
$\bar{M} \times 10^2$	8.85			6.51		4.54		5.60		

deflection on account of axial tension arising from the friction at the contact in the presence of a fluid. According to both Jones and Elias, the glass fibers had higher friction than nylon, the latter thereby incurring more slippage and having a higher slope. By this interpretation the compressibility of the glass fiber mats is governed largely by bending.

In Fig. 12 there also appears a significant separation of three lines. The cause of the actual displacement needs to be examined. The separation of the low-modulus from the high-modulus nylon is probably due to a minor difference in the unstressed structure which has so far been assumed to be constant. Stiffer fibers have more chances for higher z-orientations which makes a less compact structure according to Onogi-Sasaguri theory. Then a higher modulus would lead to a lower solid fraction at the same pressure-modulus ratio. In this sense the alignment of nylon with dacron is likely to be fortuitous in view of their widely different moduli. A possible compensating factor seems again to be slippage. If the dacron fibers had a higher friction, less slippage would have occurred, as an opposing effect of high z-orientations on the mat structure. In the case of glass fibers, a major part of the very low value of M_b is attributed to the high value of N. The remainder could again be accounted for by the low initial solid fraction due to the high z-orientations of the stiff glass fibers.

Initial Structure

The initial structure of a fiber mat is governed largely by the mode of packing. If the Onogi-Sasaguri equation applies to the unstressed structure, the initial solid fraction becomes

$$\frac{c_o}{\rho_f} = \frac{\pi^3}{16}\frac{d_f}{L_{s,o}} = \frac{\pi^3}{8}\frac{d_f}{L_f}\frac{N_c}{N_f} \qquad (18),$$

where N_c/N_f is the number of contacts per fiber. Elias contended that the fibers in a filtration-formed mat would have 2 contacts per fiber as a minimum for a stable structure. Then his glass fibers with axis ratios from 151 to 630 would yield values of c_o/ρ_f from 0.051 to 0.012. Experimental values of c_o/ρ_f by various extrapolation techniques range from 0.04 to 0.02 at the comparable axis ratios. For mechanically conditioned fiber mats the minimum number of contacts per fiber should be somewhat higher as a result of closer packing.

It is reasonable to expect that the larger the initial solid fraction, the more resistant will be the mat response to compression (smaller N) and the lower will be the final solid fraction at a given compression (smaller M).

If compressibility is dependent on the initial solid fraction, the fiber density would enter into the function in a more complicated way, rather than the direct proportionality between c and ρ_f as previously assumed. A reasonable compressibility function in the linear region would be of a form such as

$$\frac{c}{\rho_f} = M_b\left(\frac{\rho_f}{c_o}, \frac{d_f}{L_f}, \frac{1}{K_n}\right)\left(\frac{P_f}{E}\right)^{N(\rho_f/c_o,\ L_f/d_f,\ K_n)} \qquad (19),$$

in which M_b and N are two unspecified functions increasing with the stated parameters.

ADDITIONAL COMPLEXITY

Most fibers are viscoelastic. They exhibit not only elastic deformation but also creep and relaxation which are time dependent. When a

mat of these fibers is subject to external forces the individual fibers and their contact areas develop both instantaneous and delayed compressive, tensile, and shearing stresses. In addition, because of inter- and intrafiber frictions due to relative movement and configuration change as well as viscous action caused by fluid motion, irreversible effects are always involved. The mat compressibility is ultimately governed by the stress distributions and friction effects.

First Compression

For filtration analysis the pertinent compressibility is first compression which is, however, a misnomer. A freshly formed compressible mat has undergone partial recovery before the initial mechanical load is applied. Generally speaking, the lower pressure drop is used in forming the mat, the earlier starts the linear region. On the other hand, the upper limit of the simple power function appears to be uncertain within the pressure range of the known experiments. It is reasonable to expect that if the pressure is increased indefinitely the compressibility behavior will necessarily change to a different pattern. In terms of all three possible mechanisms of fiber bending, slipping, and conforming, a complete compressibility curve would resemble more or less an elongated S shape in a log-log plot.

Irreversible Deformation

The irreversible deformation may be attributed to four causes. In the order of importance, they are (1) fiber conformation at the contact areas, (2) fiber slippage along the contact surfaces, (3) fiber reorientation with respect to the z-direction, and (4) viscous action in fluid flow. The magnitude of hysteresis in compression-recovery cycles is dependent on these

irreversible effects. For elastic fibers in the absence of friction, there would be no manifestation of hysteresis. Because of the higher viscoelasticity of wood fibers, the hysteresis is more pronounced than those for synthetic fibers.

The frictions involved in compressibility are dependent not only on the nature of fiber surfaces (external and internal) but also on the rheological properties of the fluid. Elias has shown the effect of fluid on the hysteresis of the glass fiber mats. His results are summarized in Table VII. The higher friction of oil results in larger hysteresis than in the case of water. However, the hysteresis for a dry mat is intermediate between those saturated with oil and water. This is probably a manifestation of the glass surface roughness compared with the viscous nature of the fluids.

TABLE VII

HYSTERESIS OF GLASS FIBER MATS

$\underline{L_f}$ = 2.26 mm. $\underline{d_f}$ = 7.22 microns

$\underline{\rho_f}$ = 2.54 g./cm.^{3} $\underline{E}$ = 73.9 x 10^9 g./cm.^{2}

Fluid	Cycle	Work Expended in Compression, g. cm./g.	Work Regained in Recovery, g. cm./g.	Net Work Lost, g. cm./g.
Oil	1	221	149	72
	2	202	152	50
	3	200	154	46
	4	205	160	45
	5	193	151	42
Air	1	237	197	48
	3	208	177	31
Water	1	205	173	32
	3	196	170	26

It should also be mentioned from Jones' work on both glass and nylon fibers that the irreversible deformation may be correlated with the axis ratio by a concave-downward curve with the maximum located approximately at the beginning of the flat region (Fig. 13 and 14). With very short fibers slippage tends to lose contact points, while with very long fibers slippage becomes infrequent. Most slippage, therefore, takes place in the intermediate range of fiber length.

Fiber Deswelling

A swollen fiber contains a swelling fluid within its own porous structure. The specific swollen volume is customarily defined as

$$v = \frac{V_f + V}{V_f \rho_f} \qquad (20),$$

V_f and V being the volumes of dry fiber and fluid, respectively. In this definition any interaction between the fiber and the fluid is ignored. For solid fibers v is simply the reciprocal of ρ_f.

When swollen fibers are subject to deformation, a part of the internal fluid is likely to be squeezed out. In a mat of swollen fibers a large part of stresses is concentrated in the contact area, causing deswelling in conjunction with conformation. Thus, v decreases with increasing P_f. The static compressibility test as measured by mat density involves both changes in porosity and specific volume, which have different dependence on the compacting pressure, and the two factors are yet inseparable by the present techniques.

Because of deswelling and conforming the fiber thickness is reduced by compression, especially at the contact areas, and as a consequence the rate

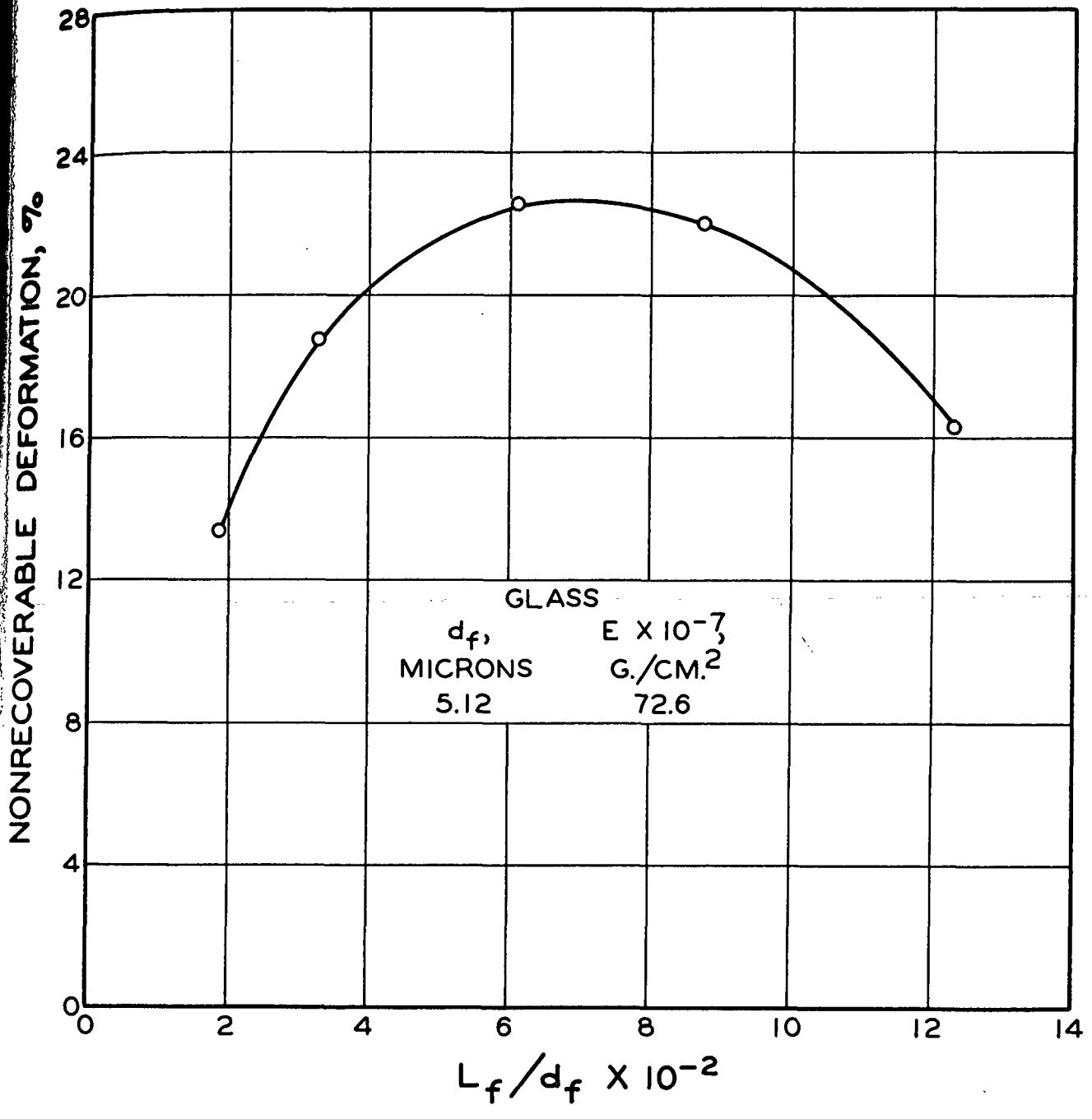

Figure 13. Irreversible Effects in Glass Fiber Mats

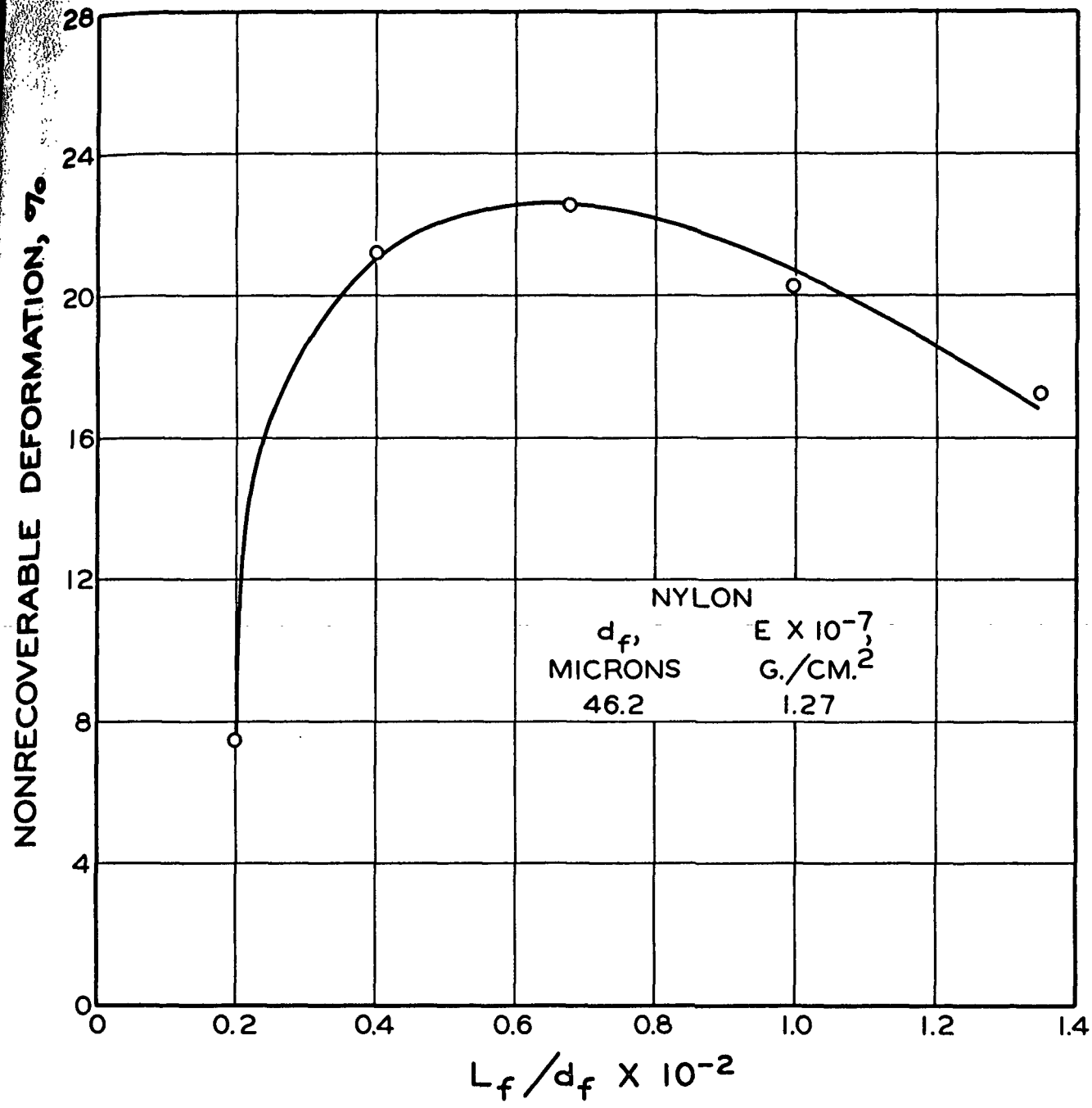

Figure 14. Irreversible Effects in Nylon Fiber Mats

of compressibility change becomes larger than pure bending. The value of N for highly viscoelastic fibers such as wood pulp would be expected to be higher than 1/3. In fact, most cellulosic fibers have N values for first compression in the range of 0.35 to 0.45. This is partly due to curved fibers (15).

Time Dependence

All the irreversible effects are time dependent. Different durations are required to complete the processes of conformation, slippage, reorientation, and flow. For slow compression (creep) and recovery, Wilder (20) has incorporated the time effect in the simple power function with a logarithmic term in M while N is independent of time as follows:

$$c = (M_1 + M_2 \log t)P_f^N \qquad (21),$$

which is applicable to times as short as 10^{-1} sec. However, for fast compression the expression of water from a mat is so rapid that the mat structure undergoes drastic changes or even disrupture, rendering the static compressibility function invalid. The problem of dynamic compressibility will be discussed in the following section on Filterability.

EMPIRICAL CORRELATIONS

Compressibility data are usually correlated in various empirical forms, among which the equations of Ingmanson (21) and Wilder (20) are most popular. The former is merely an extension of the simple power function to fit approximately the curved region:

$$c - c_0 = MP_f^N \qquad (22).$$

The latter is an independent modification of the equation of Van Wyk (22):

$$c^3 - c_o^3 = \left(\frac{\rho_f^3}{K_n E}\right) P_f \qquad (23) .$$

Wilder has incorporated an adjustable parameter γ_o in order to extend the range of compressibility. His final equation is

$$c^{4\gamma_o - 1} - c_o^{4\gamma_o - 1} = \frac{M^p \rho_f^5 (4\gamma_o - 1)}{K_n E c_o^{6-4\gamma_o}} P_f \qquad (24) ,$$

where both γ_o and M^p are pure numbers. When $c_o \ll c$, all the three equations reduced to the simple power function (15).

Using Jones' data for mechanically conditioned mats of glass fibers and kraft pulp, the correlations of Ingmanson and Wilder are compared in Fig. 15 and 16. It is seen that both forms fit the high range satisfactorily, but the deviations in the low range are considerable. It appears that Wilder's form is slightly superior to Ingmanson's at very low pressures. There is no significance in the extrapolated values of c_o in both correlations.

In Table VIII are presented a comprehensive set of compression data for both mechanically conditioned and freshly formed mats, which have been accumulated in the past years since Ingmanson's initial work. Both synthetic and cellulosic fibers are included. Among the latter the majority is of the wood origin while the range extends from bagasse to cotton. The processes for the preparation of these natural fibers were extremely diverse, covering the conventional commercial pulps as well as some laboratory specialties. The compressibility data are represented by the values of M and N. In addition, average values of specific surface S_w on a mass basis and the specific volume v are listed.

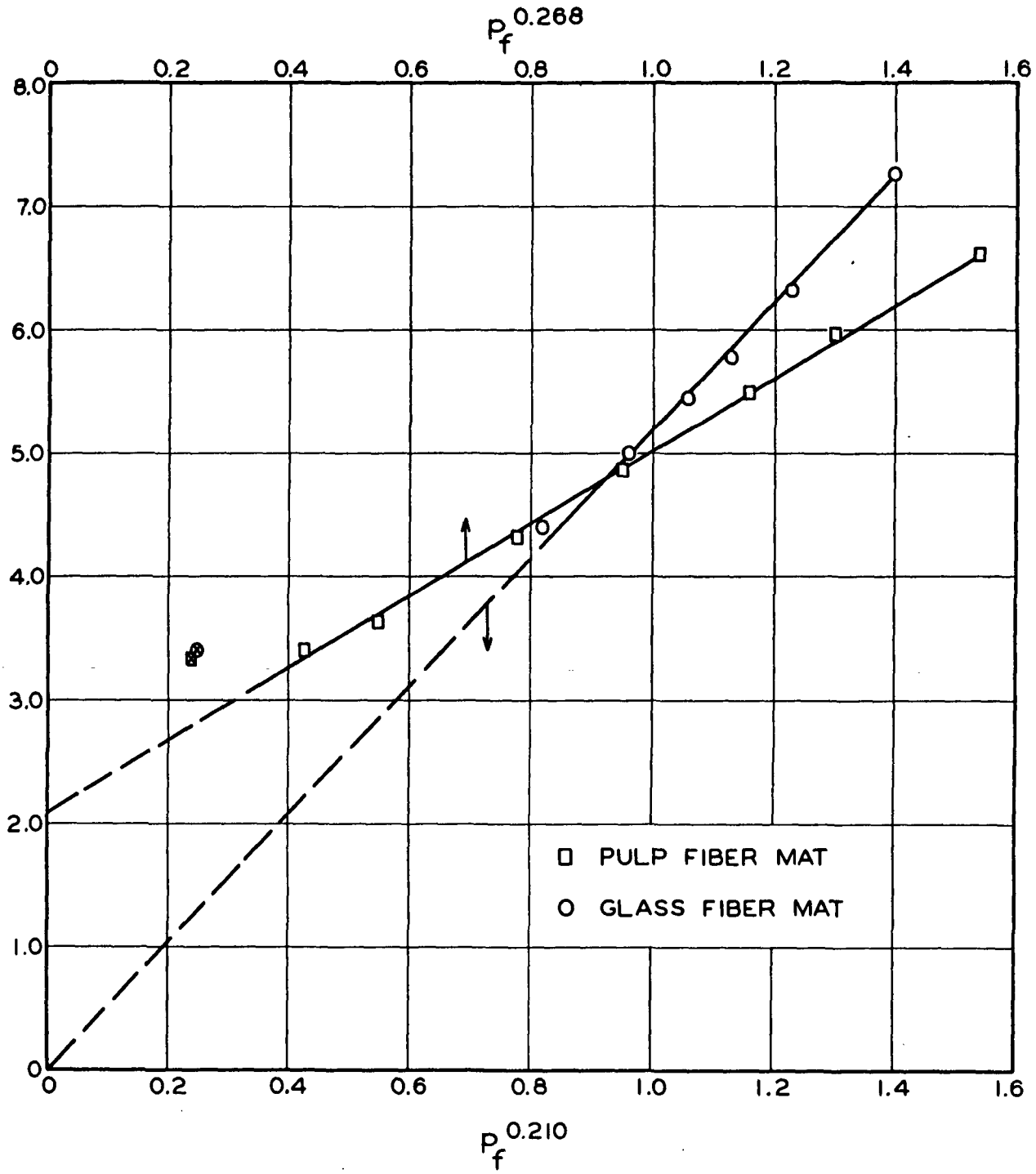

Figure 15. Test of Ingmanscn's Compressibility Function

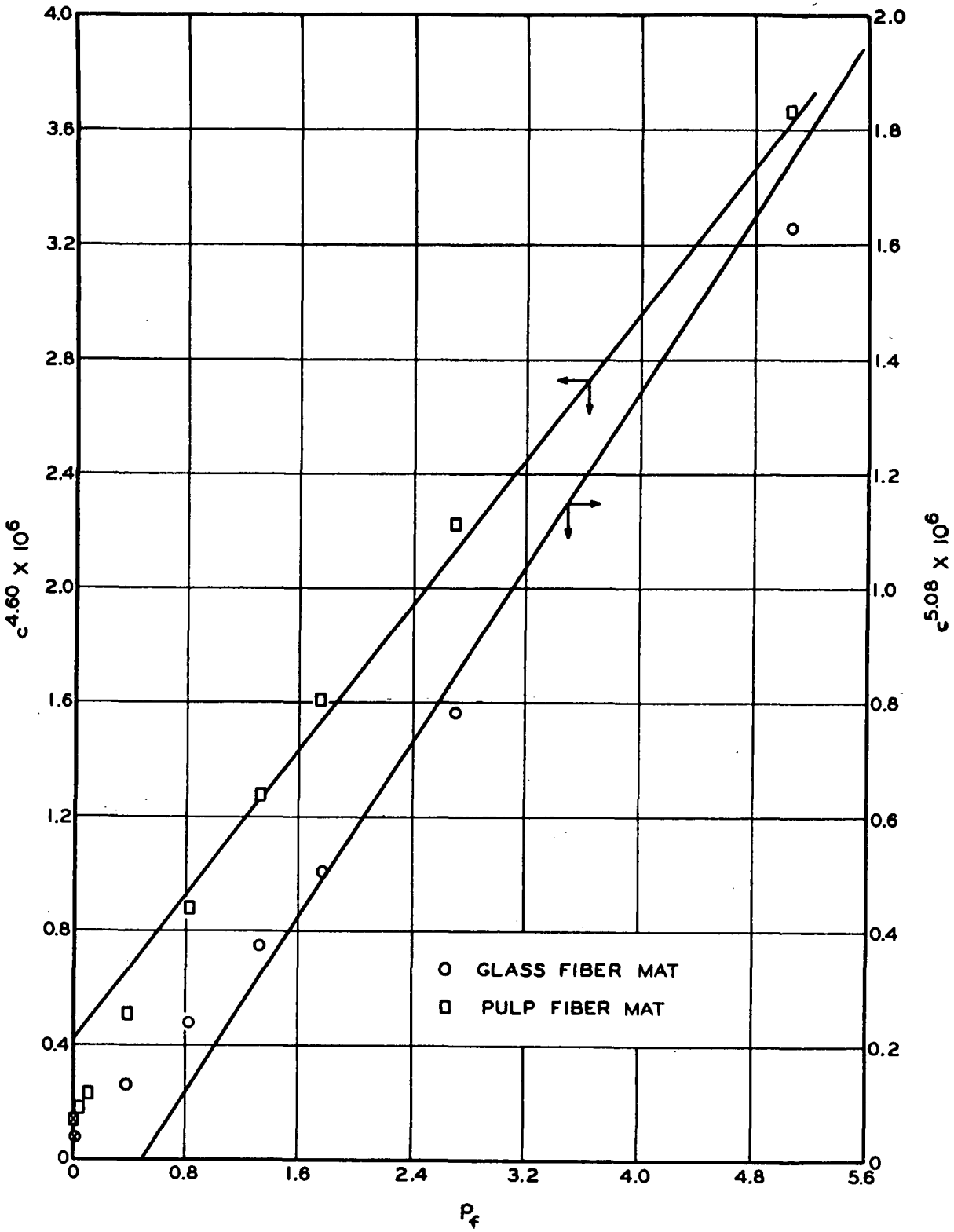

Figure 16. Test of Wilder's Compressibility Function

TABLE VIII

COMPRESSIBILITY CONSTANTS, SPECIFIC SURFACE, AND SPECIFIC VOLUME

	L_f, mm.	d_f, microns	ρ_f, g./cm.^{3}	$E \times 10^{-7}$, g./cm.^{2}	N	$M \times 10^3$, c.g.s. units[a]	$\langle \bar{v} \rangle$, cm.^{3}/g.	$\langle \bar{S}_w \rangle$, cm.^{2}/g.
Nylon, cylindrical	0.96	46.2	1.14	1.27	0.066	110	0.904	0.63
Glass, cylindrical	0.96	12.9	2.56	74.4	0.119	43	0.391	1.22
Glass, cylindrical	0.96	9.14	2.85	103	0.151	27	0.351	1.54
Glass, cylindrical	0.96	9.12	2.56	71.2	0.165	21	0.391	1.71
Nylon, cylindrical	1.68	46.2	1.14	1.27	0.165	26	0.904	0.63
Glass, cylindrical	1.68	12.9	2.56	74.4	0.175	22	0.391	1.22
Glass, cylindrical	0.96	5.12	2.56	72.6	0.195	16	0.391	3.06
Nylon, cylindrical	3.13	46.2	1.14	1.27	0.195	15	0.904	0.63
Nylon, cylindrical	6.30	46.2	1.14	1.27	0.200	12	0.904	0.63
Glass, cylindrical	4.60	9.14	2.85	103	0.200	15	0.351	1.54
Nylon, cylindrical	4.60	46.2	1.14	1.27	0.202	13	0.904	0.63
Glass, cylindrical	4.60	5.12	2.56	72.6	0.212	9.2	0.391	3.06
Glass, cylindrical	1.68	5.12	2.56	72.6	0.215	9.3	0.391	3.06
Glass, cylindrical	6.30	12.9	2.56	74.4	0.220	9.0	0.391	1.22
Nylon 66, cylindrical	6.47	19.5	1.14	0.3-1.3	0.225	10	0.904	1.83
Bagasse, depithed	--	--	1.59	--	0.230	8.7	3.38	8.3
Dacron, cylindrical	5.28	17.1	1.41	10-14	0.254	6.6	0.725	1.66
Glass, cylindrical	--	6.5	2.56	70-75	0.271	6.3	0.391	2.4
Cotton, α-cellulose	--	--	1.59	--	0.276	6.6	1.57	12.3
Orlon, dog-boned	6.64	31.1	1.21	3-4	0.286	4.6	0.826	2.19
Cotton, high H.E.[b] subst.	--	--	1.59	10-30	0.298	4.8	1.80	2.0
Loblolly pine, kraft summerwood	2.48	43.6[c]	1.59	10-30	0.311	3.0	3.62	4.08
Cotton, mod. H.E.[b] subst.	--	--	1.59	10-30	0.318	4.2	1.53	3.70
Aspen, conventional G.W.	--	--	1.59	10-30	0.326	4.0	2.85	53.9
Hemlock, sulfite diss. grade	--	--	1.59	10-30	0.327	3.9	2.46	9.9
Cotton, linters	--	--	1.59	10-30	0.332	3.1	1.43	7.9
Douglas-fir, bleached kraft summerwood	2.46	32.6[c]	1.59	10-30	0.362	1.9	2.54	5.7
Cotton, low H.E.[b] subst.	--	--	1.59	10-30	0.366	2.6	1.65	4.02
Hemlock, bleached sulfite	2.04	39[c]	1.59	10-30	0.370	2.3	1.95	12.3
Aspen, chlorited	--	--	1.59	10-30	0.373	2.1	2.51	11.1
Hemlock, bleached sulfite, high brightness	--	--	1.59	10-30	0.375	2.2	2.35	5.35
Douglas-fir, chlorited summerwood	2.55	37.3[c]	1.59	22	0.383	1.5	2.35	4.9
Spruce, unbleached kraft, NaOH extracted	--	--	1.59	10-30	0.387	1.8	2.55	10
Jack pine, unbleached kraft	--	--	1.59	10-30	0.391	1.3	3.42	13.3
Jack pine, unbleached kraft, NaOH extracted	--	--	1.59	10-30	0.395	1.6	2.52	9.3
Douglas-fir, bleached kraft, springwood	2.01	61.1[c]	1.59	10-30	0.396	1.3	3.75	16.8
Aspen, chlorited	--	--	1.59	10-30	0.400	1.5	2.96	14.8
Spruce, unbleached kraft, NaOH extracted	---	--	1.59	10-30	0.406	1.6	2.55	11.7
Jack pine, unbleached kraft	--	--	1.59	10-30	0.415	1.2	3.48	21.1
Douglas-fir, chlorited springwood	2.00	64.2[c]	1.59	9.0	0.437	0.78	4.12	15.6
Southern pine, kraft, chemically modified	--	--	1.59	--	0.451	0.71	2.54	5.3

[a] $(g./cm.^3)/(dynes/cm.^2)^N$

[b] Hydroxyethylated

[c] Fiber width, microns

The most striking general feature of compressibility is the large decrease of $\underline{M}$ with increasing $\underline{N}$. This fact is correlated in Fig. 17 on a semilog plot. All the data may be represented by a line within ± 20%. The scattering of the data points may be attributed to the variations of previously stated parameters. Apparently, some of their effects on $\underline{M}$ and $\underline{N}$ are in opposite directions, which appears to be consistent with the formulation of the compressibility function (19). In this sense a comparison of $\underline{M}$ or $\underline{N}$ alone is not adequate to clarify the compressibility behavior. A much wider range of pressures would be desired for establishing the change of compressibility with the practical papermaking properties in the forming, pressing, drying, and calendering operations.

Within the apparent $\underline{M}$-$\underline{N}$ correlation, systematic data do show minor variations of other factors yet unaccounted for. First, as may be expected, bleaching tends to lower the modulus of elasticity and therefore to increase the compressibility coefficient, as illustrated in Table IX. Secondly, for unbleached pulps, beating or refining does not influence $\underline{N}$ appreciably, but does increase $\underline{M}$ to some extent (Table X). Thirdly, for bleached pulps there is shown little effect of conventional refining over a wide range on their compressibility (Table XI). In contradistinction, with high-consistency refining a single experimental evidence indicates the same values of $\underline{N}$, but slightly increasing $\underline{M}$ as shown in Fig. 18. The comparison of conventional and high-consistency refining of a bleached pulp is demonstrated in Fig. 19, which appears to be consistent with the last two facts. However, these statements cannot be construed as rigid rules, especially in comparing different pulps.

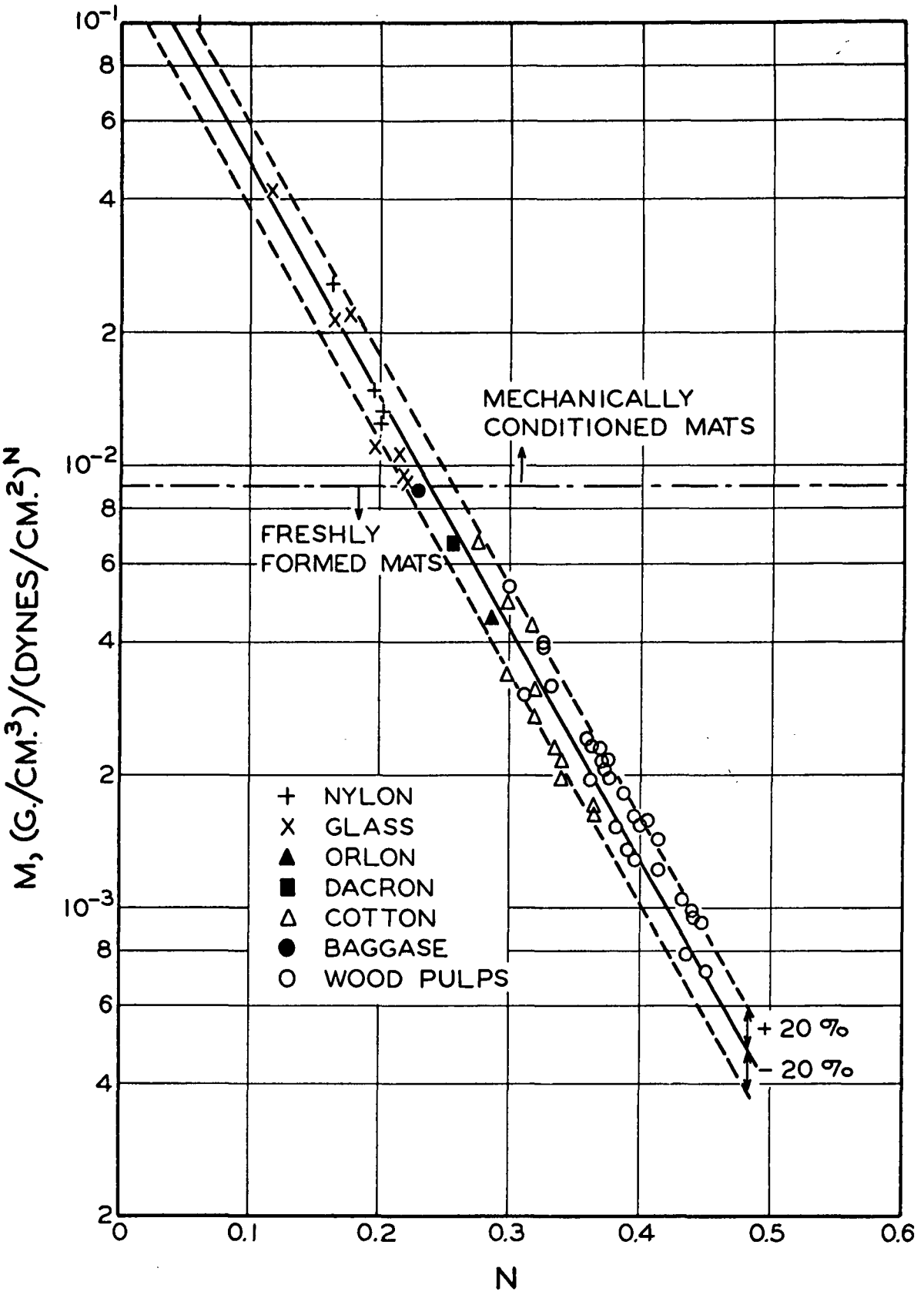

Figure 17. The M-N Correlation

TABLE IX

FIRST COMPRESSION OF NORTHERN SPRUCE KRAFT

	$\underline{N}$	$\underline{M} \times 10^3$, c.g.s. units[a]
Raw stock	0.397	1.06
Unbleached stock	0.394	1.21
Bleached stock	0.368	1.91

TABLE X

FIRST COMPRESSION OF UNBLEACHED REFINED PULPS

Pulp	Refining Time, min.	$\underline{N}$	$\underline{M} \times 10^3$, c.g.s. units[a]
A	0	0.328	2.52
	15	0.328	2.67
	30	0.328	2.77
B	0	0.337	2.33
	20	0.337	2.53
	27	0.337	2.59
C	0	0.343	2.12
	15	0.343	2.29
	30	0.343	2.38

TABLE XI

FIRST COMPRESSION OF BLEACHED PULP REFINED IN A BALL MILL

Refining Time, min.	$\underline{N}$	$\underline{M} \times 10^3$, c.g.s. units[a]
0	0.375	2.15
20	0.375	2.15
50	0.375	2.15
100	0.375	2.15
150	0.375	2.15
200	0.375	2.15

[a] $(g./cm.^3)/(dynes/cm.^2)^{\underline{N}}$

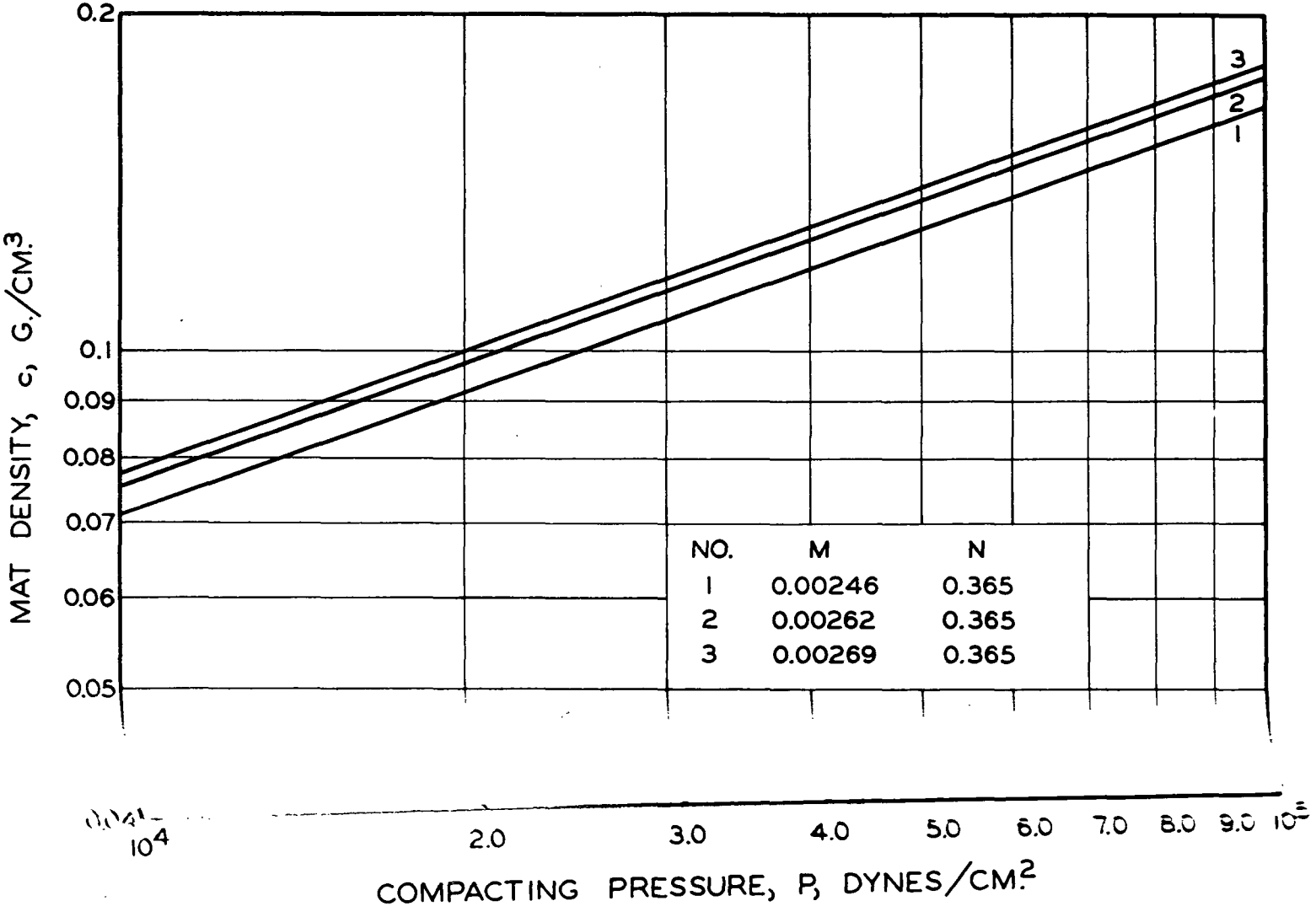

Figure 18. First-Compression Data for a High-Consistency Refined Pulp

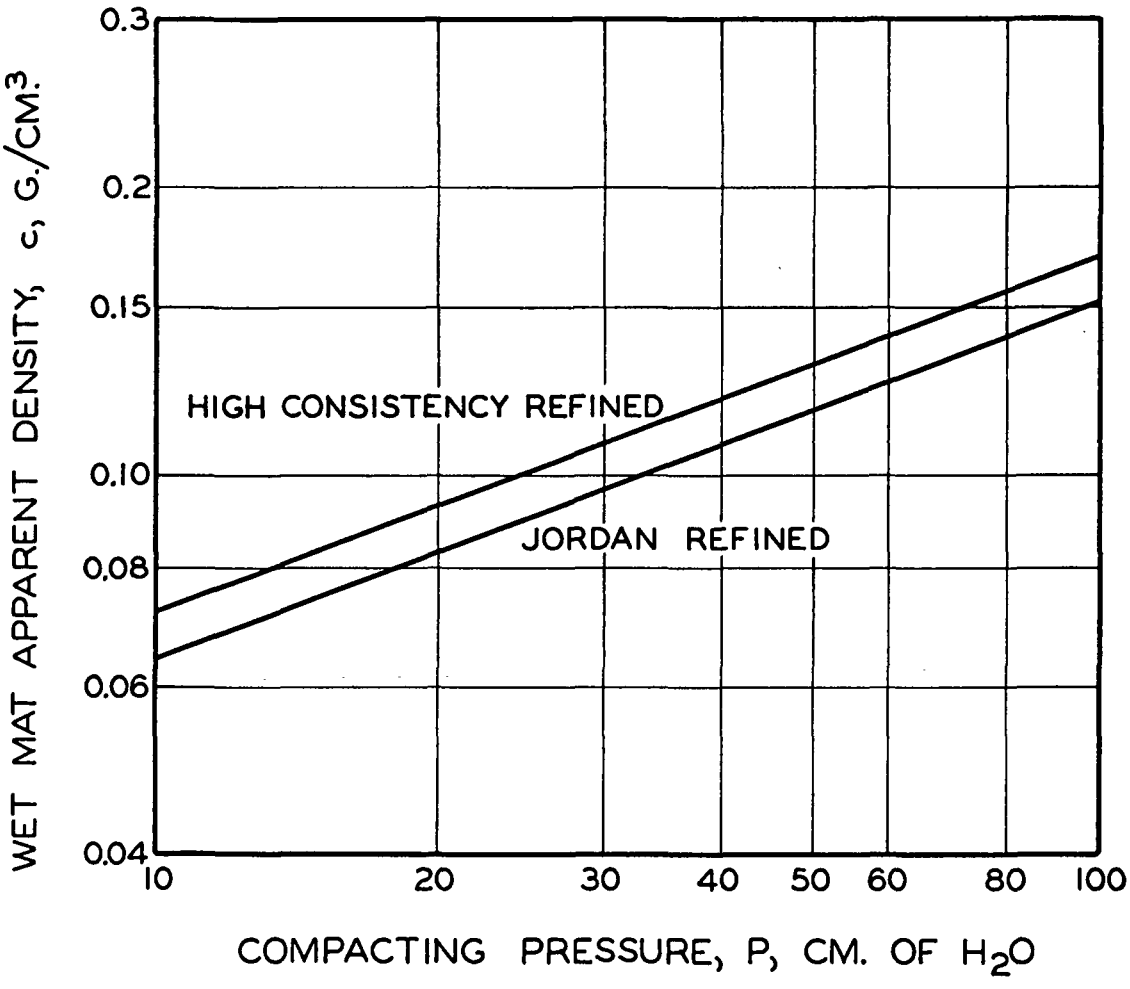

Figure 19. Compressibility of Jordan and High-Consistency Refined Pulp

In general, a higher value of $\underline{N}$ indicates more conformability of fibers, other factors being approximately the same.

APPROXIMATE THEORIES

Van Wyk's development of his compressibility function was based on a structure of three-dimensional orientations of fibers. His resulting equation (23) is obviously very limited for expressing experimental data. Wilder's development was much closer to the structure of mechanically conditioned filtration-formed mats, but his assumptions were not entirely consistent with the recent experimental evidence. At this time we attempt to refine Wilder's derivation with the hope that the resulting function will be more realistic though still oversimplified.

Accepting the Onogi-Sasaguri theory in its simplest form (14), the change of mat density from an initial to final structure may be related to the corresponding change of segment length:

$$\frac{c}{c_o} = \frac{L_{s,o}}{L_s} \qquad (25),$$

in which it is implied that the mode of packing in a mat structure remains constant. The increase of mat density in an initially unstressed structure is due simply to the increase of the number of contacts.

If a mat of unit area is imagined to consist of $\underline{n}$ similar layers, each 1 fiber diameter thick, then the initial mat density would be

$$c_o = \frac{W}{L_o} = \frac{(\pi d_f^2/4)N_f L_f \rho_f}{n d_f} \qquad (26),$$

where L_o is the thickness of the initial mat. The number of contacts per layer adjacent to two other layers is

$$n_c = \frac{N_f L_f}{2L_s n} \qquad (27) .$$

Upon application of an infinitesimal load, the incremental force sustained by each contact in the layer is dP_f/n_c . Using the beam theory, the reduction in thickness of the layer is

$$-\frac{dL}{n} = \frac{L_n^3}{K_n EI} \frac{dP_f}{n_c} \qquad (28) ,$$

where

$$L = \frac{W}{c} \qquad (29) .$$

Assuming, for the sake of simplicity, that the contacts are distributed alternately above and below fibers, the span length is then twice the segment length. Utilizing Relations (26) and (29), the above equation is expressed in terms of mat density as follows:

$$\frac{dc}{c^2} = \frac{(2L_s)^3}{K_n EI d_f c_o} \frac{dP_f}{n_c} \qquad (30) .$$

For cylindrical fibers,

$$I = \pi d_f^4/64 \qquad (31) .$$

By substituting Equations (25), (27), and (31) for L_s , n_c , and I , the final differential equation becomes

$$c^2 dc = \frac{\pi^{12}}{16^2} \frac{\rho_f^6}{c_o^2 K_n E} dP_f \qquad (32) .$$

Integrating for the whole mat between the limits c_o at $P_f = 0$ and c at P_f, the resulting expression is

$$c^3 - c_o^3 = \left(\frac{3\pi^{12}}{16^2} \frac{\rho_f^6}{c_o^2 K_n E}\right) P_f \qquad (33) ,$$

which is similar to Van Wyk's equation in form.

However, from the previous interpretation of load distributions, it seems more logical to consider K_n as a variable, rather than a constant. In the analysis of Wilder's compressibility function, Elias contended K_n to be a strong function of P_f in agreement with the proposed concept of increasing complexity of load distribution upon increasing compression. Elias' data for the third compression of a glass fiber mat after complicated manipulations are replotted in Fig. 20 on log-log scales, resulting in a linear relationship, which may be represented by a simple power function as

$$K_n = \alpha (P_f/E)^{\beta} \qquad (34) ,$$

where α and β are two constants, β being less than unity. The inclusion of the modulus of elasticity is not only to render the correlation dimensionless, but more importantly also implies the additional dependence of the bending mechanism in a multiple-beam system on the modulus. With this contention the refined compressibility function takes the form:

$$c^3 - c_o^3 = \left[\frac{M'}{\alpha(1-\beta)} \frac{\rho_f^6}{c_o^2 E^{1-\beta}}\right] P_f^{1-\beta} \qquad (35) ,$$

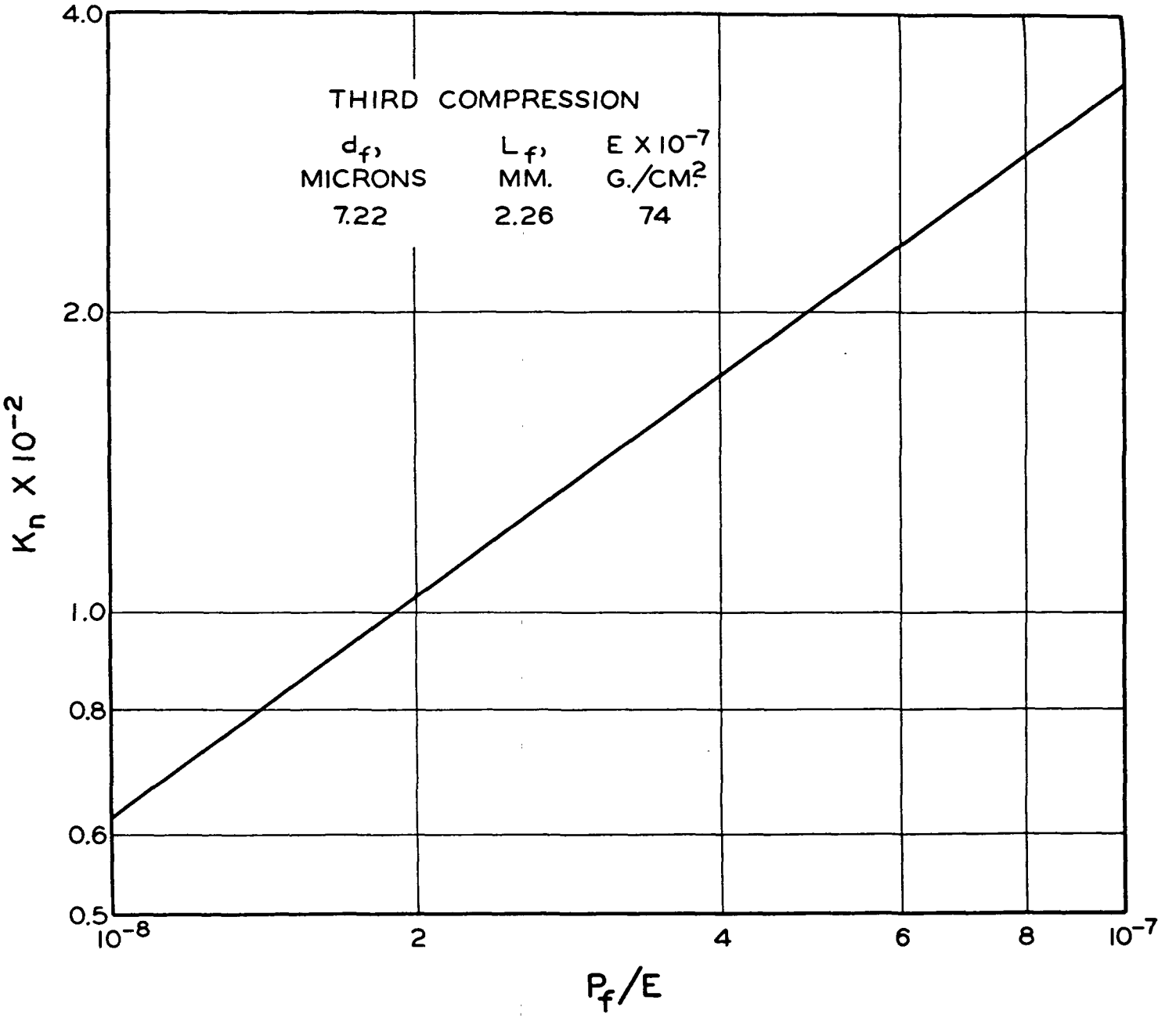

Figure 20. Change of Bending Constant in Compression

where $\underline{M}'$ has absorbed all the numerical values. This expression would be expected to be applicable to the compressibility of mechanically conditioned mats controlled by bending with some extent of fiber slipping provided by the adjustable factors α and β. Elias further showed that the value of β was smaller for the second compression, indicating the possible increase of slope with less conditioning.

The compressibility equation so developed, however, is inadequate for taking fiber conformation into account. Lacking the understanding of the mechanism, we boldly assume the same power function (34), with negative β. By this adjustment the final compressibility functions in a dimensionless form is

$$\left(\frac{c}{\rho_f}\right)^3 - \left(\frac{c_o}{\rho_f}\right)^3 = \left[\frac{M'}{\alpha(1-\beta)(c_o/\rho_f)^2}\right]\left(\frac{P_f}{E}\right)^{1-\beta} \qquad (36),$$

where β is always less than unity and may be either positive or negative. When $\underline{c_o} \ll \underline{c}$, this reduces to

$$c = \left[\frac{M'\rho_f^5}{\alpha(1-\beta)c_o^2 E^{1-\beta}}\right]^{1/3} P_f^{(1-\beta)/3} = MP_f^N \qquad (37).$$

If the fiber-fiber friction is small, allowing much slippage, the quantity $1-\beta$ permits a smaller value of $\underline{N}$ less than 1/3 and a larger value of $\underline{M}$. On the other hand, if the friction is large so that fiber conformation becomes an important factor affecting bending, the value of $(1-\beta)$, now larger than unity, results in a larger $\underline{N}$ and smaller $\underline{M}$. This feature is in qualitative agreement with the previous correlation of decreasing $\underline{M}$ with increasing $\underline{N}$.

It is to be mentioned that there are inherent inconsistencies in the present development of the compressibility function. A more rigorous analysis is under consideration.

FILTERABILITY

FILTRATION CONDITIONS

The consolidation of solid particles suspended in a fluid flowing through a septum is commonly called filtration. It may be treated as an unsteady process of permeation involving drainage of the excess fluid through a continuously growing porous structure as the particles accumulate on the septum. The resistance offered by the porous structure to flow of the fluid therefore follows the same laws of permeation. If the filtration process is carried out under well-defined conditions, the result may be interpreted in terms of the permeability of the material.

For the purposes of determining filtration resistance, the constant-rate method has been generally adopted. The latest version of the apparatus designed by Ingmanson has been refined to a high degree. Its essential feature is the recording of the pressure rise at a known flow rate. The conditions of filtration are specified as follows:

1. A dilute suspension of well soaked, deaerated, and dispersed fibers kept in mild agitation and constant temperature flows smoothly into a filtration tube filled with filtered water.

2. A relatively thick mat is formed at a slow rate on a thoroughly cleaned and wetted septum covered with a fine wire screen.

3. The filtrate is removed at a constant rate without pulsations or vibrations.

The first condition is to attain a uniform mat by deposition of individual fibers. A consistency of about 0.01% is generally low enough for

good dispersion. The flow of the suspension in the filtration tube should be slightly turbulent (Reynolds number $\approx$ 2500) to avoid reflocculation. The tube size should be sufficiently large (tube diameter/fiber length $\approx$ 50) to minimize wall effects.

For the second condition the initial part of filtration, which involves the complex fiber-wire interaction, is to be ignored. The mat should be thick enough (basis weight >50 g./sq. m.) so that the retention of the fibers becomes complete and the correction for the septum resistance is small, if not negligible. The flow rate should be sufficiently low to fall well within Darcy's region. In most cases the pressure range from 10 to 100 cm. of water is usable.

The purpose of the third condition is simply to avoid mechanical conditioning of the mat, which tends to increase the filtration resistance in an uncertain manner. The pressure rise should be as smooth as possible without the aid of damping.

AVERAGE RESISTANCE

When the suspension is dilute, the superficial velocity in a compressible mat is practically constant throughout its thickness because that part of water being squeezed out of the mat as a result of compression by the fluid frictional forces is negligible, compared with the flow through the mat. Then Darcy's law is directly applicable to an infinitesimal layer of the mat provided the flow is slow,

$$U = -\frac{K}{\mu}\frac{dP}{dz} \qquad (38),$$

where the z-coordinate is in the downward direction with its origin located at the mat face.

In dealing with filtration it is more convenient to use the basis of mass rather than thickness. Let w be the mass of fibers per unit area of the mat between 0 and z ; then the local mat density c is simply dw/dz . Similarly, the permeability coefficient may be expressed in terms of a resistance on the mass basis:

$$K = \frac{1}{Rc} \qquad (39) ,$$

where R is called the specific filtration resistance with the dimension of length per unit mass. With these transformations the Darcy equation is now in the form

$$U = -\frac{1}{\mu R}\frac{dP}{dw} \qquad (40) .$$

Upon integration at constant flow and temperature for the whole mat of basis weight W , the result is

$$\mu UW = -\int_{P_o}^{P_L} \frac{dP}{R} = \frac{\Delta P}{\bar{R}} \qquad (41) ,$$

where $\bar{R}$ is defined as the average specific filtration resistance at the overall pressure drop ΔP .

Instead of drying and weighing the mat, the basis weight may be calculated from a material balance:

$$W = s\rho Ut \qquad (42) ,$$

in which the small amount of water associated with the wet mat is justifiably neglected for filtration of a dilute suspension with consistency s and density ρ. By substitution, the final constant-rate filtration equation becomes

$$\bar{R} = \frac{\Delta P}{s\rho\mu U^2 t} = B\frac{\Delta P}{t} \qquad (43),$$

where B is called the filtration constant. In this way $\bar{R}$ as a function of ΔP is obtained from the recorded pressure drops at the corresponding times in a single filtration run.

RESISTANCE ANALYSIS

From the permeation correlation established for cylindrical fibers, Equation (11), the specific filtration resistance is related to the mat density by

$$R = k_1 (S_v^2/\rho_f)(c/\rho_f)^{\gamma/2}[1 + k_2(c/\rho_f)^3] \qquad (44).$$

If it is assumed that dynamic compression of a fiber mat is the same as first compression in a static test and the mat density at the mat-suspension boundary is practically zero at zero compacting pressure, the simple power function may be used to relate c with P_f. The relation between P_f and P can be demonstrated to be

$$P_f = P_0 - P \qquad (45).$$

In the Davis-Ingmanson correlation the term containing k_2 is negligible for porosities larger than 0.9. Thus, the integral in Equation (41) may be evaluated from

$$-\int_{P_o}^{P_L} \frac{dP}{R} = \frac{\rho_f^{3/2}}{k_1 S_v^2 M^{1/2}} \int_0^{\Delta P} P_f^{-N/2}\, dP_f \qquad (46) .$$

Resistance Integration

Upon integration of the filtration equation, the average specific filtration resistance is obtained as

$$\bar{R} = k_1 (S_v^2/\rho_f^{3/2})(1 - N/2)[M(\Delta P)^N]^{1/2} \qquad (47) .$$

If the integration is carried out numerically for lower porosities (0.7-0.9), using the Davis-Ingmanson correlation in its complete form, the results are not more than 7% lower than those based on the average mat density defined below. Furthermore, the small discrepancies are nearly the same for several kinds of fibers. It is therefore justifiable to extend the porosity range for the calculation of the average specific filtration resistance:

$$\bar{R} = k_1 (S_v^2/\rho_f)(\bar{c}/\rho_f)^{1/2}[1 + k_2(\bar{c}/\rho_f)^3] \qquad (48) ,$$

where

$$\bar{c} = \rho_f(1 - \bar{\epsilon}) = (1 - N/2)^2 M(\Delta P)^N \qquad (49) .$$

Experimental Verification

The practical validity of Equation (48) was experimentally demonstrated by Ingmanson (8,9). By integrating the Darcy equation in its original form for high porosities with the abbreviated Davis-Ingmanson correlation, the constant-rate filtration expression on the thickness basis is

$$\frac{\Delta P}{L} = k_1 \mu (S_v^2/\rho_f^{3/2}) U(1 - 3N/2)[M(\Delta P)^N]^{3/2} \qquad (50) .$$

A similar expression may be derived on the mass basis to be

$$\frac{\Delta P}{W} = k_1 \mu (S_v^2/\rho_f^{3/2}) U(1 - N/2)[M(\Delta P)^N]^{1/2} \qquad (51) .$$

Dividing one by another the result is

$$c^o = \frac{W}{L} = [\frac{2 - 3N}{2 - N}]M(\Delta P)^N \qquad (52) ,$$

where the overall mat density, $\underline{c}^o$, is experimentally measurable. For nylon fibers this equation is shown as a solid line in Fig. 21 and compared with the experimental data. The agreement is very satisfactory over a large range of pressure drops. The top line in the same figure represents the static compressibility function. It appears from the graph that the simple power function is applicable to much lower pressure drops in filtration than indicated by the static compressibility.

Further experimental support of the applicability of the simple compressibility function to filtration was provided by Ingmanson in Fig. 22, which is a plot of flow correlation in a wide range of velocities. The curve represents the following equation:

$$\frac{\bar{\epsilon}^3 \rho_f \Delta P}{\sqrt{\bar{k}}\, S_v \rho U^2 W} = \frac{\sqrt{\bar{k}}\,(1 - \bar{\epsilon}) S_v \mu}{\rho U} + b' \qquad (53) ,$$

where

$$\bar{\epsilon} = 1 - (1 - N/2)^2 M(\Delta P)^N/\rho_f \qquad (54) ,$$

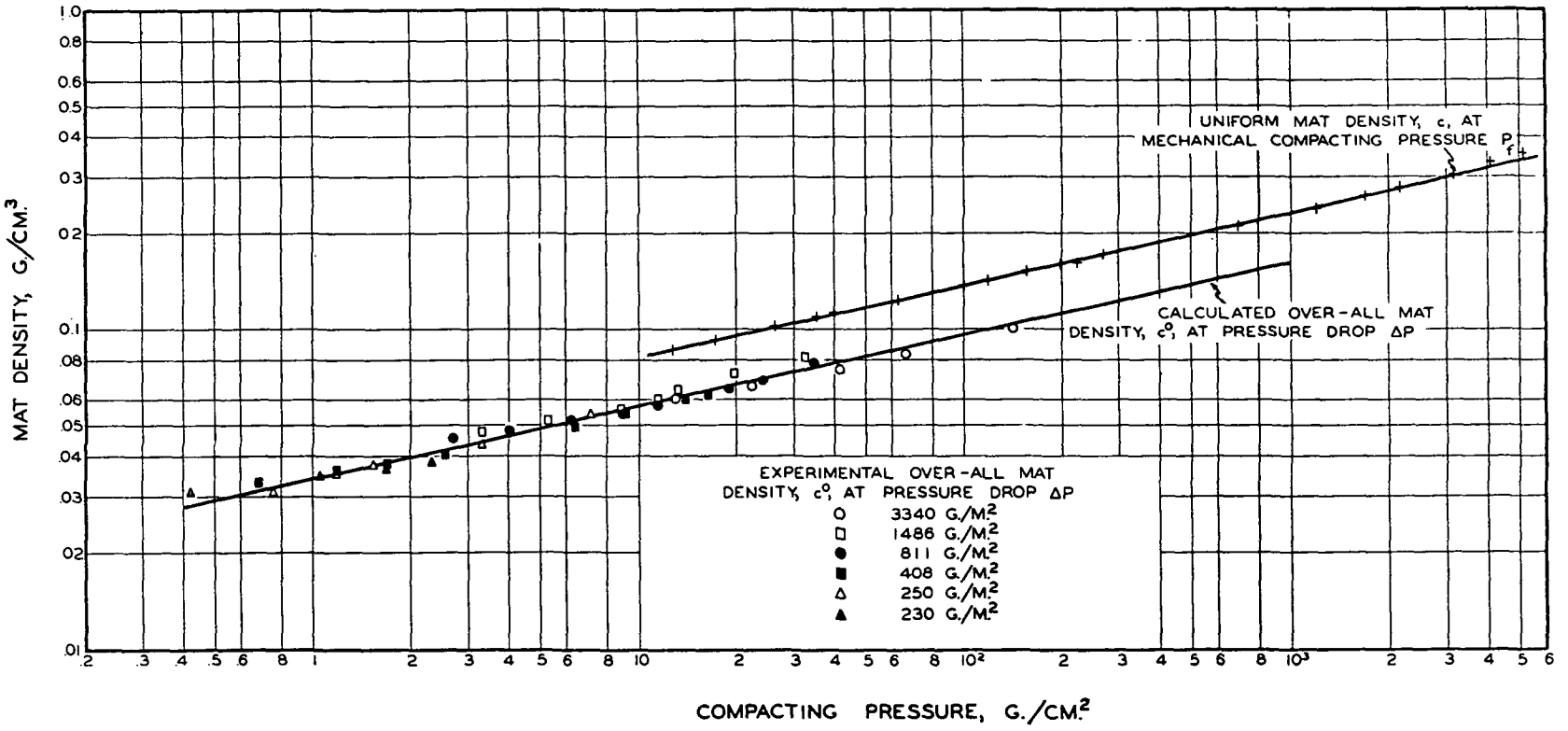

Figure 21. Comparison of Uniform and Overall Mat Densities

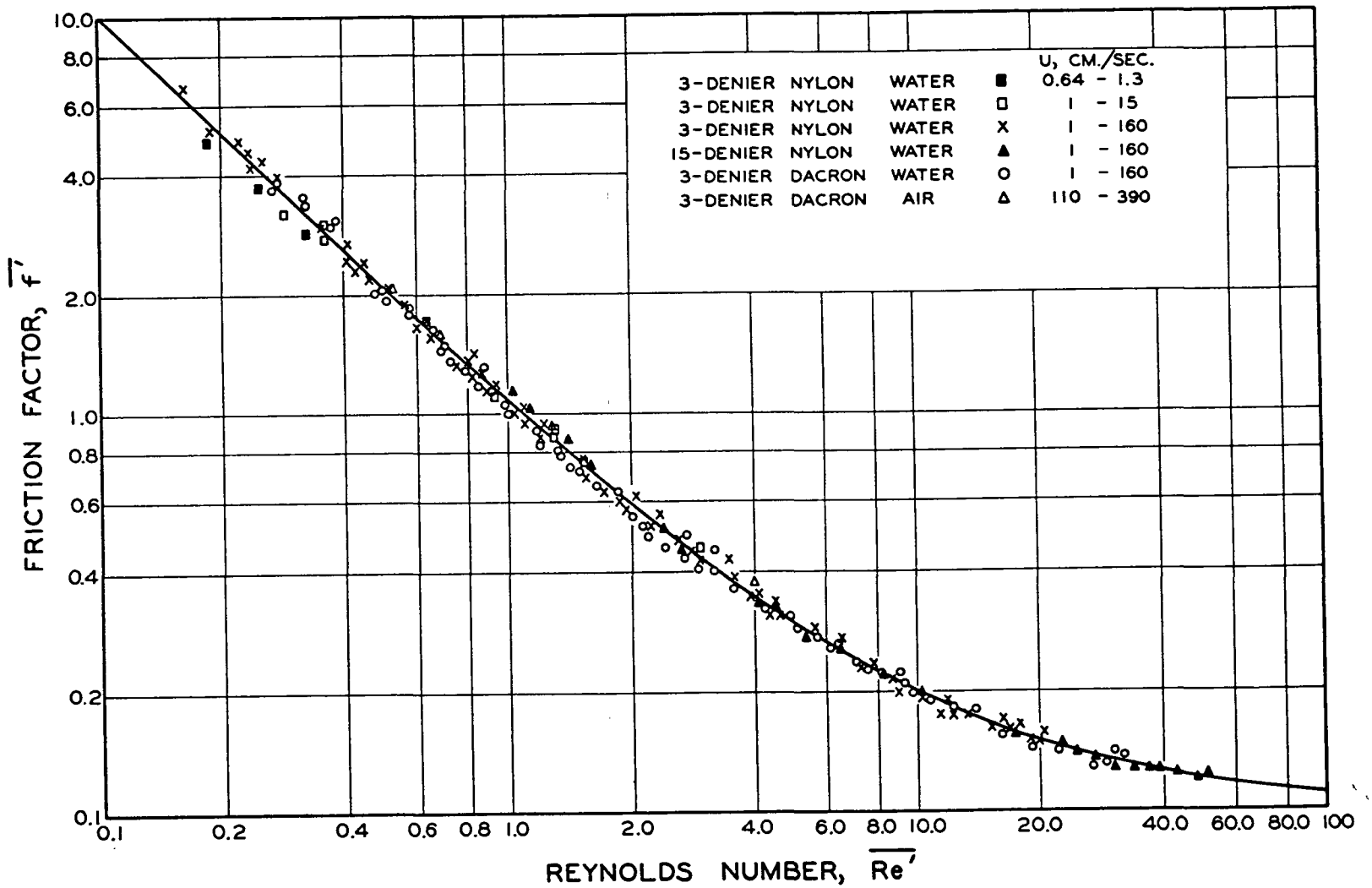

Figure 22. Correlation of Flow Data for Cylindrical-Fiber Mats

$$\bar{k} = k_1 \frac{\bar{\epsilon}^3}{(1 - \bar{\epsilon})^{1/2}} [1 + k_2 (1 - \bar{\epsilon})^3] \qquad (55),$$

and $\underline{b}'$ is the inertial constant. The same equation may be put in the simple form:

$$\bar{f}' = \frac{1}{\overline{Re}'} + b' \qquad (56).$$

The values of the constants $\underline{k}_1$, $\underline{k}_2$, and $\underline{b}'$ are 3.5, 53, and 0.1, respectively. Flow below unity $\overline{Re}'$ may be considered to be in Darcy's region. At higher $\overline{Re}'$ the inertial effects become increasingly important. For example, in terms of pressure drop, the inertial resistance is 9% at unity $\overline{Re}'$ and 91% at 100.

Compensating Factors

In the above analysis of filtration, the major assumption involved is the use of static compressibility in its simple form of a power function. In this assumption there are four aspects to be clarified: (1) the difference between mechanical and frictional compression, (2) the time dependence of compressibility, (3) the omission of the initial mat density, and (4) the fictitious boundary condition at the mat-suspension interface.

In static compression the mechanical load is distributed over the points of contact while in fluid compression the drag forces act continuously along the free spans of the fibers. According to the simple beam theory, continuous loading would result in less bending than distributed loading. However, the fluid drag forces are cumulative in the direction of flow by transmission through the contact points. The fibers in a "layer" are not only experiencing the compacting force due to the drag over this layer alone

but all the frictional forces acting on the fibers from above and transmitted through the contacts to the layer.

When the drag forces acting locally on the fibers become negligible compared with those transmitted through the distributed contact points, the load distribution in the dynamic case would approach the static case. Thus, the thicker the mat, the closer would the frictional compression response come to the static behavior. In this limiting case, the maximum deflection of the fibers would still follow Equation (17) with the value of $\underline{K}_{\underline{n}}$ of the order of 10^2 in the case of a simple beam.

In constant-rate filtration the mat is subject to continuously rising pressure while in a static test the mat is allowed to come to a nearly equilibrium state. At the same compacting pressure the mat density under dynamic conditions would be smaller than that under static conditions. Furthermore, the omission of $\underline{c}_{\underline{p}}$ would introduce an error in overestimating the mat density in the filtration analysis. There is a third error concerning mat density which has been assumed to vanish at the mat-suspension boundary. The fiber structure at the boundary should be finite in reality although there must be a continuous change of fiber orientations from two dimensions to three dimensions within a thickness of approximately one fiber length. The mat density right at the mat face should be larger than that of the approaching suspension. These errors in the calculation of mat density or porosity in the filtration analysis would tend to compensate with each other to some extent in the early part of filtration, and would become inconsequential in the latter part of a long, slow filtration.

CELLULOSIC FIBERS

For hydrodynamic evaluation of the specific surface and volume of swollen fibers, the differential constant-rate filtration equation may be rearranged into the so-called rectified form:

$$\frac{d(\Delta P)}{\sqrt{c}\, dt} = \frac{k_1 S_w^2}{B\sqrt{v}} (1 + k_2 v^3 c^3) \qquad (57),$$

where S_w, the specific surface based on the fiber mass, is equal to vS_v, and the effect of fiber shape is neglected. The mat density c at the septum is calculated from the simple compressibility function. By taking the derivatives from the corrected pressure-time chart recorded during filtration, Equation (57) may be plotted as the first term $vs.\ c^3$. If the resulting plot is a straight line, then S_w and v can be evaluated from its slope and intercept. This procedure generally involves some loss of experimental precision.

Instead of taking derivatives, the pressure drop across the mat may be read and corrected for the septum pressure drop from the chart at various chosen times. The rectified equation now takes the integrated form:

$$\frac{\Delta P}{\sqrt{c}\, t} = \frac{k_1 (1 - N/2) S_w^2}{B\sqrt{v}} [1 + k_2 v^3 (1 - N/2)^6 c^3] \qquad (58).$$

By introducing the average mat density in accordance with its previously established definition:

$$\bar{c} = (1 - \bar{\epsilon})/v = (1 - N/2)^2 M(\Delta P)^N = (1 - N/2)^2 c \qquad (59),$$

the alternative form of the rectified equation becomes

$$\frac{\Delta P}{\sqrt{c}\, t} = \frac{k_1 S_w^2}{B\sqrt{v}} [1 + k_2 (v\bar{c})^3] \qquad (60) .$$

In all the above treatments both S_w and v have been assumed to be constant.

The following example may be given as an illustration of the method of evaluation:

Pulp	Classified bleached sulfite
U	1.80 cm./sec.
μ	0.827×10^{-2} g./(cm.)(sec.)
s	0.0196×10^{-2} g./g.
ρ	1.0 g./cm.^{3}
B	1.90×10^5 (cm.^{2})(sec.^{3})/g.^{2}
k_1	3.5
k_2	57

The original filtration and first-compression data for the case are shown in Fig. 23. They are then replotted in the above rectified form in Fig. 24. The result is nonlinear, curving concavely downward. If linearity is forced to fit most of the data points and extrapolated to zero mat density, such as shown by the dashed line, the resulting values for specific surface and volume are 5030 cm.^{2}/g. and 2.16 cm.^{3}/g., respectively. These are obviously the averages for the range of ΔP used in the evaluation.

The data for wood pulp indicate that for the intermediate porosity range the deviation from linearity is the least. This may involve a fortuitous compensation by an additional factor which is thought to be the deswelling of

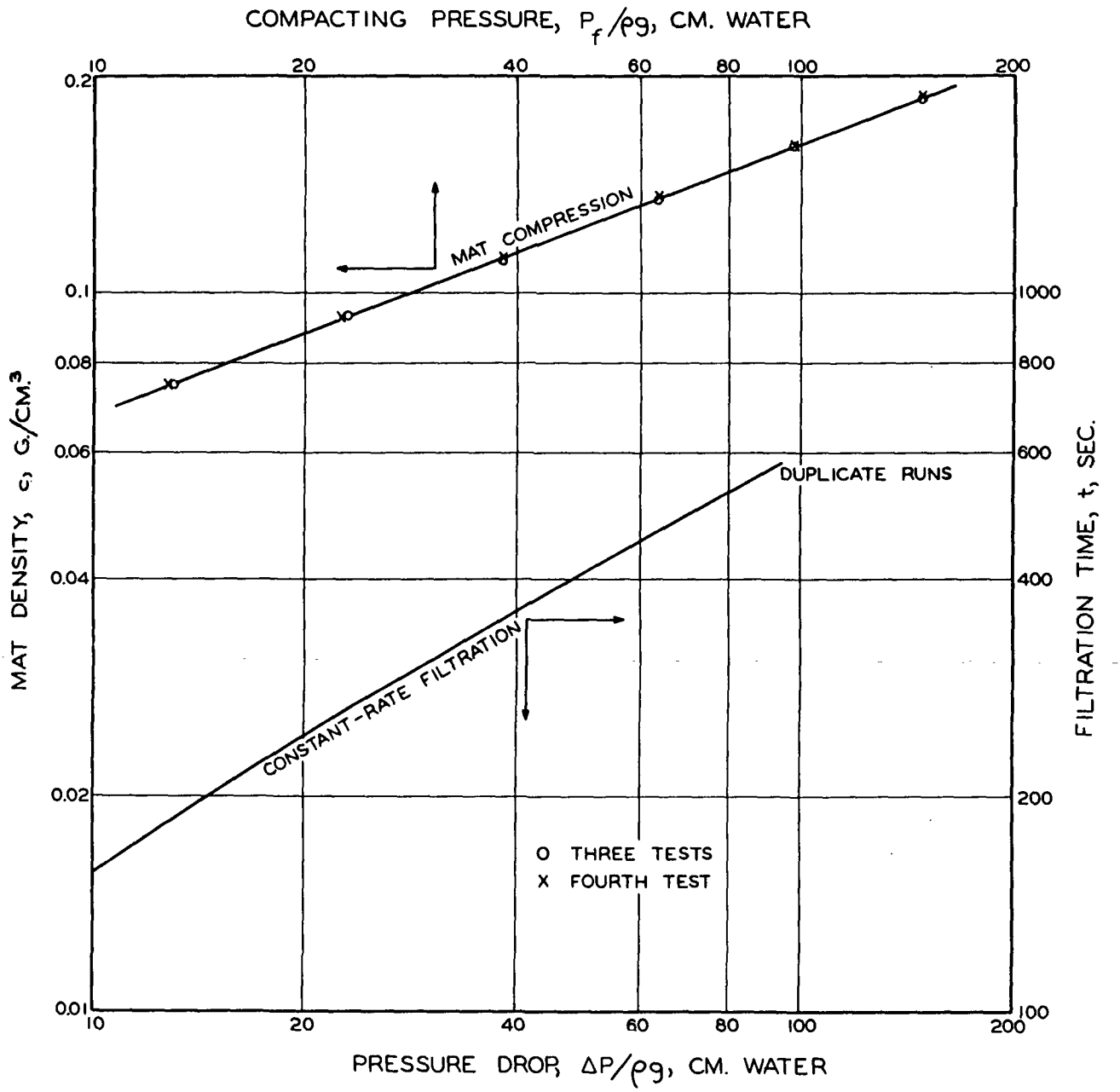

Figure 23. Example of Filtration and Compressibility Data

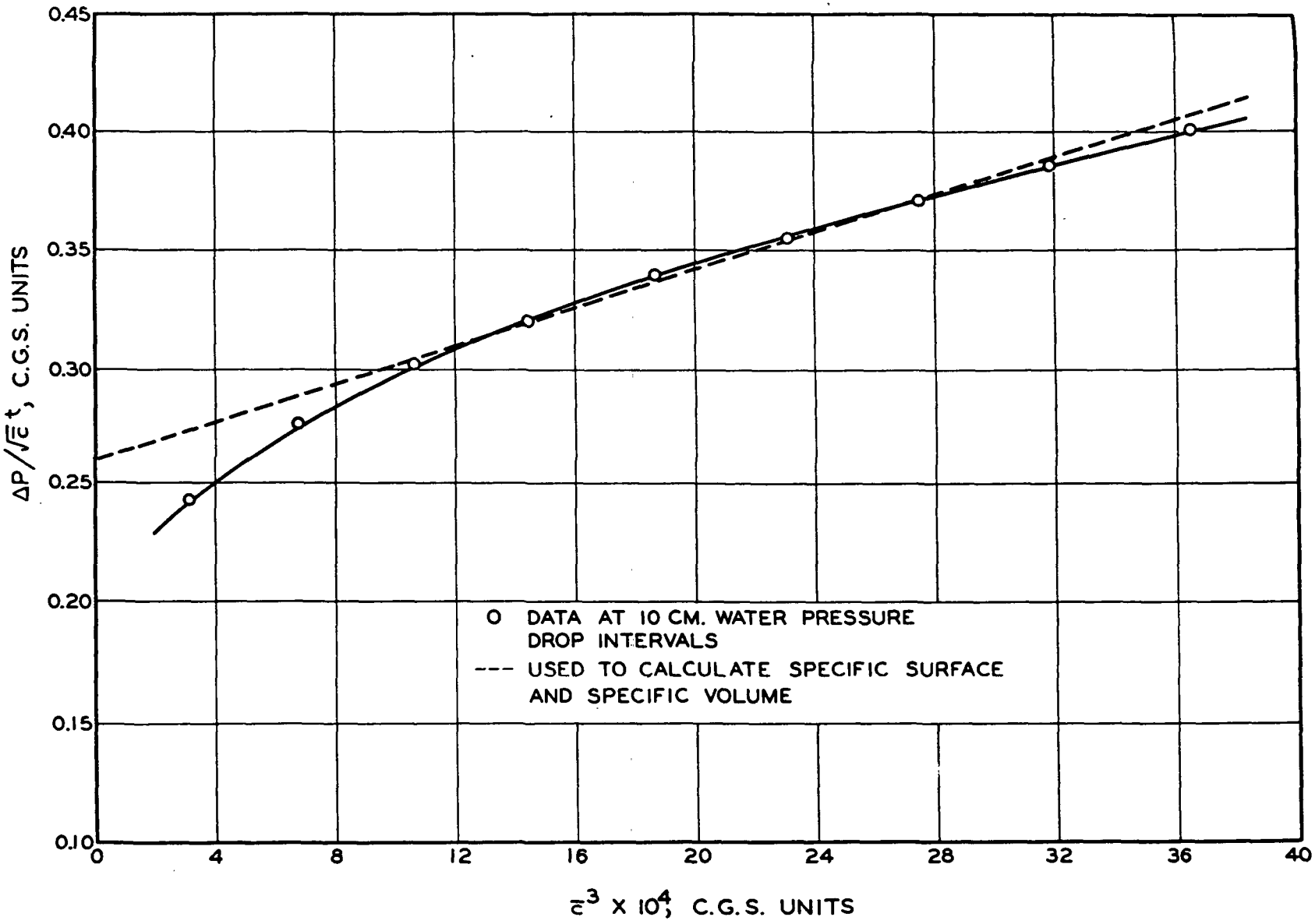

Figure 24. Rectified Plot of Filtration Data

cellulosic fibers under pressure. Deswelling will cause a higher porosity or lower resistance at the same mat density. The inclusion of the deswelling factor would also account for the larger deviations of both high and low porosities. As the pressure rises, deswelling increases the interfiber porosity while the Kozeny factor becomes higher at the actual porosity. Thus, the discrepancy would become larger with the increasing mat density. In the other direction, as the pressure drop decreases the Kozeny factor tends toward the assumed value whereas deswelling continues to increase the actual porosity, resulting in a lower porosity than expected.

In light of the deviation and its interpretation, Meyer (23) suggested an approximate method of finding the pressure dependence of specific surface and volume. The rectified equation is simplified to

$$P^* = k_1^* \frac{\bar{S}_w^2}{\sqrt{\bar{v}}} [1 + k_2 (\bar{v}\bar{c})^3] \qquad (61) .$$

Assuming $\bar{S}_w$ and $\bar{v}$ to have some representative mean values for any two points 1 and 2 along a short segment of the rectified curve and using Lagrange's interpolation formula, their dependence on pressure may be estimated from the following equations:

$$\bar{S}_w = \left[\frac{\bar{c}_1^3 P_2^* - \bar{c}_2^3 P_1^*}{k_1^* (\bar{c}_1^3 - \bar{c}_2^3)}\right]^{1/2} \bar{v}^{1/4} \qquad (62) ,$$

and

$$\bar{v} = \left[\frac{P_1^* - P_2^*}{k_2 (\bar{c}_1^3 P_2^* - \bar{c}_2^3 P_1^*)}\right]^{1/3} \qquad (63) .$$

The results of such calculations for the same sulfite pulp are shown in Fig. 25. It is seen while the specific volume decreases pronouncedly with increasing pressure as expected, the slight increase of the specific surface is inconsistent with the previous interpretation of fiber conformability. The two circles represent the pressure-average values and may be designated as $\langle \bar{S}_w \rangle$ and $\langle \bar{v} \rangle$.

A further refinement by Meyer from the basic filtration theory has corrected the inconsistent pressure dependence of specific surface. The new equation is as follows:

$$\bar{S}_w = \left[\frac{\bar{c}_1^3 P_2^* - \bar{c}_2^3 P_1^*}{k_1^*(\bar{c}_1^3 - \bar{c}_2^3)} \frac{\rho_f - \rho + \rho\rho_f \bar{v}}{\rho_f - \rho + \rho\rho_f v_0} \right]^{1/2} \frac{1}{v^{1/4}} \qquad (64),$$

where the bar now indicates the average over the mat. This equation cannot be solved until the values of v_0, the specific volume at zero stress, is known. Assuming a reasonable value of 4.0 cc./g. for sulfite pulp, the specific surface is depicted to be a decreasing function of pressure in Fig. 25.

In this treatment the equation for $\bar{v}$ remains the same as before. The previous specific surface and volume obtained by Ingmanson under the simplified assumptions can now be seen to be really average values under the specific filtration conditions. Further refinements call for the establishment of the specific surface and volume as functions of both position and time (pressure) as a mat is being formed during filtration. When such functions are obtained, their appropriate average values will be representative of the hydrodynamic properties describing a wet mat under the laboratory filtration conditions.

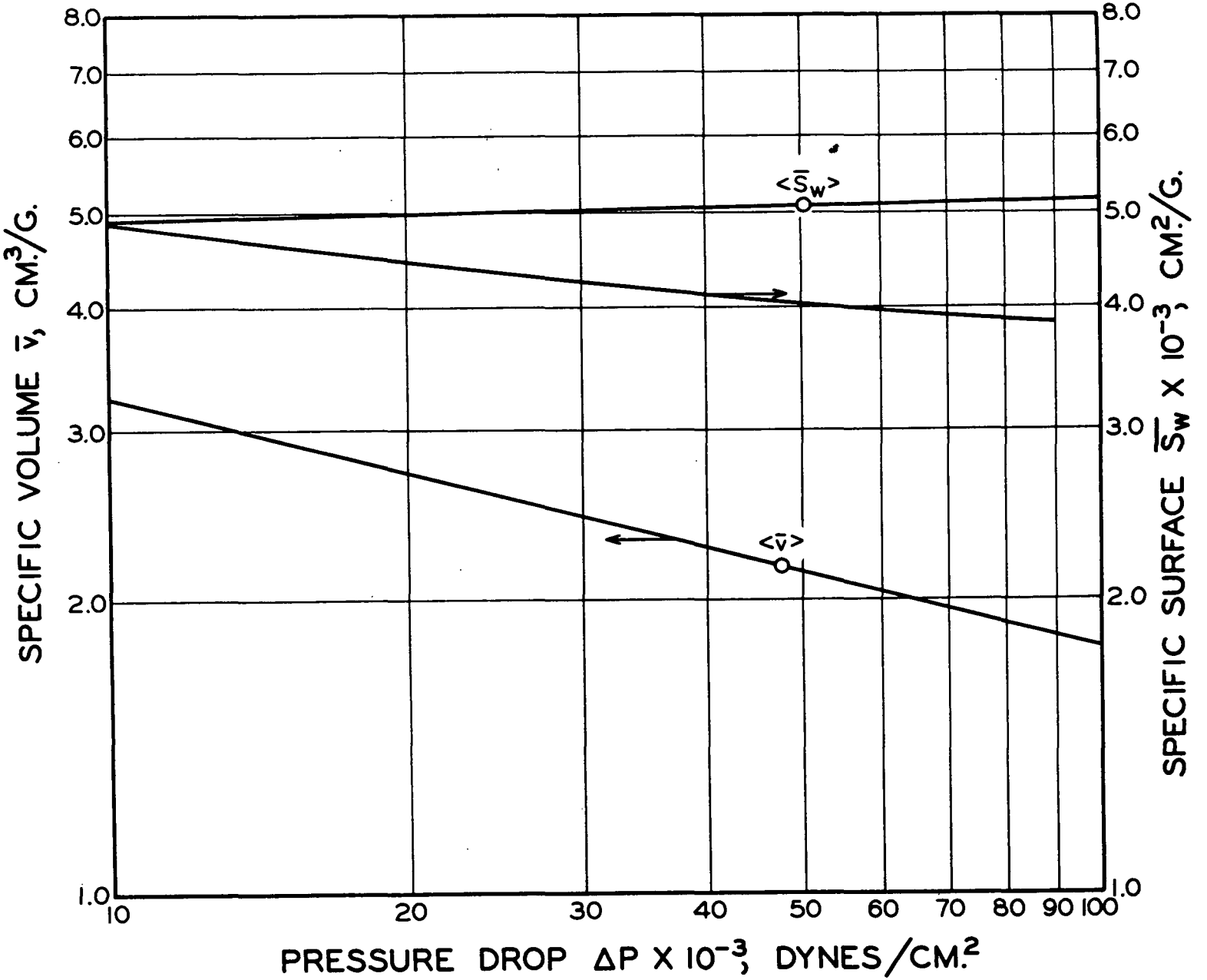

Figure 25. Variation of Specific Volume and Surface under Fluid Compression

FREENESS EVALUATION

In Fig. 26 and 27 are reproduced a comprehensive collection of filtration resistance data for cellulosic fibers in the pressure range of 10-100 cm. water in conjunction with the approximate correspondence of Schopper-Riegler freeness in both low and high regions. The family of curves are more or less concave upward in the log-log plots, indicating the rise of resistance with increasing pressure on account of the mat compressibility.

A correlation of the average specific filtration resistance at 10 cm. water with Schopper-Riegler freeness is illustrated in Fig. 28. The choice of the pressure is arbitrary. It is obvious that freeness is much less sensitive than filtration resistance in both high and low regions. Other freeness tests such as Canadian standard and Williams show similar patterns. In view of the popularity of the various freeness or drainage tests, some explanations of their usefulness and limitations are in order.

Simple Operation

Compared with the constant-rate filtration test, there is no doubt about the simplicity and rapidity of the freeness tests for routine purposes. Even the newly developed Drainage Resistance Analyzer (A.I.L. Type 273) simplified from the Institute's research model is still a slower though more sophisticated tester. From the previous comparison of freeness with filtration resistance, the former is deemed suitable for moderately refined pulps, provided every care is taken to insure a proper test operation. With such precautions, however, a large part of its appeal is lost.

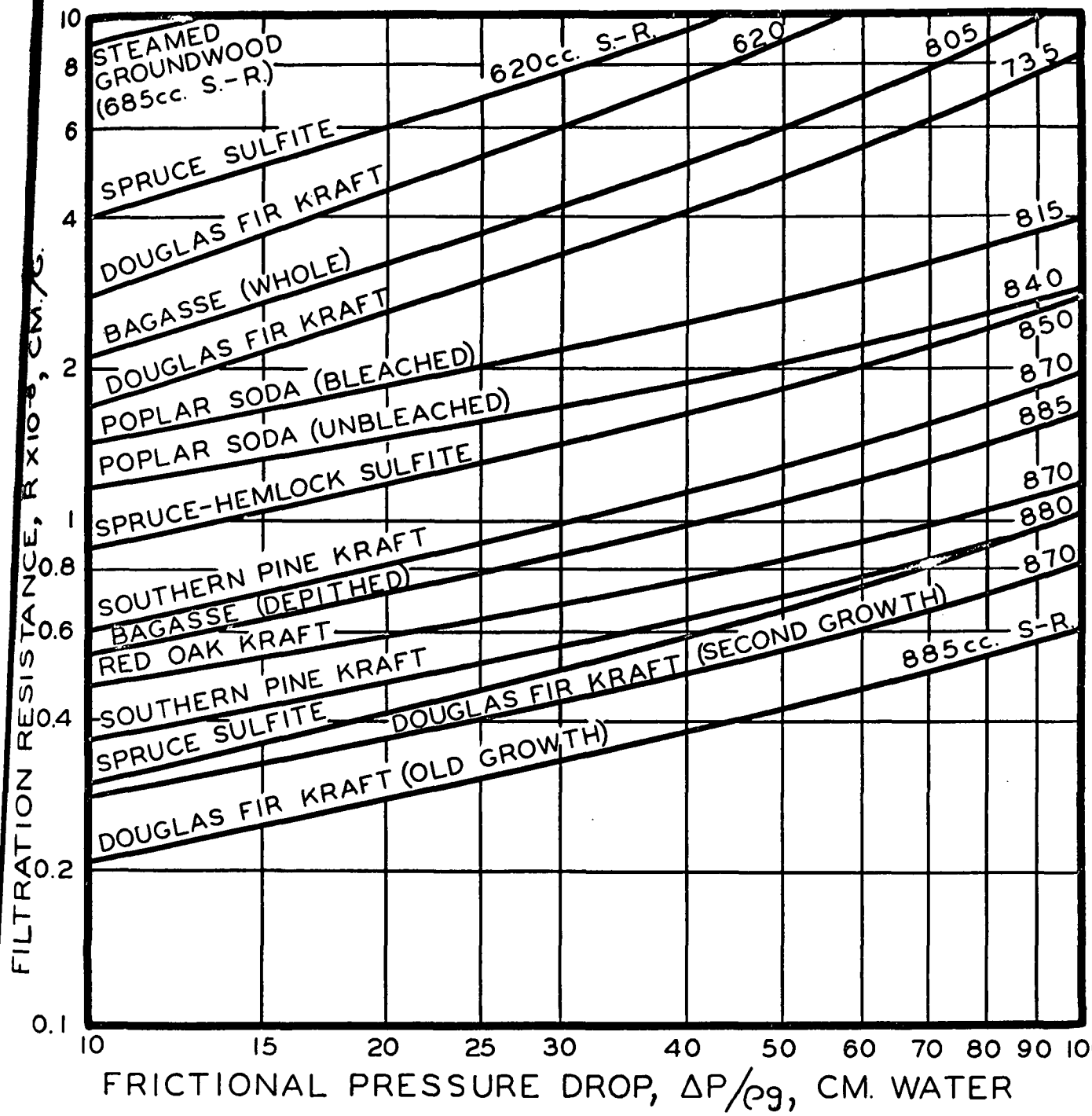

Figure 26. Filtration Resistances of Cellulosic Fibers (Low Range)

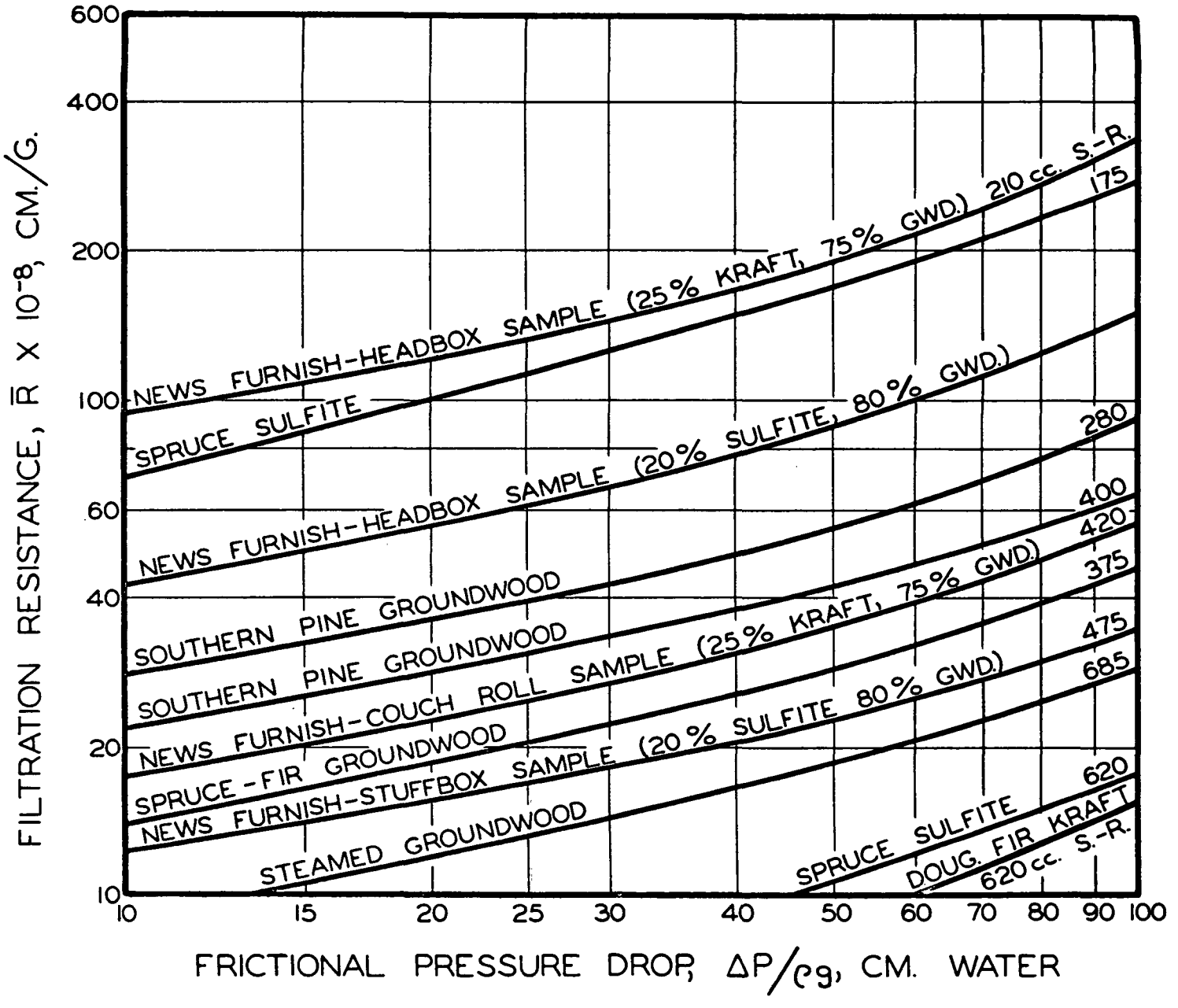

Figure 27. Filtration Resistances of Cellulosic Fibers (High Range)

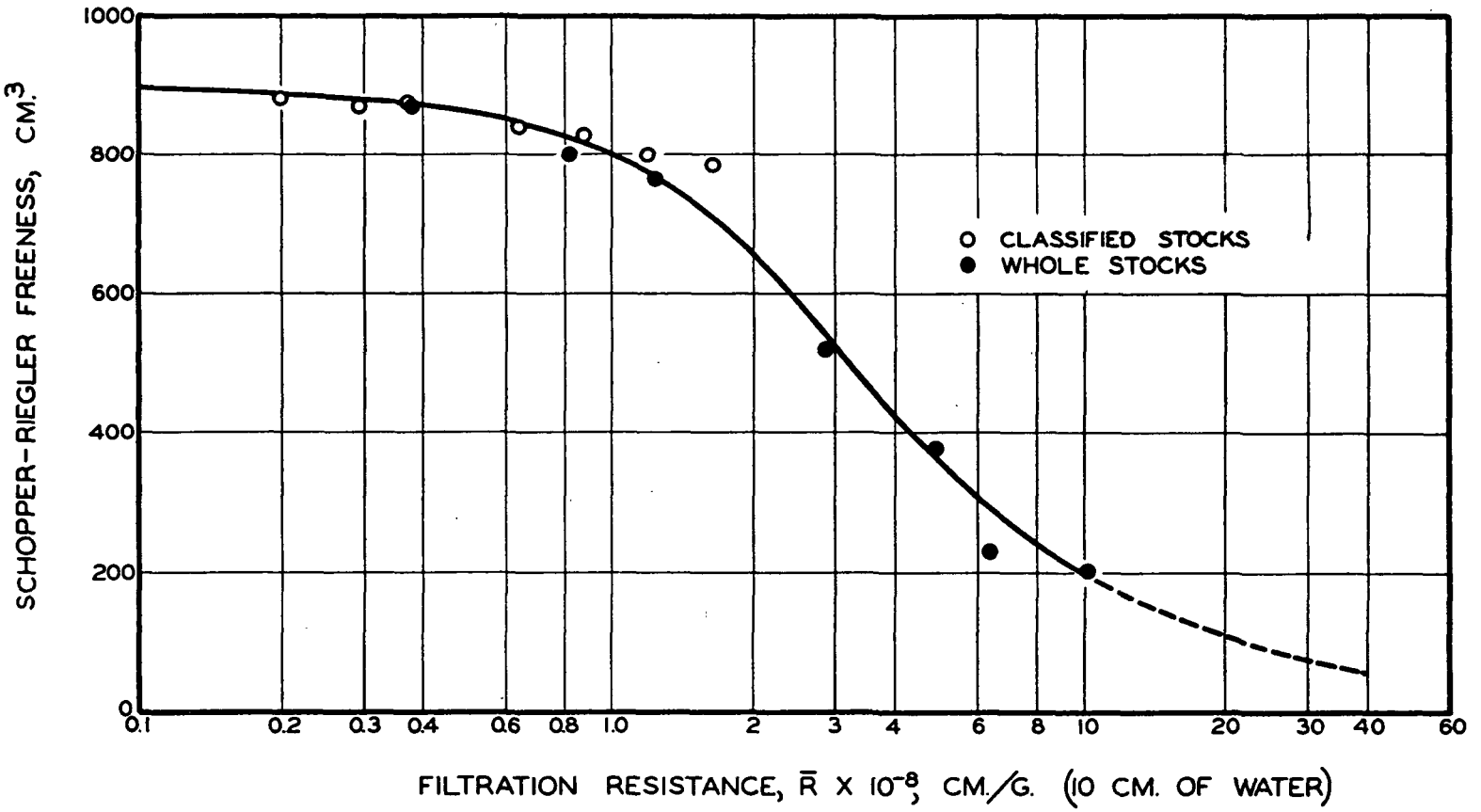

Figure 28. Correlation of Filtration Resistance with Freeness

Septum Resistance

A freeness test generally involves a complete filtration process from the beginning to the end of drainage. It is obvious that the resistance of the septum plays an undesirable role in the initial part of forming a mat. Of much more importance is the well established fiber-wire interaction which causes a higher overall pressure drop than the mere combination of the wire and the thin mat. The fiber-wire interaction becomes ngeligible when the mat reaches a basis weight of about 30 g./sq. cm. The wire-mat resistances are additive above 50 g./sq. cm. and the wire resistance needs no correction over a basis weight of 300. (The final basis weight in a freeness test is usually in the range of 200-600 g./sq. cm.) As a consequence the errors introduced by the septum are appreciable in the drainage measurement in terms of either volume or time.

Falling Head

All freeness tests use a fixed volume of suspension, usually 1000 cc. For very free pulps the initial part of drainage may not follow Darcy's law because of the high head. As drainage proceeds, the hydraulic head drops in proportion to the volume. The decrease of pressure drop by itself is not a serious defect for the purpose of evaluation. The filtration resistance simply decreases correspondingly. But its inherent consequence is an ill-defined effect on the mat structure. The part of the mat already formed tends to recover under the decreasing head. As mentioned before, recovery is a more complicated phenomenon in compressibility. It rarely attains the full extent, resulting in a higher mat density at a given pressure than that in first compression. According to Wilder (20), recovery of a wet mat of cellulosic fibers takes a longer time than creep. This is partly due to the difficulty in reswelling of the fibers.

On account of these complications, recovery tends to increase the filtration resistance in a spurious and uncertain manner. Furthermore, the decrease of pressure drop accompanied by the increase of recovery exerts opposing effects on the filtration resistance which might exhibit a pseudo phenomenon as if the mat were imcompressible. As an illustration, Ingmanson in his initial filtration work analyzed the Williams drainage tester and found the apparent resistance to be relatively constant. It is of some interest to cite his analysis here. If the filtration equation based on Darcy's law applies,

$$\int_o^V \frac{V dV}{V_o - V} = \frac{A}{\mu s \rho R} \int_o^t dt \qquad (65) ,$$

where V_o is the volume corresponding to the initial head and R is tentatively supposed to be constant. Upon integration it yields

$$V_o \ln \left(\frac{V_o}{V_o - V}\right) - V = Ct \qquad (66) .$$

Using a free pulp with a Schopper-Riegler freeness of 805, he obtained the following data:

t, sec.	V, cm.^{3}	C
5	510	24.4
10	670	23.8
15	760	21.8
20	840	21.4
25	910	21.5
32.2	1000	22.4

The apparent constancy of C or R is in contrast to the well established

compressibility of pulp mats. This defect possibly accounts for a part of the insensitivity of a freeness test for very free pulps.

Fines Loss

In the initial part of a freeness test there occurs loss of fibers, which is not taken into account in the drainage result. With highly refined pulps the partial loss of fines is also inevitable in the absence of a flocculating action. The retention of fines in a mat increases in the direction of flow, the maximum being at the bottom of the mat provided no disturbances are incurred. In such cases drainage is partially controlled by the retained fines. This introduces another uncertainty to freeness measurement unless both whole and classified stocks are compared in the same test. As a matter of fact, it has been found that when waste paper is progressively refined, there occurs a slight inversion of freeness at some point, the more refined stock having a higher freeness due to the large loss of fines.

Fiber Settling

Again, for highly refined pulps the drainage becomes very slow. After the initial dispersion the fibers may settle from the suspension during the test, which induces another uncertainty in the result because by settling the mat structure is rather different than by drainage. The last-mentioned two factors may explain the sometimes observed peculiar results in the low freeness range.

In view of these implicit complications and uncertainties the continuing wide use of freeness tests is mainly by their deceptive appeal of convenience. In the rapid advance of technology, what is needed is an instrument capable of measuring the filtration and compressibility under

controlled conditions in a simple and rapid operation with results amenable to further analysis into parameters useful for pulp evaluation. Hopefully, the instrument will eventually incorporate a continuous feature with dynamic effects taken into account for the control of papermaking operations.

UTILITY

PULP EVALUATION

Hydrodynamic evaluation of pulps has been used in research and practice. We conclude this review by citing a number of such applications to illustrate its power as well as limitations. For certain reasons, references to the actual cases are omitted, and they should not be quoted in any manner.

Sheet Strength

The correlations of hydrodynamic properties of wood pulps with handsheet tensile have been fairly well established. Figures 29 and 30 show the correspondence of sheet tensile with specific surface and specific volume, respectively, for a bleached sulfite pulp, whole and classified. The increase of surface area by refining contributes to tensile at a decreasing rate, while the increase in swollen volume is almost linear with tensile within the moderate range. Conventional refining unravels fiber surfaces but also creates fines, some of which do not assist in bonding to a significant extent. Swelling, however, enhances fiber conformability in wet pressing, and therefore improves bonding for a given pulp.

Surface Unravelling

Classified unbleached sulfite fibers were stirred in a British disintegrator for the purpose of unravelling the fiber surfaces. The original and resulting fibers were analyzed by filtration tests and checked against sheet tensile, as follows.

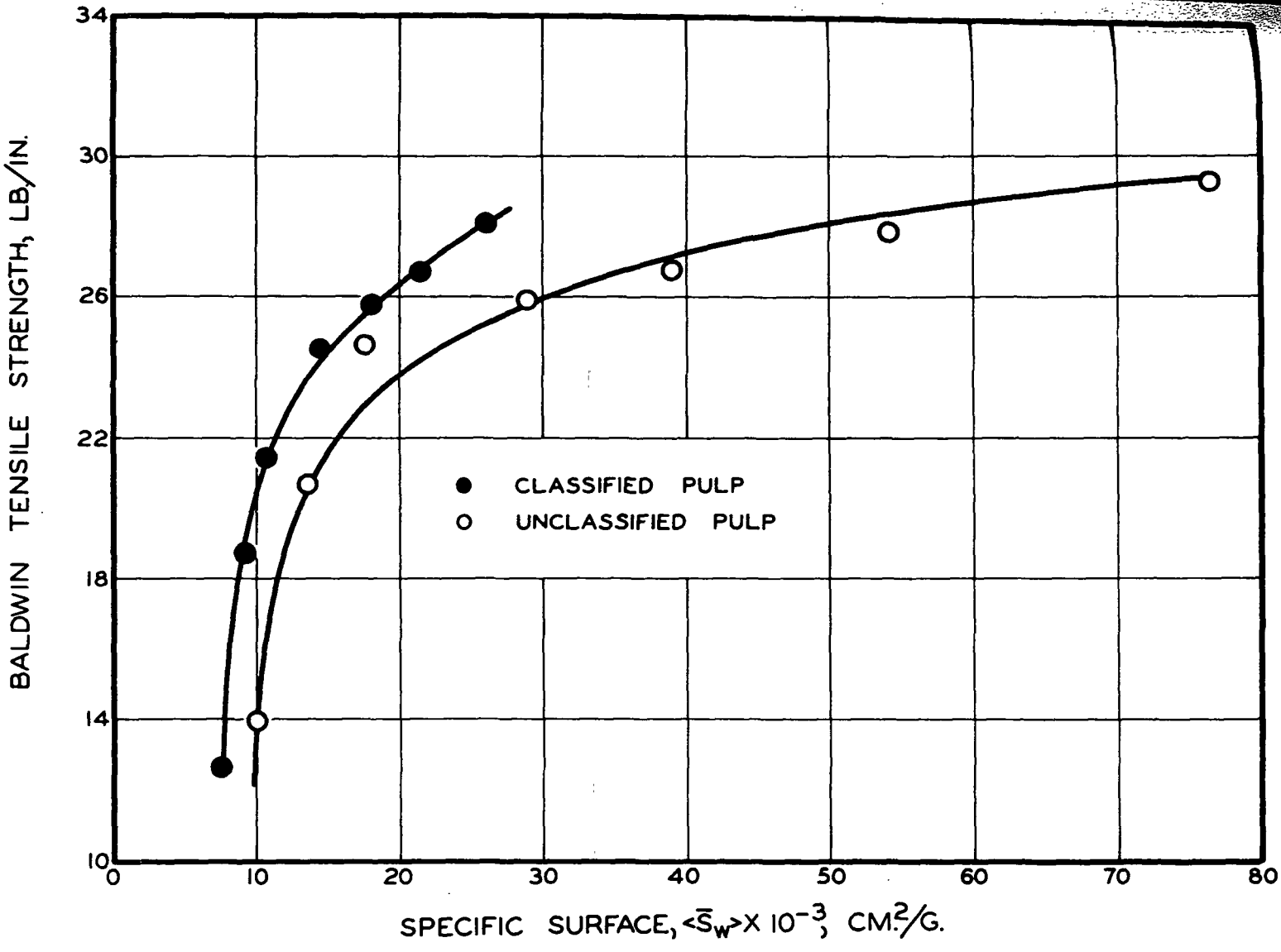

Figure 29. Correlation of Handsheet Tensile with Specific Surface

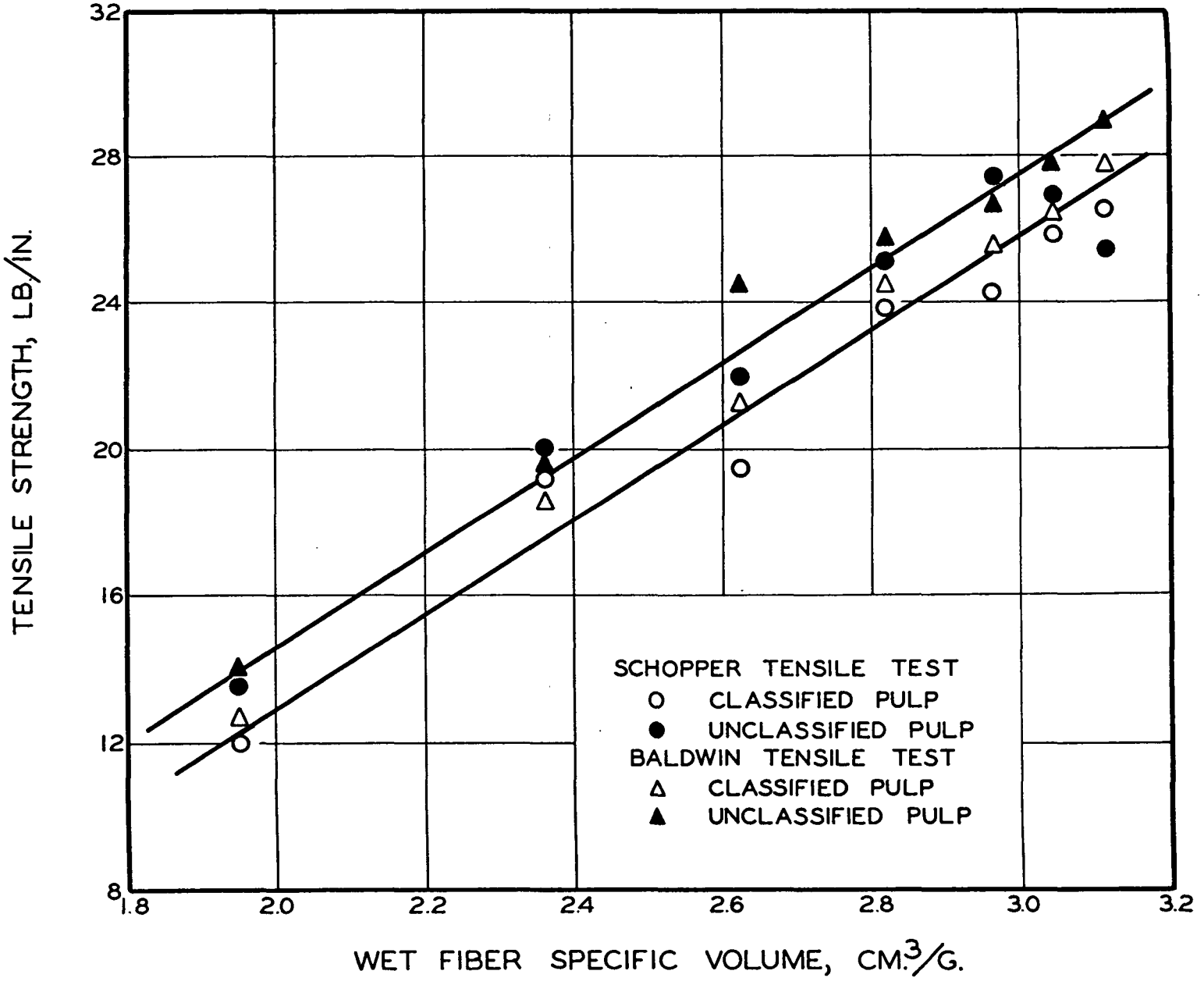

Figure 30. Correlation of Handsheet Tensile with Specific Volume

Fibers	Original	15,000 Counts	300,000 Counts
$\langle \bar{S}_w \rangle$, sq. cm./g.	10,780	38,400	70,800
$\langle \bar{v} \rangle$, cu. cm./g.	0.96	3.21	3.88
Tensile, lb./in.	29.9	42.7	14.4

Most of the newly created surface areas were due to the unravelled primary and outer secondary wall fragments which comprised only about 3% of the classified fiber mass and contributed considerably to bonding. However, the additional surfaces created by prolonged unravelling appeared to be detrimental to bonding, in spite of the increase in swelling.

Hemicellulose Sorption

Additives such as locust bean gum are often adsorbed on fiber surfaces to enhance bonding. The rate of sorption is dependent on specific surface as demonstrated below with the sorption of partially methylated gum on sulfite fibers.

$\langle \bar{S}_w \rangle$, sq. cm./g.	Initial Rate x 10^6, $sec.^{-1}$
9,260	14.8
11,780	16.1
15,610	17.9
29,900	26.5

These data indicate a linear relationship. However, for different pulps and refining conditions the accessibility of the hydrodynamic surfaces for sorption should also be taken into consideration.

Cellulose Modification

Sodium carboxymethylation of cotton linters was found to increase swollen volume and bonding without significant effect on surface area.

Degree of Substitution	$\langle \bar{S}_w \rangle$, sq. cm./g.	$\langle \bar{v} \rangle$, cu. cm./g.	Relative Bonding
0.002 (control)	20,250	1.48	1
0.019	19,600	2.14	1.5
0.040	22,800	2.32	2

Decrystallization of highly purified cotton cellulose by aqueous ethylamine was found to increase specific volume and decrease specific surface. A corresponding decrease in fiber strength was also noted.

Crystallinity index	70.1	69.4	62.8	56.0	52.1
$\langle \bar{v} \rangle$, g./cu. cm.	2.40	2.38	3.02	3.08	3.00
$\langle \bar{S}_w \rangle$, sq. cm./g.	4100	3920	3520	3350	3240
Zero-span tensile, kg./sq. m.	24.8	24.7	21.0	20.9	20.2

Hypochlorite Bleaching

Hypochlorite bleaching of neutral sulfite semichemical aspen pulp indicated that the specific volume of the bleached pulps was linear with their residual Klason lignin content. The specific surface increased mildly. The strength of handhseets improved considerably.

Conventional Refining

The filtration resistance of a pulp during conventional beating or refining increases rapidly primarily because of the increase of specific

surface. Their correlation is shown in Fig. 31 for several pulps with different refiners. The slope of the line on the log-log plot indicates $\underline{\bar{R}}$ to be closely proportional to $\langle \underline{\bar{S}}_w \rangle$ squared in agreement with the previous analysis. The minor discrepancy is attributable to the change of swollen volume. Thus, in practice the decrease of freeness in refining is a less precise index of the increase of surface area on account of the loss of fines.

High-Consistency Refining

Conventional refining of pulps does not alter the mat compressibility to a significant extent because of the counterbalancing effects of fiber-length reduction and fines production. High-consistency refining showed an increase of compressibility by 15% for a kraft pulp over conventional refining (Fig. 19), although the compressibility was practically independent of the level of refining just as in conventional refining. In the compacting pressure range of 10-100 cm. of water the values of $\underline{N}$ remained the same for both cases. At the same freeness level, high-consistency refining indicated about the same degree of fiber swelling as, but considerably lower surface area than, conventional refining.

	Unrefined	Conventionally Refined		High-Consistency Refined	
		High Freeness	Low Freeness	High Freeness	Low Freeness
$\langle \underline{\bar{S}}_w \rangle$, sq. cm./g.	7,800	18,700	37,600	14,600	20,800
$\langle \underline{\bar{v}} \rangle$, cu. cm./g.	2.60	3.00	3.27	2.93	3.16
$\underline{c}$, g./cu. cm. at 50 cm. water	0.118	0.118	0.118	0.130	0.130

Microscopic examination of high-consistency refined pulps showed little fiber-length reduction, near absence of fines, and gentle peeling of

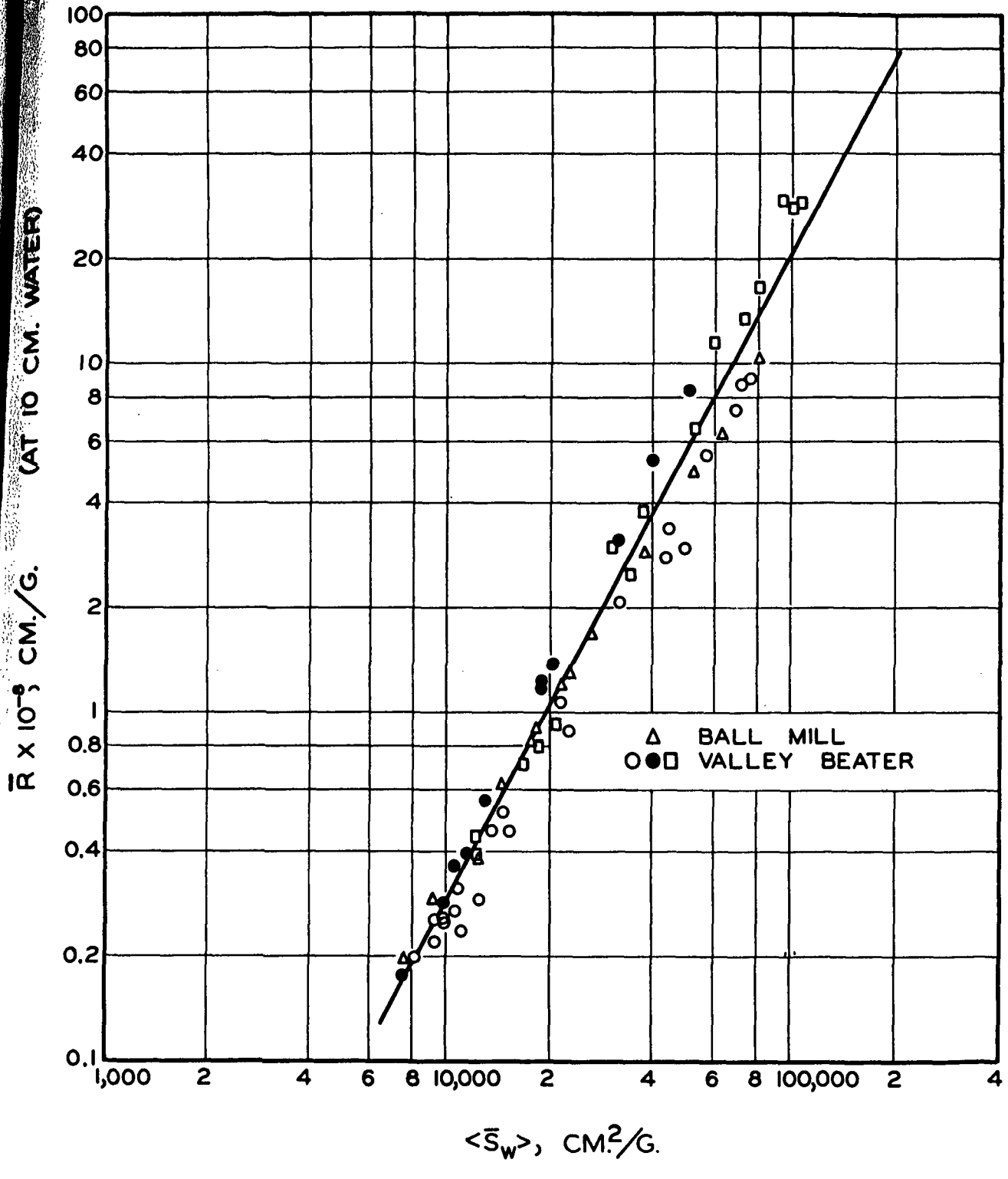

Figure 31. The Dominant Effect of Specific Surface on Filtration Resistance

the outer secondary walls. All these factors tended to contribute to tear, tensile, and burst.

Axial compression of fibers is thought to be the major effect of high-consistency refining (24). If this interpretation is correct, the stress distribution in compressibility badly needs investigation.

MACHINE OPERATION

Wet Breaks

A mill substituted a foreign pulp for its own pulp on one paper machine and encountered less frequent wet breaks at the couch roll. All conventional methods (freeness, beating curves, and handsheet tests) failed to reveal significant differences in the two pulps. By filtration tests samples of the two pulps showed close filtration resistances. However, in conjunction with compressibility tests, it was found that the foreign pulp had a significantly higher specific volume, 2.5 cm.^{3}/g. as compared with 1.8 for the original pulp. By further refining of the original pulp the machine runnability was improved as expected.

Furnish Adjustment

A fourdrinier machine developed occasional difficulties in producing satisfactory corrugating medium. Samples from the stuffbox and the reel under good and poor conditions were submitted for analysis. The results are summarized as follows:

Board sample:	Good	Poor
Basis weight, lb./1000 sq. ft.	32.4	27.0
Caliper x 10^3	11.6	10.3
Apparent density	2.8	2.6
Burst, pt./100 lb.	179	146
Tensile, lb./(in.)(100 lb.), M.D.	154	133
C.D.	75	59
Thwing formation	4.5	4.8
Stock sample:		
C.S. freeness	285	360
$\langle \bar{S}_w \rangle$, sq. cm./g.	36,300	31,100
$\langle \bar{v} \rangle$, cu. cm./g.	2.77	2.41
Repulped board sample:		
$\langle \bar{S}_w \rangle$, sq. cm./g.	25,350	28,900
$\langle \bar{v} \rangle$, cu. cm./g.	1.85	1.78

The 20% larger burst and tensile of the good board was attributed primarily to the 15% greater specific volume, indicating pulping and refining differences between the good and poor pulps. The reverse of specific surface in the corresponding repulped samples was also noted. This was thought to be due to a greater loss of fines from the white water system when the machine was making good board. By classifying the stock and repulped board samples and considering the fraction through 150-mesh screen as fines, it was estimated that 7.6% of the inlet stocks were lost from the white water system for good and poor board, respectively, in agreement with the filtration data. By adjusting pulping and refining to increase the specific volume of the poor pulp and reducing fines retention in the poor board, the problem was eventually solved.

Ply Difference

Difficulties were experienced in maintaining drying rate and burst of jute linerboard on a cylinder machine. Samples of the furnishes and board were taken for examination.

Machine	Operation	Sample	$\langle \bar{S}_w \rangle$, sq. cm./g.	$\langle \bar{v} \rangle$, cu. cm./g.
A	normal	filler	39,350	1.92
		top liner	54,800	2.14
		wet web	39,700	1.98
B	good	filler	36,300	1.95
		top liner	42,400	2.18
		wet web	41,400	1.60
B	poor	filler	42,900	1.91
		top liner	45,300	2.38
		wet web	40,200	1.70

As the filtration resistance of the three web samples showed only 5% variations, the rate of water removal at the wet end should be about the same in spite of the different furnishes. The good and poor board from Machine B should also have nearly the same strength. By repulping these web samples the following test results on handsheets were obtained:

	Good Web	Poor Web
Basis weight, lb./1000 sq. ft.	13.5	13.6
Caliper, points	4.7	4.8
Burst, pt./100 lb.	42	48
Tensile, lb./in.	12.6	13.6

It turned out that the "poor" web was somewhat better than the "good" web, in conformance with the filtration results. Therefore, the difficulties were not in the wet end, nor with the furnishes.

Temperature Increase

A special twin-cylinder machine was manufacturing insulation board. It was desired to increase the production by raising the stock temperature. Wet samples of two grades of board were tested for filtration resistance at two temperatures. Board B was made from the same stock as Board A, except for the addition of 22% resin.

$\Delta P/\rho g$, cm. H_2O	$\bar{R} \times 10^{-8}$, cm./g. 25°C. Board A	25°C. Board B	48°C. Board A	48°C. Board B
50	1.26	1.16	1.65	1.40
60	1.35	1.25	1.79	1.53
70	1.44	1.33	1.92	1.65
80	1.53	1.42	2.04	1.75
90	1.61	1.51	2.16	1.87

It was concluded that 25°C. the increase in production with Board B over Board A was 9% by area. By raising the stock temperature the production of A would gain 1% per °C. and that of B, 1-1/2% per °C. These predictions were confirmed in actual operations. The compressibility tests on the same samples indicated a 25% increase in apparent density of Board B over A. The hydrodynamic properties were evaluated to be as follows:

	$\langle \bar{S}_w \rangle$, sq. cm./g.	$\langle \bar{v} \rangle$, cu. cm./g.
Board A	11,900	2.45
Board B	9,650	2.31

As Board B contained resin, a part of the fines in the stock would be agglomerated through adhesion, accounting for its lower specific surface.

Furthermore, there would be more uniform distribution of fines in the board. Fines agglomeration and adhesion to the fibers would be enhanced at higher temperatures due to the presence of the resin. These factors could contribute to a 50% better temperature effect on drainage than for Board A, as revealed by the filtration results.

In concluding this review, we consider the hydrodynamic evaluation of surface area and swollen volume by constant-rate filtration, pioneered by the late William L. Ingmanson twenty years ago, is basically sound in principle and technique and is a useful tool for research and practice. Further refinements are possible through more sophisticated investigations. In view of the complicating and compensating factors involved in wet fibrous structures, the most critical need of future research on the subject is the construction of a physical theory or a mathematical model for simulating the compressibility of fiber mats under both static and dynamic conditions. This ambitious objective calls for considerable intellectual effort, and if successful will bring important rewards to the paper industry.

Meanwhile, we hope that the present hydrodynamic method of pulp evaluation will be used more and more for solving actual pertinent problems wherever feasible. The results of its application may be not only profitable to the practice but also helpful to continuing research in this and related areas. In this connection, more frequent dialogs between the industry and the Institute would be extremely desirable in order that the technology may be more rapidly advanced.

NOMENCLATURE

Capitals:

A	=	area
B	=	filtration constant
C	=	constant
E	=	modulus of elasticity
G	=	correlation function
I	=	moment of inertia
K	=	permeability; beam constant
L	=	length; thickness
M	=	compressibility coefficient
M'	=	numerical coefficient
N	=	number; compressibility power
P	=	sum of static and gravitational pressures
R	=	specific filtration resistance
Re'	=	Reynolds number for porous media
S	=	specific surface; correlation function
U	=	superficial velocity
V	=	volume
W	=	basis weight

Lower case:

b'	=	inertial constant
c	=	mat density
d	=	diameter
f'	=	friction factor for porous media
g	=	gravitational constant

$\underline{h}$ = fluid head

$\underline{k}$ = Kozeny factor; constant

$\underline{m}$ = hydraulic radius

$\underline{n}$ = number

$\underline{p}$ = pressure

$\underline{s}$ = consistency

$\underline{t}$ = time

$\underline{v}$ = specific volume

$\underline{w}$ = mass of fibers per unit area

$\underline{x}$ = $\underline{x}$ coordinate

$\underline{y}$ = $\underline{y}$ coordinate

$\underline{z}$ = $\underline{z}$ coordinate

Greek symbols:

α = coefficient

β = power

γ = power

Δ = finite difference

δ = length of a vector; deflection of a beam

ϵ = porosity

μ = viscosity

ρ = density

Subscripts:

$\underline{c}$ = contact

$\underline{f}$ = fiber

$\underline{L}$ = mat-septum boundary

$\underline{n}$ = number

$_o$ = mat-suspension boundary; specific reference (see text)

$_s$ = segment

$_v$ = per unit volume of fiber

$_w$ = per unit mass of fiber

Miscellaneous:

$\bar{}$, <> = average

$\rightarrow$ = vector

^{o}, * = explained in text

exp = exponential function

$f()$ = function

∞ = infinity

$\int$ = integral

log = common logarithm

LITERATURE CITED

1. Darcy, H. Les fontaines publiques de la ville de Dijon. Paris, Victor Dalmint, 1856.

2. Prager, S., Phys. of Fluids 4, no. 12:1477(1961).

3. Debye, P., Anderson, H. R., Jr., and Brumberger, H., J. Appl. Phys. 28, no. 6:679(1957).

4. Carman, P. C., Trans. Inst. Chem. Engrs. (London) 15:150(1937).

5. Snyder, L. J., and Stewart, W. E., A.I.Ch.E. Journal 12, no. 1:167(1966).

6. Happel, J., A.I.Ch.E. Journal 5, no. 2:174(1959).

7. Davis, C. N., Proc. Inst. Mech. Engrs. (London) B 1:185(1952).

8. Ingmanson, W. L., Andrews, B. D., and Johnson, R. C., Tappi 42, no. 10:840 (1959).

9. Ingmanson, W. L., and Andrews, B. D., Tappi 46, no. 3:150(1963).

10. Carroll, C. W. Private communication, 1965.

11. Bliesner, W. C. A study of the porous structure of fibrous sheets using permeability techniques. Doctor's Dissertation. Appleton, Wis., The Institute of Paper Chemistry, 1963; Tappi 47, no. 7:392-400(1964).

12. Labrecque, R. P. An investigation of the effects of fiber cross-sectional shape on the resistance to the flow of fluids through fiber mats. Doctor's Dissertation. Appleton, Wis., The Institute of Paper Chemistry, 1967.

13. Onogi, S., and Sasaguri, K., Tappi 44, no. 12:874(1961).

14. Van den Akker, J. A. Unpublished work. Appleton, Wis., The Institute of Paper Chemistry, 1963.

15. Jones, R. L. An investigation of the effect of fiber structural properties on the compression response of fibrous beds. Doctor's Dissertation. Appleton, Wis., The Institute of Paper Chemistry, 1962; Tappi 46, no. 1:20 (1963).

16. Elias, T. C. An investigation of the compression response of ideal unbonded fibrous structures by direct observation. Doctor's Dissertation. Appleton, Wis., The Institute of Paper Chemistry, 1965.

17. Qviller, O., Papir-J. 26, no. 23:312(Dec. 15, 1938).

18. Campbell, W. B., Pulp Paper Mag. Can. 48, no. 3:103(1947).

19. Ingmanson, W. L. An investigation of the mechanism of water removal from pulp slurries. Doctor's Dissertation. Appleton, Wis., The Institute of Paper Chemistry, 1951: Tappi 35, no. 10:439(1952).

20. Wilder, H. D. The compression creep properties of wet pulp mats. Doctor's Dissertation. Appleton, Wis., The Institute of Paper Chemistry, 1959; Tappi 43, no. 8:715(1960).

21. Ingmanson, W. L., and Whitney, R. P., Tappi 37, no. 11:523(1954).

22. Van Wyk, C. M., J. Textile Inst. 37:T-285(1946).

23. Meyer, H. Unpublished work. Appleton, Wis., The Institute of Paper Chemistry, 1965.

24. Page, D. H., Pulp Paper Mag. Can. 67, no. 1:T2-12(1966).

ACKNOWLEDGMENT

The considerable work of Mr. Bruce D. Andrews in the preparation of this review is gratefully acknowledged. Thanks are also due to Mrs. Elizabeth A. Cary for her editing and typing of the text. Without their assistance the completion of the paper on schedule would not have been possible.

THE INSTITUTE OF PAPER CHEMISTRY
Appleton, Wisconsin

S. T. Han

S. T. Han